ADDIS ABABA INSTITUTE OF TECHNOLOGY

School of Civil and Environmental Engineering

Parametric Study of the Axial Load Behavior of Concrete Filled Double Circular Steel Tube Short Columns

A THESIS SUBMITTED IN PARTIAL FULFILLMENT OF THE REQUIREMENTS FOR
MASTER OF SCIENCE (STRUCTURAL ENGINEERING)

By
Melekte Muluken Tamiru

February 2021
Addis Ababa, Ethiopia

ADDIS ABABA UNIVERSITY
ADDIS ABABA INSTITUTE OF TECHNOLOGY
SCHOOL OF CIVIL AND ENVIRONMENTAL ENGINEERING

Parametric Study of the Axial Load Behavior of Concrete Filled Double Circular Steel Tube Short Columns

By Melekte Muluken

Approved by the Board of Examiners:

Dr. -Ing. Girma Zerayohannes Advisor	____________ Signature	____________ Date
______________________________ Internal Examiner	____________ Signature	____________ Date
______________________________ External Examiner	____________ Signature	____________ Date
______________________________ Chairperson	____________ Signature	____________ Date

DECLARATION

I declare that this thesis entitled "Parametric Study of the Axial Load Behavior of Concrete Filled Double Circular Steel Tube Short Columns" provided with following the required academic instructions and the document has never been presented for any other universities and it is my original work.

Melekte Muluken

ABSTRACT

Concrete filled double circular steel tube (CFDCST) columns are exceedingly efficient categories of composite columns, which can be considered as modified sorts of circular concrete-filled steel tube (CFST) columns. They also possess the properties of circular CFST columns with extra improvements. The double confinement effect observed in CFDCST short columns is an important aspect, which tremendously improves the load-bearing capacity of the column and the CFDCST's performance depends on the constituent material's individual property and combined action effects. These types of short CFDCST columns are importantly used in composite multistory building structures for taking most of the earthquake forces acting on the system and they could be used in slopped grounds as footing columns and also positioned in the requirement of an intermediate beam for supporting heavy compression loads.

Despite the CFDCST column's vast advantages, very limited researches have been carried specifically in examining the influential factors related to the change in material's strength, and geometrical properties. There is also complexity in accompanying finite element (FE) analysis, especially in defining the materials' combined action. Therefore, in conducting a parametric study using FE analysis; this paper provides a basic understanding of the axial load performance of CFDCST short columns. Besides, the possible advantages of using CFDCST columns instead of CFSTs are discussed in detail.

Possible FE analyzing techniques used in this study were verified by experimentally conducted and published seven CFST and four CFDCST column tests. Moreover, seven basic sections of model specimens are classified to study the axial load behavior of circular CFST and CFDCST short columns in a total of fifty-eight model analyses. Different parameters are also studied regarding the change in material strength and geometrical variations.

The analysis result assures that CFDCST columns are much better in providing extra-axial resistance through the development of a higher confinement tendency. It is also found that the insertion of an internal steel tube has a great influence to tolerate the variation in the external D/t ratios, which can be taken as a measure to enhance the capacity of CFST columns. In addition, no immediate failure occurred in CFDCST columns and failure modes tend to develop lower lateral displacement at the average height of the column due to the presence of the internal steel tube.

Keywords: - CFST and CFDCST short columns, Dual confinement effect

NOMENCLATURE

Latin upper case letters

A_c	Cross-sectional area of concrete in CFST column
$A_{c,sw}$, $A_{c,core}$	Cross-sectional area of sandwich and core concrete in CFDCST columns, respectively
A_s	Cross-sectional area of steel in CFST column
A_{sc}	Total cross-sectional area of a CFST or CFDCST column
$A_{s,ext}$, $A_{s,int}$	Cross-sectional area of external and internal steel tubes in CFDCST columns, respectively
CFDCST	Concrete filled double circular steel tube
CFST	Concrete filled steel tube (Circular)
D	Diameter of the steel tube in CFST column
D_{ext}	Diameter of the external steel tube in CFDCST column
D_{int}	Diameter of the internal steel tube in CFDCST column
EI_{eff}	Effective flexural stiffness
E_s	Modulus of elasticity of steel
FE	Finite element
FEM	Finite element modeling
L	Column Length (for either CFST or CFDCST columns)
N_{EC-4}	Ultimate axial strength of CFST or CFDCST columns as per the Eurocode−4 predictions
N_{Exp}	Experimentally predicted ultimate axial strength of CFST or CFDCST column
N_{FEA}	Ultimate axial strength of CFST or CFDCST columns predicted from Finite element analysis
$N_{pl,Rd}$	Design plastic resistance of the axially loaded member
P_1	Lateral pressure of the interface between sandwich concrete and external steel tube
P_2	Lateral pressure of the interface between sandwich concrete and internal steel tube
P_3	Lateral pressure of the interface between core concrete and internal steel tube

Latin lower case letters

f_1	Lateral confining pressure
f'_c	Compressive cylindrical strength of concrete
$f'_{c,c}$, $\varepsilon_{c,c}$	Maximum stress of confined concrete and the corresponding strain
f_{cu}	Cubic compressive strength of concrete
f_u	Ultimate strength of structural steel in CFST column
$f_{u,ext}$, $f_{u,int}$	Ultimate strength of external and internal steel tubes respectively in CFDCST columns

f_y	Yield strength of structural steel in CFST column
$f_{y,ext}$, $f_{y,int}$	Yield strength of external and internal steel tubes respectively in CFDCST columns
r_1, r_3	Outside radius of external and internal steel tubes, respectively
r_2, r_4	Inside radius of external and internal steel tubes, respectively
t	Thickness of the steel tube in CFST column
t_{ext}	Thickness of external steel tube in CFDCST column
t_{int}	Thickness of internal steel tube in CFDCST column

Greek lower case letters

δ	Steel contribution ratio of composite columns
δ_{FEA}	Finite element analysis based axial deflection at peak load
$\varepsilon_{c,o}$	Strain at peak stress of unconfined concrete
ε_y	Strain at yielding stress of steel tube in CFST columns
$\bar{\lambda}$	Relative slenderness
μ_C	Poisson's ratio of concrete
μ_S	Poisson's ratio of steel
ξ_c	Confinement factor of a CFST column
$\xi_{c,eqv}$	Equivalent confinement factor of a CFDCST short column
${\sigma^c}_{sw}$	Sandwiched concrete lateral stress in CFDCST columns
σ^s	Lateral stress of steel tube in CFST column
${\sigma^s}_{ext}$	Lateral stress of external steel tube in CFDCST columns
${\sigma^s}_{int}$	Lateral stress of internal steel tube in CFDCST columns
ψ	Dilation angle of concrete

Table of Contents

List of figures

List of tables

CHAPTER-1 Introduction

1.1 Background

Concrete filled steel tube (CFST) columns are extensive advancements of reinforced concrete column structures. The idea of enhancing concrete column's overall strength related to bearing capacity, ductility, stiffness, and energy-absorption capacity had developed the concept of well-sophisticated straps, transversal and longitudinal reinforcement which eventually led to the use of steel tube as full shell confinement. Therefore, circular, square, rectangular, and other types of CFST columns are becoming important in the construction sector. CFST columns are useful in civil engineering structures for their excellent ductility and energy absorption capacity. Unlike other types, circular CFST columns are well suited for providing uniform confining pressure in all the radial directions (Musthafa et al., 2016). They are extremely effective types and for further structural enhancement, circular CFST columns are nowadays constructed with an additional internal circular steel tube profile, which collectively termed as concrete-filled double circular steel tube (CFDCST) columns.

(a). Circular CFST column (b). CFDCST column

Figure 1: Cross-sectional shape of circular CFST and CFDCST columns

CFDCST columns possess the properties of circular CFST columns with extra improvement. The double confinement effect observed in CFDCST short columns is an important aspect, which tremendously improves the load-bearing capacity of the column. Fire resisting tendency due to the presence of a fully encased internal steel tube is also considered as a particular advantage in the CFDCST column's usage. Besides, the reduction in the amount of concrete caused by the placement of the inner steel tube results in lighter self-weight which further enhances the damping characteristics.

The performance of CFDCST columns highly depends on its constituent material's strength and geometrical properties. The strength of concrete and steel tubes has a great impact on the overall structural responses. Geometric variations including cross-sectional size and steel tube thickness tremendously influence the ultimate load-bearing capacity of the column.

Moreover, the performance of CFDCST columns affected by materials combined action due to bond interaction and confinement effect. The combined action effect of the steel tube and the concrete core in the CFST column results in a triaxial stress state toward the concrete and alters the stress-strain relationship of the concrete in the manner of increasing the load-carrying capacity of the whole structure. Similarly, the surrounding steel which provides the confining pressure also stiffened by the concrete from the inside and results to have an outward buckling that creates delays from reaching its ultimate load-carrying capacity earlier. Therefore, the effect of confinement is an important concept in the analysis and design of circular CFST and CFDCST short columns, and it still keeps being a challenge. The interaction between the steel tube and the concrete core also possesses difficulties in the determination of the material's combined property.

In concerning circular CFST columns, different scholars have conducted behavioral studies in different aspects through providing effective experimental, numerical, and finite element analysis. However, studies are still required to achieve their most advantages and to make the design more simplified and economical in its application. Besides this, very limited research has been done in studying CFDCST columns, especially in examining the influential factors affecting their performance in terms of changes in geometrical aspects, confinement, and slenderness effects.

This paper is concerned with conducting a parametric study on the axial force resistance of short CFDCST columns under varied material's strength and geometrical properties by using finite element analysis with a consideration of strength modification due to confinement effects. A comparative evaluation between circular CFST and CFDCST columns is also provided in this document.

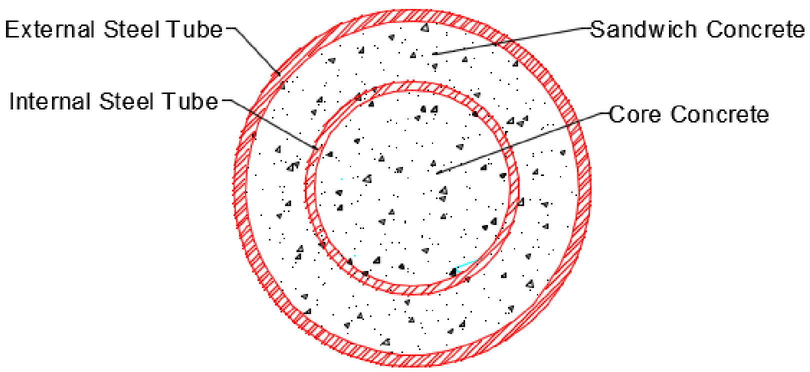

Figure 2: CFDCST column cross-section

Note: -

- The term 'short' is used to describe a CFST or CFDCST column whose length is sufficiently small compared to its cross-sectional dimension in which crushing failure tends to develop due to axial loading.
- In this paper, the term 'CFST' (concrete-filled steel tube) is used to describe a circular concrete-filled steel tube.

1.2 Significance of the study

CFDCST columns are exceedingly efficient categories of composite columns, which can be considered as modified sorts of CFST columns. However, very few studies have been conducted in exploiting their most important advantages. Detailed studies on the effect of change in geometrical properties and materials strength of CFDCST columns are still required. There is also complexity in conducting finite element (FE) analysis, especially in defining the materials' combined property. Therefore, with conducting parametric studies using finite element modeling; this paper has an impact on understanding the performance of CFDCST short columns under axial loadings. Besides, the possible advantages of using CFDCSTs instead of CFST columns are exposed depending on some structural aspects. This paper also discusses potential FE modeling techniques.

Further, Eurocode-4 provides a design guideline for CFST columns and presents a simplified method for computing the plastic resistance. However, this code considers the internal steel tube of a CFDCST column as an inner reinforcement that entirely ignores the double-tube configuration effect of confinement in the core concrete. This may result in a very conservative approach toward the estimation of axial load carrying capacities. Therefore, a comparative study on EC-4 presented and possible FE analysis mechanisms toward the consideration of confinement in the core concrete of the CFDCST columns discussed in this paper.

1.3 Objectives

1.3.1 General objectives

This paper plans to conduct a parametric study on the axial load behavior of CFDCST short columns and stand to set a comparative study over CFST columns using finite element model analyses.

1.3.2 Specific objectives

a) Conduct possible methodological techniques for the finite element analysis and restructure effective ways of including the combined properties of materials for use in FE analysis.
b) Assess the effect of change in geometrical properties and materials' strength on the performance of axially loaded CFST and CFDCST short columns.

1.4 Outline of the study

There are four major sections in this paper presented to justify the required objectives of the study. The first section, which is listed as chapter 2 presents a literature review on the axial load behavior of CFST and CFDCST short columns. Experimental tests and nonlinear analysis of past research works are also conducted. In addition, the analysis and design standards of the Eurocodes-4 are described.

In chapter-3 of this study, possible FE modeling techniques and numerical suggestions are described for both CFST and CFDCST columns. Chapter-4 is also concerned with validating the proposed techniques of the finite element analysis and it mainly targets to verify the numerical suggestions. This section illustrates how the proposed techniques of the FE analysis were verified using experimentally tested seven CFST and four CFDCST short columns.

In the final main section of this paper (chapter-5), parametric studies on the analyses of 15 models of CFST and 43 models of CFDCST columns are shown regarding the change in materials' strength and geometrical properties. This section contains seven groups of models, which are classified according to the variation in the internal steel tube diameter, external and internal steel tube thickness, concrete and steel strength, short column slenderness ratio, and combined effect of change in the internal steel tube D/t ratio and material's strength. Finally, reliable assessments on test results are discussed, and appropriate comparative studies are given for CFST and CFDCST short columns.

CHAPTER-2 Literature Review

2.1 General overview

Composite columns could be constructed with the combinations of concrete and steel materials in the manner of achieving their composed structural benefits. There are different composite column sections known these days, and these are classified into three major groups; the fully encased column (FEC), partially encased columns (PEC), and concrete-filled steel tube (CFST) columns. In CFST columns, the structural steel fully confines the concrete core cast inside, and additional internal steel sections can be included for further structural improvements like in the case of CFDCST columns.

CFST columns are favored for earthquake-resilient structures and widely deployed in high-rise buildings, and high strain rate subjected bridges. They are also becoming popular in various structures. CFST columns have an advantage in reducing construction time and costs associated with formwork. Moreover, CFST columns provide high compressive and torsional resistance when compared with concrete-encased steel composite and reinforced concrete columns. They have also high levels of ductility nature and they are considered as the most effective forms of composite columns in assuring all the above-mentioned advantages.

Within the different categories of CFST columns, CFDCST columns are introduced with two concentrically placed steel tubes for further structural advancements in which the internal steel tube is fully surrounded with concrete from its internal and external faces. Therefore, the concrete separates into two different concrete classes known as sandwich and core concrete as shown in figure 2.

In comparison with CFST columns, CFDCST columns have a higher axial strength, ductility performance, and fire rating capacity. In the situation of a fire, CFDCST columns have a better tendency to resist elevated temperatures as the internal steel tube confine the inside concrete core without being affected by fire due to the full protection and encasement of sandwich concrete. Besides, CFDCSTs have better damping characteristics, due to the amount of concrete reduced by the inner steel tube filling. Therefore, these types of short CFDCST columns are importantly used in composite multistory building structures for taking most of the earthquake forces acting on the system and they could be used in slopped grounds as footing columns and also positioned in the requirement of an intermediate beam for supporting heavy compression loads.

In studying the behavior of CFDCST columns, it is primarily important to deal with CFST columns. Wan and Zha (2016) also state the CFDCST column inherits similar behavior from the CFST column.

2.2 Studies on circular CFST columns

Before the beginning of the 1960s, extensive researches on CFST columns were not happening (Abdalla, 2012). But later, Furlong (1967) provided experimental beam-column data in determining the accuracy of his theoretical estimates. The tests were performed on round and square columns by applying a constant concentric axial force and moment. Conclusions on the theoretical result were also given. After Furlong (1967), a growing amount of research work concerning CFST columns has been published worldwide. These works include experimental, theoretical, analytical, and finite element simulations to understand the composite actions, nonlinear behavior, bond effects, local buckling, and other responses of CFST members. Parametric studies and new modifications are also continuing and the works of these scholars have a great deal of effect in understanding the structures, formulating design methods, and provisions of standard codes.

Some scholars conducted experimental studies on CFST columns (Schneider, 1998; Huang et al., 2002; Giakoumelis and Lam, 2004; Sakino et al., 2004; Abdalla, 2012; Wang et al., 2016; Zhao et al., 2018; Lin et al., 2018; He et al., 2019). Researchers have also investigated the property and performance of CFST columns by using finite element simulations and currently, the finite element technique is becoming popular for modeling CFST columns. Some of the researchers that conducted finite element analysis using the ABAQUS software program includes Hu et al. (2003), Tao et al. (2013), Abbas (2016), Yadav and Chen (2017), Goel and Tiwart (2018), Du et al. (2018), Zhao et al. (2018). Even though finite element simulation permits more precise analysis circumstances and straightforward modeling techniques on imperfections, and boundary conditions, it is also surrounded by challenging aspects of setting parameters related to material's characteristics. Especially in composite structures, it is importantly required to understand the combined response of each material. This solely requires setting up guidelines for FE analysis depending on experimental test results. Following this, some researchers have done lots of work and conducted successful FE modeling of CFST short columns that closely match with experimental results.

The axial force resisting capacity of the CFST column is highly influenced by the diameter-to-thickness (D/t) ratio, length-to-diameter (L/D) ratio, and material strength of concrete and steel tubes. For small-dimensional CFST columns, smaller D/t ratios tend to modify the force-resisting capacity of columns with an increased yield strength and favorable post-yield behavior (Schneider, 1998; Huang et al., 2002). Similarly, higher L/D ratios affect the structural response, failure mode, and load-carrying capacity of the column. CFST columns classify into short, intermediate, and slender members depending on their relative slenderness or L/D ratios. The increment of column slenderness weakens load-carrying capacity; and to consider this reduction in the plastic resistance of a column, EC-4 uses European-bucking curves depending on the relative slenderness ratios of the members.

Likewise, the changes in the material's strength affect the structural response of CFST columns. Yadav and Chen (2017) conducted a parametric study on CFST columns and suggested that the axial force resistance capacity linearly increases with an increment in the concrete compressive strength and yield strength of the steel tube. Moreover, the study predicted that increases in the concrete strength from 30 MPa to 70 MPa results in a 54.3% increment in the ultimate load-carrying capacity of the CFST column. Similarly, the increase in yield strength of steel tube improves the concrete ductility and axial load carrying capacity of the column.

Concerning the steel tube and concrete bond interaction, Giakoumelis and Lam (2004) remark that increment in concrete strength tends to develop a higher influence on the bond strength of concrete and steel tube. However, the effect of bond strength of the axial load behavior of a column was found to be negligible for concrete strength with normal grades. Further, the conducted finite element analysis of Goel and Tiwary (2018) claims the effect of the frictional coefficient between the steel tube and concrete in the CFST column has no substantial effect on the axial load capacity. Besides, short CFST columns were noticed to develop the most common failure type of local buckling.

Hu et al. (2003) also proposed material constitutive models for CFST circular and square columns and introduce the empirical equation of lateral confining pressure depending on the cross-sectional size and steel tube's strength. Degradation parameter introduced to quantify the properties of confined concrete stress-strain curves and equations were suggested based on the concept that both lateral confining pressure and the material degradation parameter decrease with an increase in diameter-to-thickness ratio (D/t). The study also suggests that when the thickness of the steel tube is relatively thicker in comparison with the diameter of the concrete, the steel tubes provide strong lateral support to the concrete core resulting in a very large value confining pressure. Material degradation parameter also equals 1; indicating that the concrete strength does not degrade beyond this ultimate point. The active confinement pressure suggestion of Mander et al. (1988) was also adopted and the stress-strain relationship proposed by Saenz (1964) was used in assuming the descending line of the stress-strain curve that terminates at a point equals to the confined concrete strength multiplied by the degradation factor.

The model presented by Hu et al. (2003) was analyzed using ABAQUS software and verified with experimental works, which were done by Schneider (1998), and Huang et al. (2002). The effect of steel confining pressure and the geometric properties of CFST columns under uniaxial performance were studied and discussed. The study also explains that circular sections provide much better confinement in comparison to the square sections, especially when the diameter to thickness ratio is getting smaller.

Tao et al. (2013) also performed a finite element model analysis on concrete-filled short columns; different experimental data were studied to develop refined finite element modeling techniques in simulating CFST short columns under axial loadings. The study discusses different aspects related to the concrete damage plasticity model and it proposes an empirical equation for dilation angle and claims an equation used to estimate the ultimate yield strength of steel tubes. For confined concrete, strain hardening/softening rules are presented, and good results also found in modeling short CFST columns.

2.3 Studies on CFDCST columns

Concerning the performance of CFDCST columns, some researchers conduct numerical analysis, experimental tests, and FE model analysis including Romero et al. (2015), Wan and Zha (2016), Ekmekyapar, and AL-Eliwi (2017), Ji et al. (2018).

Romero et al. (2015) investigated experimental studies on slender columns. Two double-tube concrete-filled steel tubular columns devoid of core concrete and four CFDCST slender columns were examined under elevated and room temperatures with the application of concentric loading. The effect of using a thicker tube size in internal or external steel tubes and usage of ultra-high-strength core concrete was discussed to maximize the axial resistance of a slender column. At room temperature, test results showed buckling failures in all the slender sections, and no local buckling developed at the mid-height and ends of the columns. With approximately the same total area of steel, the effectiveness of using a thicker external or internal steel tube was tested and founded that thicker external steel tube results in developing increased ultimate load resistance due to the increase in the moment of inertia of the whole section, which reduces the influence of second-order effects. It also indicated that increasing core concrete strength from normal concrete strength (42MPa) to ultra-high concrete of 134MPa results in only a 9% increment in the load-bearing capacity of a slender column with a buckling length of 3315mm. However, costs spend on ultra-high-strength concrete were approximately found to be 5 times the cost of the nominal concrete grades.

Wan and Zha (2016) performed analytical, experimental, and finite element analysis on short and slender CFDCST columns. In the numerical section, a design formula for computing the compressive strength of axially loaded CFDCST short and slender columns was provided. FE model analyses were conducted and compared using experimental results of six short and two slender CFDCST columns. The failure mode of the experimental tests of short columns showed an outward local buckling in the external steel tube near the position of the bottom, top, and middle-heights. However, slender columns showed an unstable failure of compression bending failure. Moreover, one short and one slender CFST columns were tested for comparison purposes and results show the CFDCST column possesses the stronger bearing capacity, ductility, and stiffness capacity in contrast with the CFST column due to additional confining effects of the internal steel tube. Besides, increment in the internal steel tube yield strength with constant steel ratio results to develop higher load-bearing capacity in CFDCST columns.

Ekmekyapar and AL-Eliwi (2017) performed experimental studies on short CFDCST columns for the improvement in the efficiency of composite members and results showed that the CFDCST column’s configuration is very effective to enhance compression, ductility, and stiffness performances of the compression members. The statistical analysis also advocates the property of an external steel tube is more effective than the core and sandwiched concretes in its contribution to the collapse load of a CFDCST short column. The percentage contribution of an external steel tube has also been estimated to be 82.37% of the collapse load of a short CFST column. The existence of an internal steel tube was also found to improve the ductility and toughness of the columns, especially for a column with high core and sandwiched concrete strength. It also suggested that damaged CFST columns could be strengthened with full shell steel tube jacketing which results in the formation of CFDCST column configurations. Experimental tests also showed repaired CFST columns exhibit very close performance to that of the CFDCST counterpart.

2.4 Analysis and design of CFST columns according to the Eurocode-4

2.4.1 General requirements

Eurocode-4 provides a simplified design method to deal with CFST columns. This method does not apply to laced or battened CFST columns, which consist of two, or more discontinuously connected sections. The scope of this simplified method is also bounded on sections with relative slenderness lower than 2 and the steel contribution ratio (δ) should fulfill the condition of $0.2 \leq \delta \leq 0.9$.

$$\delta = \frac{A_a f_{yd} + A_e f_{ed}}{N_{pl,Rd}} \tag{1}$$

Where:-

A_a, A_e: Cross-sectional area of steel tube and encased steel section respectively

f_{yd}, f_{ed}: Design strength of steel tube and encased steel section respectively

$N_{pl,Rd}$: Plastic resistance to the composite section

EC-4 (Part1-1) S6.7.1 states the applicability of the simplified method is limited to normal concrete strength classes C20/25 to C60/75 and for steel grades S235 to S460. In the design of steel sections, the influence of local buckling needed to be taken into account. However, this effect may also be neglected for steel sections that are fully encased in concrete or for cross-sections satisfying the following requirements.

For circular CFST: $\frac{D}{t} \leq 90\varepsilon^2$, where $\varepsilon = \left(\frac{235}{f_y}\right)^{0.5}$ And f_y in MPa (2)

Further, EC-4 (Part1-1) S6.7.2 specifies that creep and shrinkage effects could be ignored if the increase in the first-order bending moments due to creep deformations and longitudinal force results from permanent loads is not greater than 10%.

2.4.2 Cross-sectional resistance

According to Eurocode-4, the plastic resistance to compression $N_{pl,Rd}$ of a composite cross-section could be calculated by adding the plastic resistances of its components.

$$N_{pl,Rd} = A_a f_{yd} + A_c f_{cd} + A_e f_{ed} \tag{3}$$

Where:-

A_c: Cross-sectional area of concrete

For circular cross-sections, accounts are allowed to be taken for the increase in strength of concrete caused by a confinement in the limit of relative slenderness ratio does not exceed 0.5 and e/d considered to be less than 0.1.

Where: e: Eccentricity of loading given by MEd/NEd

d: External diameter of the column

Therefore, modified plastic resistance to compression can be calculated from the following expression in considering the effect of confinement as expressed in Eurocode-4:

$$N_{pl,Rd} = \eta_a A_a f_{yd} + A_c f_{cd}\left(1 + \eta_c \frac{t}{d}\frac{f_y}{f_{ck}}\right) + A_e f_{ed} \tag{4}$$

For members with zero eccentricity

$$\eta_a = 0.25(3 + 2\bar{\lambda}) \text{ but } \leq 1.0 \qquad \eta_c = 4.9 - 18.5\bar{\lambda} + 17\bar{\lambda}^2 \text{ but } \geq 0 \tag{5}$$

Based on Eurocode-4, the relative slenderness ratio of a typical cross-section of a concrete-filled steel tube column in the plane of bending is shown in equation (6).

$$\bar{\lambda} = \sqrt{\frac{N_{pl,Rk}}{N_{cr}}} \tag{6}$$

Where:-

$N_{pl,Rk}$: The characteristic value of the plastic resistance to compression, where the design strength is replaced by characteristic values

N_{cr} : The elastic critical normal force for the relevant buckling mode

The elastic critical normal force can be found from the Euler buckling load as shown below.

$$N_{cr} = \frac{\pi^2 (EI)_{eff}}{L^2}, \quad \text{Where } (EI)_{eff} \text{ is the effective flexural stiffness} \tag{7}$$

EC-4, S6.7.3.3 (3) determines the characteristic value of the effective flexural stiffness $(EI)_{eff}$ of a cross-section of a composite column to be calculated as follows.

$$(EI)_{eff} = E_a I_a + E_s I_s + K_e E_{cm} I_c \qquad K_e = 0.6 \text{ and } I_c \text{ Is for un-cracked section} \tag{8}$$

Where:-

K_e : Correction factor is taken as 0.6

$I_a, I_c,$ and I_s: Second moments of area of the structural steel section, the un-cracked concrete section, and the reinforcement for the bending plane being considered.

2.4.3 The resistance of members’ in axial compression

For members in axial compression, the design value of the normal force N_{ED} should satisfy:-

$$N_{ED} \leq \chi N_{pl,Rd} \tag{9}$$

$$\chi = \frac{1}{\Phi + \sqrt{\Phi^2 - \bar{\lambda}^2}} \tag{10}$$

$$\Phi = 0.5\left(1 + \alpha\left(\bar{\lambda} - 0.2\right) + \bar{\lambda}^2\right) \tag{11}$$

Where:-

χ: Reduction factor for the relevant buckling mode

α: Imperfection factor

2.4.4 Imperfections

EC-4(Part1-1), S5.3.1 states appropriate allowances shall be incorporated in the structural analysis to cover the effects of imperfections, including residual stresses and geometrical imperfections and the assumed shape of imperfections shall take account of the elastic buckling mode of the structure or member in the plane of buckling considered in the most unfavorable direction and form.

EC-4, S5.3.2.3, (1) States design values of equivalent initial bow imperfection for composite columns and composite compression members to be taken as follow

Cross Section		Limits	Axis of buckling	Buckling curve	Imperfection Factor	Member Imperfection
Circular hollow steel sections	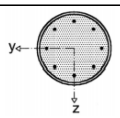	$\rho_s \leq 3\%$	Any	a	0.21	L/300
		$3\% < \rho_s \leq 6\%$	Any	b	0.34	L/200
Circular hollow steel sections with internal ‘I’ section	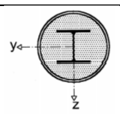		y-y z-z	b	0.34	L/200

Table 1: Member’s imperfection as given in the EC-4, part 1-1 (table 6.5)

2.4.5 Steel- concrete interaction

- EC-4, Section 6.7.4.3 provides that the surface of the steel section, which is in contact with the concrete, should be free from oil, grease, coats, and rusts. It also suggests design shear strength (τ_{RD}) standards for different cross-sections and the following value is provided for CFST columns.

Concrete filled circular hollow sections…………………… τ_{RD}= 0.55 N/mm^2

2.4.6 Euro code approach for confined concrete

In conducting non-linear analysis EC-4, S 6.7.2, (8) requires stress-strain relationships of concrete to be as per the code stated under EN 1992-1-1, 3.1.5 where the relationship between compressive stress (σ_c) and strain (ε_c) are provided for unconfined concrete with schematic, parabolic-rectangular, bilinear, and rectangular representation for purpose of structural analysis. Similarly, EN 1992-1-1, 3.1.9 suggests that, confinement of concrete results in a modification of effective stress-strain relationship in which higher strength and higher critical strains are achieved. In the absence of more precise data for design purposes, the code also suggests stress-strain relation to be used with increased characteristic strength and strains.

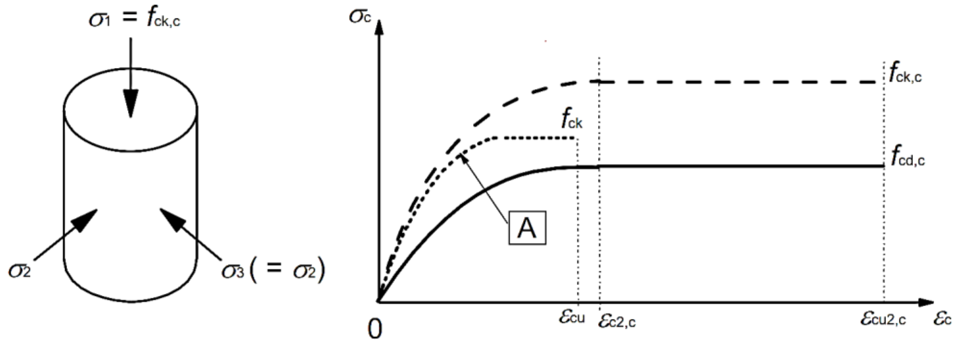

Figure 3: Stress-strain relationship for confined concrete as given in EC-2, part 1-1 (figure 3.6)

Where:-

$\sigma_2 = \sigma_3$: The effective lateral compressive stress at the ultimate limit state due to confinement

$\varepsilon_{c2}, \varepsilon_{cu2}$: Strain reaching maximum strength and ultimate strain as given in EC-2, part 1-1 (table3.1)

2.4.7 Stress-strain relationships of steel structure

Non-linear analysis of the structural steel section EC-4, S6.7.2, (8) suggests EN 1993-1-1, 5.4.3 (4) to be used where the bi-linear stress-strain relationship is recommended. For more precise details EN 1993-1-1, 5.4.3 (4) also refer to EN 1993-1-5(C.6) which presents four assumptions for finite element model (FEM) analysis. Therefore, depending on the accuracy and allowable strain required for the analysis the following assumptions for the steel material behavior may be used.

a) Elastic-plastic without strain hardening

b) Elastic-plastic with a nominal plateau slope

c) Elastic-plastic with linear strain hardening

d) True stress-strain curve modified from the test results

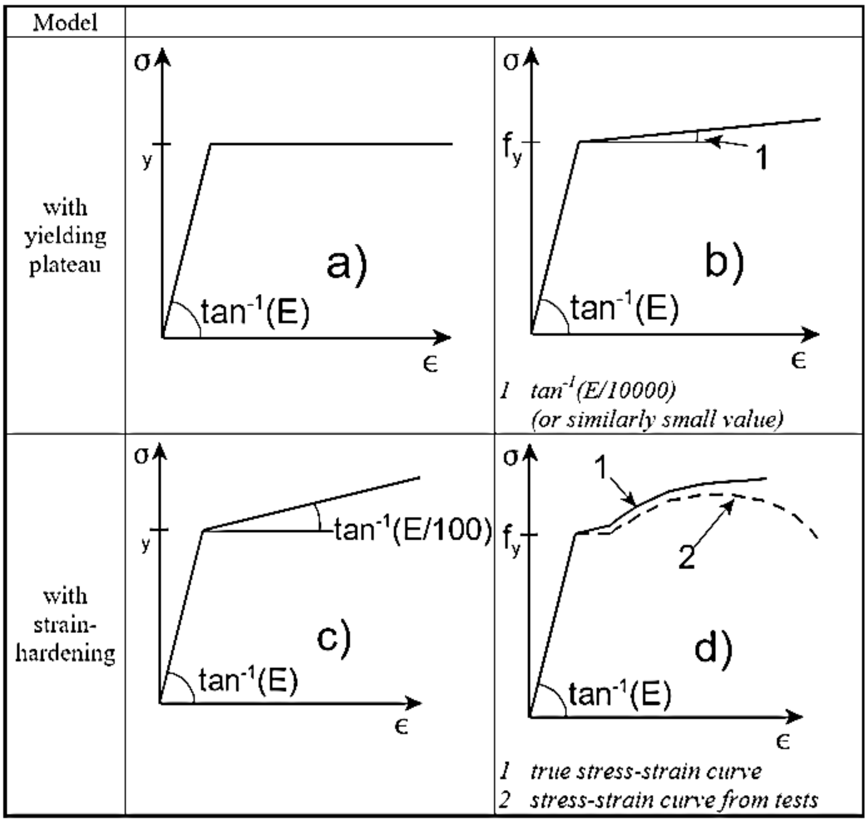

Figure 4: Stress-strain relationship for steel structures as given in EC-3, part 1-5 (figure C.2)

2.4.8 Analysis

Eurocode-4, S6.7.2 (1) specifies, design for structural stability shall take account of second-order effects, including residual stresses, geometrical imperfections, local instability, cracking of the concrete, creep and shrinkage of concrete, and yielding of structural steel and reinforcement.

EN 1993-1-5 (C6) also suggest that using FEM for design purpose should have to be done with special care in the modeling of structural components, boundary conditions, software, and documentation, use of imperfections, material properties, partial factors, modeling of loads and limit state criteria.

CHAPTER-3 Finite Element Analysis

3.1 Introduction

The finite element method or analysis is a numerical method applied in multi-physics problems with a sophisticated process of modeling, analysis, and visualizations. This method can be applied to problems with arbitrary geometry, non-homogeneous, and anisotropic materials to perform stress, thermal, fluid flow, and different other types of analyses. It also gives important solutions for problems of nonlinear fluid dynamics and plasticity in nonlinear solids with efficient considerations of boundary and loading conditions.

FEM is stabilized on the concept of dividing complicated systems into small manageable sections. Therefore, piecewise study is a crucial technique for FE analysis and it is performed by discretizing the geometry into small pieces called elements using a set of nodes. Although the FE analysis responds significantly to complex problems, it provides an approximate solution that might not have an exact value. Therefore, proper meshing and input data considerations are required in dealing with finite element modeling to obtain a valid result depending on the issue provided.

FE analysis widely deployed in engineering problems of mechanical, aerospace, thermal, and structural analysis using different simulation programs. Some general steps involved in FE analysis are presented in Figure 5, as summarized by Bathe (1996).

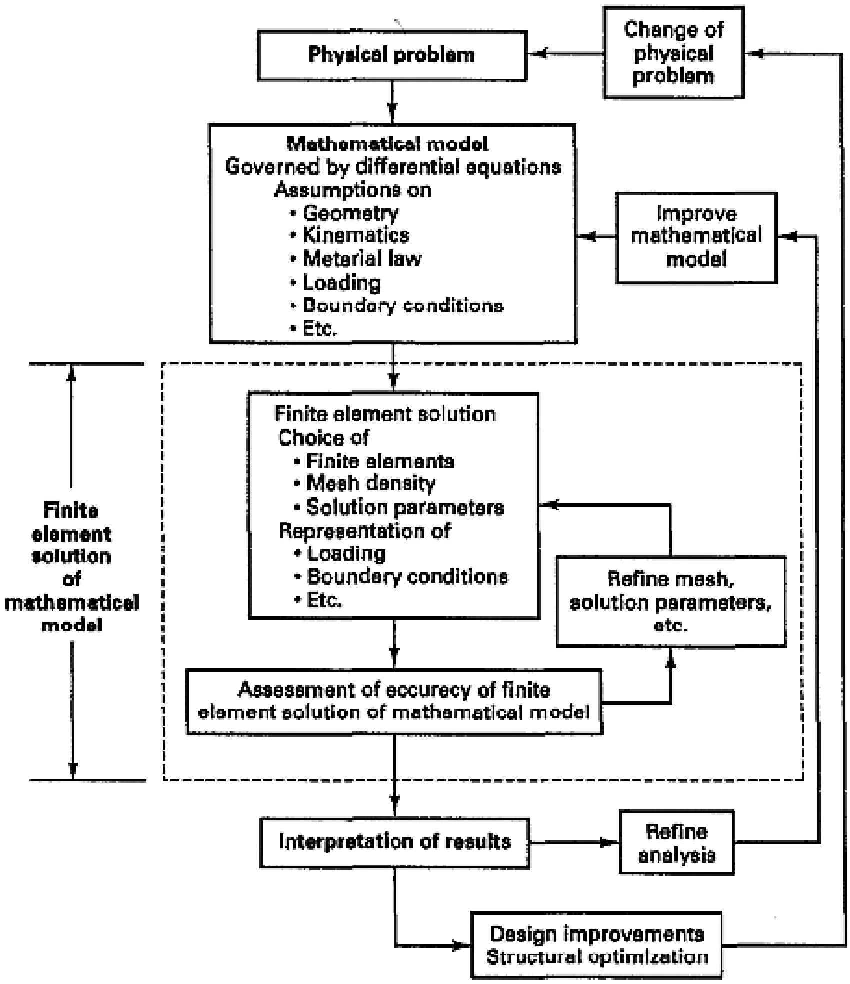

Figure 5: The process of finite element analysis

3.2 Considered finite element modeling techniques

This study uses finite element modeling software (ABAQUS/Standard version 6.18) for the simulations of required column tests. For each member, a linear analysis was primarily conducted on the external steel tube and followed by nonlinear analysis of the whole model. The linear analysis determined Eigen-modes for the application of geometrical imperfection in the structural system and managed through subspace Eigen-solver with a fixed number of three eigenvalues. Among the three possible Eigen-modes of the analysis results, the first mode was chosen by default, and its nodal displacements were used in the nonlinear analysis. It is also possible to use the second and the third modes; however, in short columns, modal variations are not such influential factors in predicting the axial force resistance of the column. Besides, slender members possibly develop single or double curvatures (bending) that strongly require detailed consideration of failure modes in the first linear analysis step. In the nonlinear analysis, a static general step was used with the Newton - Raphson method of an iterative procedure, and to reduce the analysis duration, job parallelization using multiprocessors was implemented.

In this chapter individual material characteristics, combined properties of steel and concrete, modeling techniques, and other required documents, which were used in the FE analysis of this study, are described in a very detailed and reasonable manner for both CFST and CFDCST columns.

3.2.1 Materials property

In the analysis of this study, Poisson's ratio was taken as 0.2 for un-cracked concrete and 0.3 for structural steel members. The mean value of inclination of the stress-strain curve of the steel was taken as 200,000 N/mm^2. Similarly, Hu et al. (2003) and Tao et al. (2013) adopted the same mean value of steel modulus of elasticity.

3.2.2 Imperfections

Structural steel or composite member's imperfection can be specified as a geometrical imperfection or imperfection results from residual stresses. Geometrical imperfections include a lack of verticality, straightness, and flatness. Residual stresses are either negative or positive stresses that remain in steel structure after uniform loading beyond the yield stress and result in plastic deformation. These stresses are also formed due to uneven heating and cooling of the structure. Tensile residual stresses develop a positive influence for a steel column in pure compression, while compressive residual stresses initiate premature yielding which results in a decrement in the structural member's capacity and stiffness.

The effect of residual stress is less likely to occur in hot rolled sections and imperfection in steel tubes can be reduced by the inside filled concrete. Similarly, concrete imperfection is not a significant problem as its effect could be reduced by the existence of evenly straightened steel tubes. The effect of imperfection in short columns would not be that much higher due to the occurrence of maximum cross-sectional capacity over the column's length and the existence of restricted boundary conditions. Therefore, in conducting nonlinear FE analysis of short CFST columns researchers like Tao et al. (2013) ignore the effect of global imperfections and residual stresses.

Nevertheless, the existence of geometric imperfection in CFSTs could rely on inaccuracies that occurred during the fabrication process of steel tubes. Lack of verticality may also arise during the erection process. This indicates that CFSTs or CFDCST member's imperfection may result due to structural steel imperfections. Therefore, geometrical imperfections are considered in this study and established in FE analysis.

3.2.2.1 A numeral expression for geometrical imperfections

Based on the European technical requirements, the executions of steel structures are specified on EN (2008). This requirement includes maximum levels for the fabrication tolerances such as a bow and local imperfection in which the extreme bow imperfection is allowed as L/750. However, the characteristic value of the geometrical imperfection used in most investigations corresponds to a mean imperfection of L/1000, which in turn corresponds to 75% of the recommended tolerance value of L/750 for steel columns (Jönsson and Stan, 2017). In the study conducted by Espinos et al.(2012) different values for the out-of-straightness of columns extended from L/2000 to L/500 were studied and it is recommended that values higher than L/500 should be avoided. Similarly, the value of L/1000 has been considered by many researchers (Espinos et al., 2012; Schaumann and Kleiboemer, 2012; Laim et al., 2012; Jönsson and Stan, 2017; Wan and Zha, 2016). In this paper also, geometrical imperfection is introduced as 75% of the recommended tolerance of EN1090-2 with a value of L/1000.

3.2.3 Steel-concrete interactions

The attached lateral surface of the concrete member and steel tube develops a rough interaction contact surface. The performance of this surface-to-surface interaction is more significant in the case of shear forces when one member slip over the other in which the separation of the interface occurred. However, for the applied axial loadings in the whole surface of short CFST or CFDCST column, both steel and concrete members develop interrelated axial translation results in a lower effect of the surface interaction. Lam et al. (2012) also suggested that short CFST columns are not highly affected by friction coefficient, as there is little or no slip between simultaneously loaded core and sandwich concrete surfaces. In the paper conducted by Goel and Tiwary (2018), the effect of steel and concrete interaction's coefficient was tested on a short CFST column (D114.3mm, T3.85mm, L300mm) in which the friction coefficients were varied from 0.05 to 0.5 and results showed almost no variation in the peak load capacity with an approximate value of 0.01% increment.

However, Eurocode-4 suggests a shear strength (τ_{RD}) value of 0.55 N/mm^2 in circular sections of the CFST columns. Based on finite element analysis made by Abdalla (2012) for CFST columns, tangential behavior was defined as a penalty with a friction coefficient of 0.3. Similarly, coefficients of 0.25, and 0.3 were also used by Schneider (1998), and Lam et al. (2012) respectively. Tao et al. (2013) adopt a 0.6 coefficient of friction between the steel tube and concrete.

As described earlier, the effect of steel-concrete interaction is not highly influential in the ultimate load-carrying capacity of the whole surface loaded short columns. However, there would be a strong impact on the column's response after the attainment of peak stress while the concrete starts crushing and possess slip over the steel tube. Therefore, in this FE analysis, a tangential contact behavior of the concrete and steel tube is considered as a value of 0.55 N/mm^2 for all CFST and CFDCSTs columns as suggested by the Eurocode-4. Hard contact behavior in the normal direction is also considered. In addition, concrete and steel surfaces were respectively defined in the ABAQUS program as 'slave' and 'master' surfaces based on the plasticity nature of the materials.

3.2.4 Meshes size and element type

In conducting FE analysis, the selection of mesh type and size has a tremendous contribution to the required results. The concept of finite element modeling depends on studying a small part of the given member by discretizing the geometry into small pieces called elements using a set of nodes. However, researchers like Hu et al. (2003) considered coarser meshes in their analysis based on the convergence study made by Wu (2000) stated that mesh refinement has very little influence on numerical results. But later on from sensitivity analysis, it is clearly shown that the finer the discretization the better the approximated results would be and the question becomes on how to measure mesh fineness. Tao et al. (2013) adopted an approximated mesh size of D/15 for CFST columns in the axial direction and 2.5 times that in the lateral direction. Espinos et al. (2012) use a maximum finite element size of 20mm based on results conducted on mesh sensitivity studies. In general, no rule has yet been established to set finer meshing; different researchers use different approaches, but they commonly adopt a very finer mesh for slave surface (concrete) and relatively increased mesh sizes for steel tubes to be defined as a master surface based on the ABAQUS program documentation.

Finite element models with better quality or finer meshing tend to develop excellent output results. However, the enlarged quantity of meshing rises the computational time and creates an obstacle in performing the required amount of analysis on time; the finer the meshing, the greater the numbers of equilibrium equations needed to be processed. Therefore, a compensating choice was made in the mesh adjustment of this study, and for concrete members in either CFST or CFDCST columns; an approximated element size of 5% and 7.5% of the overall column diameter was used along with the cross-sectional and longitudinal directions respectively. Similarly, 10% of the column's diameter was used as a mesh element size for the external steel tube (shell element). 7.5% and 10% of the column's diameter were also used for the inner steel tube (solid element) in CFDCST columns along with the cross-sectional and longitudinal directions respectively.

All the concrete models in this study were meshed based on a three-dimensional solid element (C3D8R element) available in the ABAQUS program library. This type of brick element modeling has eight nodes in each linear element and nodes are with three translational degrees of freedom. It also has to be clear that four nodded linear tetrahedron (C3D4) and six nodded linear triangular prism (C3D6) types of element modeling requires a finer mesh than that of C3D8, thus they were not chosen in this study. A sweeping technique with hex elemental shape was also used for the core and sandwiched concrete. The wedge element shape of the sweep technique was also used as a mesh control for core-concrete interior circular mesh portions. For external steel tubes, shell elements (S4R) were used with a reduced integration in 4-node linear geometric order and a sweep technique with quad-dominated element shape was assigned as a mesh control. For the internal steel tube in the CFDCST column, a three-dimensional solid element (C3D8R) was defined.

3.2.5 Boundary and loading conditions

To minimize the influence of end conditions, including local buckling of steel tube most researchers use end plates welded to both ends of a tube in the experimental tests of short CFSTs. It is also important for uniform load distribution along the whole section of the column. Researchers like Du et al. (2018) also use highly ridged endplates in conducting FE analysis to idealize the real scenario of experimental tests of short CFSTs. However, in finite element modeling, it is not mandatory to use plates; top and bottom surfaces can be tied and constrained at a certain reference point to act similarly to that of the experimental tests. It is also advantageous in saving analysis time and complexity that occurred in modeling related to surface-to-surface interactions. Tao et al. (2013) also state that FE analysis fixed at both top and bottom surfaces except the displacement at the loaded end would have a similar result to that obtained from the model with endplates.

In this study, the bottom and top surfaces of steel tubes and concrete were fixed against all degrees of freedom except for the top surface displacement toward the loading direction. In the load controlled first step linear analysis, compression, or axial point loading was applied at a central reference point where all top surface nodes were constrained. The nonlinear analysis was displacement controlled conditions and 1mm axial displacement allowed per unit time.

3.2.6 Stress and strain relationship of steel

The stress-strain relationship of a steel tube property in the FE analysis shall have to be chosen depending on the allowable strain state required to be involved in a relationship with the real situation. Therefore, in the CFST columns of this study, the bilinear elastic-plastic stress-strain curve with linear strain-hardening is used in defining the material property of the steel tube. This typical stress-strain curve can be considered for the precise simulation of steel's behavior; it consists of linear elastic and nonlinear plastic sections with a slope of E (steel modulus of elasticity) and E/100 respectively. Similarly, Jönsson and Stan (2017) and Pagoulatou et al. (2014) adopt the same technique according to EC-3.

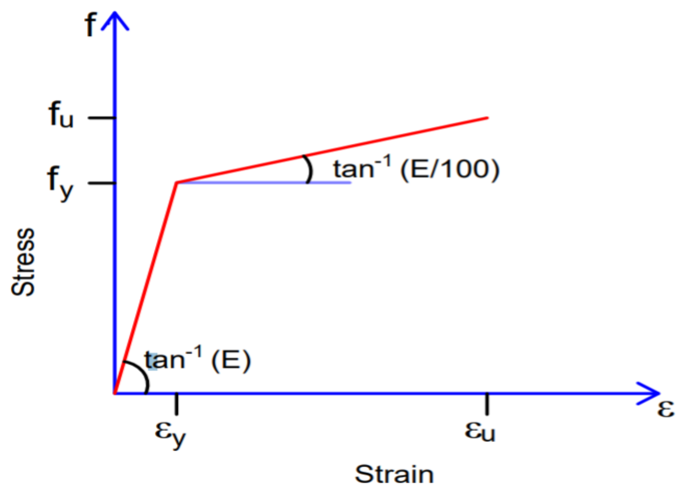

Figure 6: Stress-strain relations of structural steel tube in CFST columns

In this study, the ultimate strength of the steel is computed based on the equations proposed by Tao et al. (2013) for yield strength between 200 MPa and 800 MPa.

$$f_u = \begin{cases} \left(1.6 - 2 * 10^{-3}(f_y - 200)\right) f_y & 200\text{MPa} \le f_y \le 400\text{MPa} \\ \left(1.2 - 3.75 * 10^{-4}(f_y - 400)\right) f_y & 400\text{MPa} < f_y \le 800\text{MPa} \end{cases} \quad (12)$$

Where:-

f_y: Yield strength of structural steel

f_u: Ultimate strength of structural steel

For the external steel tube of a CFDCST column, the bilinear elastic-plastic stress-strain curve was used as shown in figure 7 (a) similar to the consideration made in CFST columns. Nevertheless, for the internal steel tube, an elastic-plastic stress-strain relationship with a nominal plateau slope as shown in figure 7 (b) was accepted. The internal steel tube's plastic nature is mainly restricted by the adjoining effect of the core and sandwich concrete. Therefore, a nominal plateau slope is considered, as it tends to develop a controlled strain state during axial loadings.

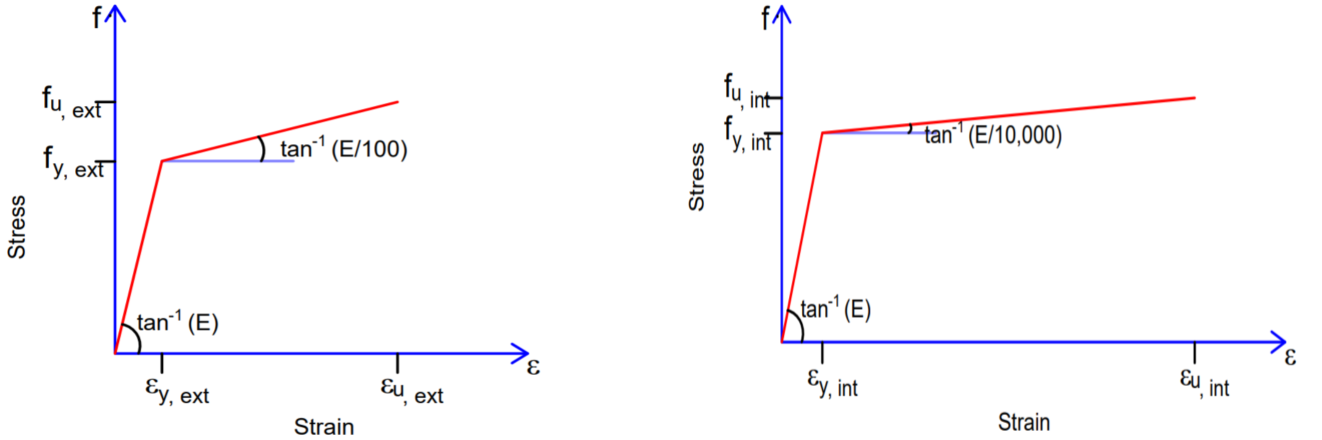

(a) Elastic-plastic with linear strain hardening (b) Elastic-plastic with a nominal plateau slope

Figure 7: Stress-strain relations of external and internal steel tubes in CFDCST columns

The ultimate strength of the steel tubes in CFDCST columns could also be found from the equation given by Tao et al. (2013) for both external and internal steel tubes.

$$f_{u,ext\,(int)} = \begin{cases} \left(1.6 - 2 * 10^{-3}\left(f_{y,ext\,(int)} - 200\right)\right) f_{y,ext\,(int)} & 200\text{MPa} \le f_{y,ext\,(int)} \le 400\text{MPa} \\ \left(1.2 - 3.75 * 10^{-4}\left(f_{,ext\,(int)} - 400\right)\right) f_{y,ext\,(int)} & 400\text{MPa} < f_{,ext\,(int)} \le 800\text{MPa} \end{cases} \quad (13)$$

Where:-

$f_{y,ext\,(int)}$: Yield strength of external or internal steel tube of CFDCST column

$f_{u,ext\,(int)}$: Ultimate strength of external or internal steel tube of CFDCST column

3.2.7 Concrete damage plasticity model key parameters

Concrete plasticity models idealize the concrete nonlinear behavior in the ABAQUS program using different techniques including Ducker-Prager (DP) and concrete damage plasticity models. The DP model was developed as a generalization of the Mohr-Coulomb criterion for soils by Drucker and Prager in 1952 and the three-dimensional pressure-dependent model was used as a failure criterion for estimating the stress state. Beyond its prior application on soils, especially for stiff clays with low friction angles, this model was also used to describe pressure-sensitive materials such as rock and concrete. However, this criterion results in errors with the increment in the confining pressure (Alejano Leandro, 2012). Therefore, this model had extended to the modified Drucker-Prager (MDP) model that is used to idealize the stress-strain behavior of confined concrete and further the concrete damage plasticity (CDP) model currently developed and become popular in modeling the stress-strain relationship of unconfined, and confined concrete. The CDP has dominantly become one of the potential models to predict the performance of concrete. CDP is importantly used for modeling concrete and quasi-brittle materials in different types of structures. The CDP model requires compressive and tensile characteristics of concrete together with some input parameters. These parameters are in form of dilation angle, eccentricity, viscosity, and concrete fracture energies, and they are calibrated to develop modeling strategies of concrete. Moreover, the tensile and compressive behavior of concrete describes the concrete's manner by presenting scalar damage values. These damage values are conversely sub-options and possible to left the requirement unfilled to get the program's calculation. Concrete damage plasticity key parameters are discussed below.

<u>Dilation angle (ψ)</u>: (Internal friction angle)

Dilation angle (ψ) is importantly used to define plastic flow potential in the allowed values of $0^{\circ} < \psi \leq 56^{\circ}$ in ABAQUS FE analysis. Besides, in the consideration of in-plane concrete, this parameter has a relationship with the steel confinement capacity; as the confinement factor increases, the dilation angle will be reduced. The dilation angle is computed in this paper based on the formulation presented by Tao et al. (2013) as a function of confinement factor (ξ_c) as shown below. In addition, it is found to have a great influence in determining the ultimate load-carrying capacity of the column.

For CFST columns:

$$\psi = \begin{cases} 56.3(1-\xi_c) & \text{for } \xi_c \leq 0.5 \\ 6.672e^{\frac{7.4}{4.64+\xi_c}} & \text{for } \xi_c > 0.5 \end{cases} \tag{14}$$

$$\xi_c = \frac{A_s f_y}{A_c\, f_c'} \tag{15}$$

Where:-

ξ_c: Confinement factor

A_c and A_s: Area of concrete and steel cross-sections

f_c': Compressive cylinder strength of concrete

f_y: Yield strength of structural steel

Equation (14) is further used to describe the CFDCST column's dilation angle with the consideration of equivalent confinement factor ($\xi_{c,eqv}$) in place of the confinement factor (ξ_c).

$$\xi_{c,eqv} = \frac{A_{s,ext} * f_{y,ext} + A_{s,int} * f_{y,int}}{A_{c,sw}\, f_{c,sw}' + A_{c,core}\, f_{c,core}'} \tag{16}$$

Where:-

$\xi_{c,eqv}$:	Equivalent confinement factor
$A_{c,ext}$, $A_{s,int}$:	Area of external and internal steel tube cross-sections
$f_{c,sw}'$, $f_{c,core}'$:	Compressive cylindrical strength of sandwich and core concrete
$f_{y,ext}$, $f_{y,int}$:	Yield strength of external and internal steel tubes

Determination of f_{bo}/f'_c: Based on the ABAQUS documentation 'f_{bo}/f'_c' is defined as "the ratio of initial equi-biaxial compressive yield stress to initial uniaxial compressive yield stress." Following the expression used by Papanikolaou and Kappos (2007), f_{bo}/f_c' is determined as follows.

For CFST columns

$$\frac{f_{bo}}{f_c'} = 1.5(f_c')^{-0.075} \tag{17}$$

In addition, it has been noted that the ultimate strength will increase slightly if a larger value of $\frac{f_{bo}}{f_c'}$ is used.

For CFDCST columns similar technique as in the case of equation (17) could be used with the replacement of cylindrical core concrete strength (f_c') with either sandwich or core concrete strength $\left(f_{c,sw(core)}'\right)$.

Determination of K_c: In according to the ABAQUS documentation " K_c" is described as "The ratio of the second stress invariant on the tensile meridian to that on the compressive meridian at initial yield for any given value of the pressure invariant such that the maximum principal stress is negative" and it must satisfy the condition of $0.5 < k_c \leq 1$.

The value of K_c was also expressed by Tao et al. (2013) to be within the range of 0.703 and 0.725 as the concrete strength reduced from 100MPa to 30MPa.

$$K_c = \frac{5.5}{5 + 2(f_c')^{0.075}} \quad (18)$$

However, some researchers adopted a fixed value of K_c equals to 2/3, which is also the default value in the ABAQUS program. Highly increased value of K_c weakens the post yielding behavior of concrete and lower assumptions tend to strengthen the entire system response. In relating to this, a rough validation was made in this study and it is found that, the value of K_c within the range of 0.71 and 0.689 shows good results for normal grade concrete strength. Therefore, a 2% decrement in the value of K_c from equation (18) is made and the formulation is rearranged as follows.

For CFST columns

$$K_c = \frac{5.39}{5 + 2(f_c')^{0.075}} \quad (19)$$

Similarly, in the case of CFDCST columns, equation (19) could be used to determine 'K_c' using the sandwich or core cylindrical concrete strength $\left(f'_{c,sw(core)}\right)$.

<u>Flow potential eccentricity (e)</u>: In according to the ABAQUS documentation, eccentricity is described as "a small positive number that defines the rate at which the hyperbolic flow potential approaches its asymptote." It can also be calculated as the ratio of the tensile strength to the compressive strength and it alters the shape of the plastic potential curve in the meridional plane. Zero eccentricity produced a straight line corresponding to the Drucker-Prager criterion. In this study, a constant value of 0.1 is considered; which is also the default value in the ABAQUS program.

<u>Viscosity Parameter</u>: used in visco-plastic regularization

A value of viscosity parameter equal to 0.0001 is adopted in this analysis referring to the works of Michał and Andrzej (2015) in which varied viscosity parameters ranged from 0 through 0.0001, 0.001 to 0.01 were tested. And it is found that for the viscosity parameter equal to 0.0001 a constant damage zone width was observed for all FE discretization.

3.2.8 Tensile behavior of concrete

For concrete stress-strain relationship under tension, various kinds of numerical equations were developed. Ellobody and Young (2010) projected that the stress-strain behavior in uniaxial tension follows a linear elastic relationship up until the value of the failure stress.

In this paper tensile stress-strain ($\sigma - \varepsilon$) relationship is assumed to be linear until the uniaxial tensile strength reaches the failure stress. The relationship after the failure peak limit is also expressed using the exponential function as shown in equation (20) in referring to the work of Dere and Koroglu (2017). The value of uni-axial tensile strength failure stress (f_t) is determined using equation (21), as considered in the Eurocode-2 for nominal concrete grades.

For CFST columns

$$\sigma = f_t \left(\frac{\varepsilon_t}{\varepsilon}\right)^{0.7+1000\varepsilon}, \text{where } \varepsilon_t = \frac{f_t}{E_{cm}} \tag{20}$$

$$f_t = 0.3 * (f_c')^{\frac{2}{3}} \tag{21}$$

Where:-

f_t: Mean uniaxial ultimate tensile strength

ε_t: Strain at the ultimate uniaxial tensile strength

E_c: Modulus of elasticity

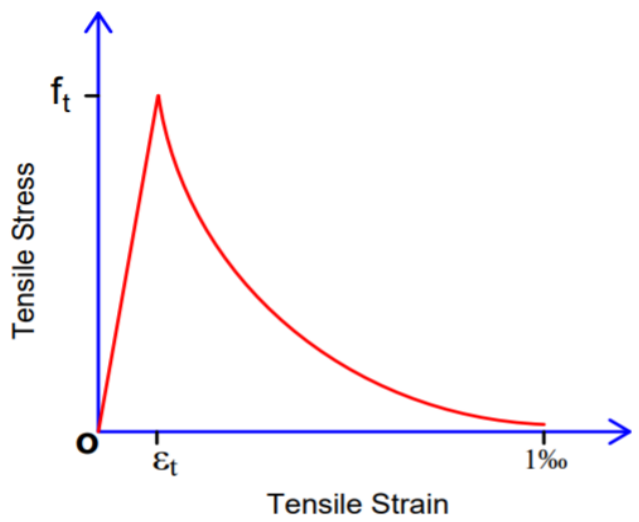

Figure 8: Tensile stress-strain relation of concrete

For CFDCST columns

$$\sigma_{sw} = f_{t,sw}\left(\frac{\varepsilon_{t,sw}}{\varepsilon_{sw}}\right)^{0.7+1000\varepsilon_{sw}} \quad \text{, where } \varepsilon_{t,sw} = \frac{f_{t,sw}}{E_{cm,sw}} \quad \text{and} \quad f_{t,sw} = 0.3 * \left(f'_{c,sw}\right)^{\frac{2}{3}} \tag{22}$$

$$\sigma_{core} = f_{t,core}\left(\frac{\varepsilon_{t,core}}{\varepsilon_{core}}\right)^{0.7+1000\varepsilon_{core}} \text{, where } \varepsilon_{t,core} = \frac{f_{t,core}}{E_{cm,core}} \quad \text{and} \quad f_{t,core} = 0.3 * \left(f'_{c,core}\right)^{\frac{2}{3}} \tag{23}$$

Where:-

$f_{t,sw}$ and $f_{t,core}$: Mean uniaxial ultimate tensile strength of sandwich and core concrete

$\varepsilon_{t,sw}$ and $\varepsilon_{t,core}$: Sandwich and core concrete strain at the ultimate uniaxial tensile strength

$E_{cm,sw}$ and $E_{cm,core}$: Modulus of elasticity of sandwich and core concrete respectively

3.2.9 Stress-strain relationship of concrete under axial compression

In axially loaded CFST short columns, the response developed by the dual action of steel and concrete materials results in a higher stiffness of the structure due to the effect of confinement. This is also the most desired and effective response of a short CFST column, in which the stress capacity of the concrete core gets modification in strength. The hoop stress developed by the steel imposes confinement (belt) toward the bulging concrete and for the applied axial force; a triaxial state of stresses would be formed in the core concrete. This scenario simply refers to the lateral confinement effect in which unconfined concrete gets modification in its strength. Similarly, the steel tube abstains from having inward buckling, and this restriction delays the steel from getting its ultimate load capacity earlier.

However, an enhancement in the concrete strength shall only be considered for short columns depending on their relative slenderness ratios. Short columns have such property to reach ultimate plastic resistance without buckling elastically. Unlike this, slender columns will buckle elastically in which the dual effect of the materials would have a different perspective. Therefore, Eurocode-4 applies modification for short columns with relative slenderness below a value of 0.5. Concerning the lateral confinement effect of short columns, different scholars have presented numerical suggestions and conduct experimental studies.

The effects of confinement and relative slenderness ratios are more related issues in the applications of axial loading; the shorter the column the more the effect of confinement would be. Short columns tend to crash without buckling or bending due to the comparatively larger diameter to height ratios. In such columns under axial compression, the expanding concrete core will be restricted from early bulging out and this effect importantly develops modification in the stress-strain relationship of the core concrete.

3.2.9.1 Studies on the confined concrete stress-strain relationship

To include strength modification in the core concrete due to the formation of confinement, different methodologies were conducted by researchers. An active hydrostatic fluid pressure confined stress-strain relationship was previously described by Mander et al. (1988) using the following equations.

$$f'_{c,c} = f'_{co} + k_1 f_1 \quad (24)$$

$$\varepsilon_{c,c} = \varepsilon_{co}\left(1 + k_2\left(\frac{f_1}{f'_c}\right)\right) \quad (25)$$

Where:

- $f'_{c,c}$: Maximum concrete stress
- $\varepsilon_{c,c}$: Maximum corresponding strain at $f'_{c,c}$
- f_1: Lateral fluid pressure
- f'_{co}: Unconfined concrete strength
- ε_{co}: Unconfined concrete strain
- k_1 and k_2: Coefficients that are functions of the concrete mix and the lateral pressure

The mean values of coefficients k_1 and k_2 found by Richart et al. (1928) as 4.1 and $5k_1$ respectively. The model presents in figure (9) expresses how the lateral confining pressure affects the ultimate compressive strength of confined concrete.

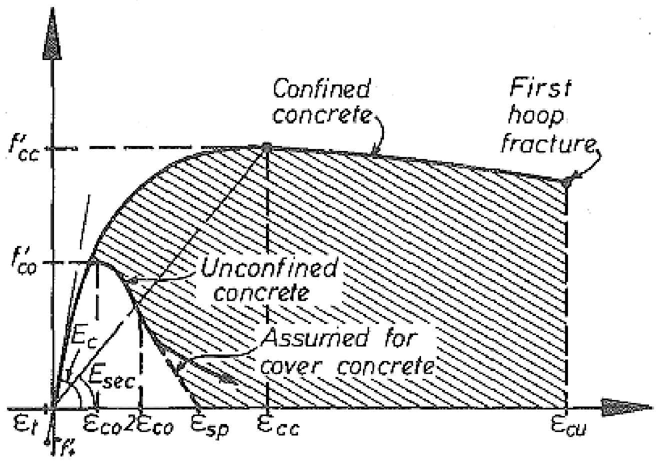

Figure 9: Stress-strain model of unconfined and confined concrete (Mander et al., 1988)

In the above-considered techniques of modifying the concrete's strength, the lateral confinement of CFST sections was defined and implemented as active confinement, but the actual case in the concrete-filled steel tubes is gradual or loading time-based confinement effect termed as passive confinement. Richart et al. (1929) projected that the lateral pressure of active confinement is approximately considered the same as the equivalent lateral pressure of the passive confinement of closely spaced spiral steels. And this situation has currently been studied by some authors. The works of Zhao et al. (2018) can be mentioned in discussing this situation by studying the effect of the loading path and formulate an equation depending on the regression analysis of selected test results.

$$f'_{c,c} = f'_c + 2.2 {f'_c}^{0.3} \sigma_{ru}^{0.81} \quad \ldots\ldots\ldots \text{ Zhao et al. (2018)} \tag{26}$$

Note that σ_{ru} can be used interchangeably with f_1 in expressing the confining pressure and f'_c can be taken as f'_{co}.

But this work was conducted by applying loads only on the concrete core. Later on, the paper published by Lin et al. (2018) discussed the stress path effect and provided the following equation with some extensions from Zhao et al. (2018) through applying load in the whole section of the steel and concrete core area.

$$f'_{c,c} = f'_c + 2.2\lambda {f'_c}^{0.3} \sigma_{ru}^{0.81} \quad \ldots\ldots\ldots \text{ Lin et al. (2018)} \tag{27}$$

$$\lambda = \begin{cases} 0.66\eta^{0.52} & , 0 \le \eta < 2.223 \\ 1.0 & , \eta \ge 2.223 \end{cases} \quad , \quad \eta = \frac{2t * f_y}{(D - 2t) * f'_c} \tag{28}$$

Where:-

σ_{ru}: Confining pressure around a concrete core

Besides the above-mentioned stress-strain model, Tao et al. (2013) develop a new technique in which the peak stress in the core concrete developed by the effect of confinement considered in the finite element simulation as it is captured by the steel-concrete interaction with a continuous strain hardening stage after the unconfined concrete peak stress.

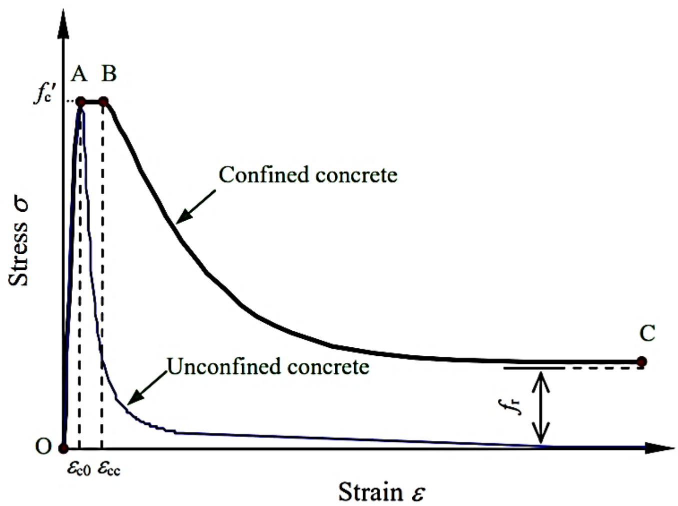

Figure 10: Stress-strain model of unconfined and confined concrete (Tao et al. (2013)

3.2.9.2 Proposed CFST short column's strain hardening/softening rule under compression

The passive nature of confinement is considered under this study and modification on stress-strain curves of concrete is made for the increase in strength and ductility performance. Regarding this, the stress-strain relationship of a short CFST column is presented as follows with some revised features and considerations from the initial suggestion of Tao et al. (2013) strain hardening or softening rule.

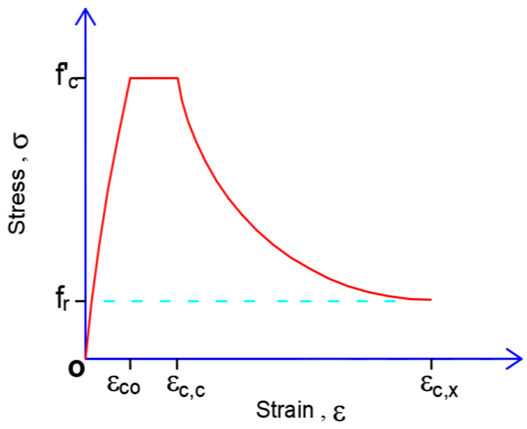

Figure 11: Stress-strain model of confined concrete in CFST columns

I. <u>First stage:</u> $(0 \leq \varepsilon \leq \varepsilon_{co})$

In the first phase of the initial loading, there is negligible interaction between the concrete core and the steel tubes up until the concrete reaches its maximum capacity before the encasement of the steel tube is initiated. Therefore, the compressive stress and shortening strain data can be considered similar to the unconfined concrete in using the equation recommended by EN 1992-1-1:2004 as shown in equation (29):

$$\sigma = f'_c\left(\frac{k * \eta - \eta^2}{1 + (k-2) * \eta}\right) \tag{29}$$

Where:

$$\eta = \frac{\varepsilon}{\varepsilon_{co}} \tag{30}$$

$$k = 1.05 * E_{cm} * \frac{\varepsilon_{co}}{f'_c} \tag{31}$$

The value of ε_{co} is determined using the equation developed by De Nicolo et al. (1994):

$$\varepsilon_{co} = 0.00076 + \sqrt{(0.626f'_c - 4.33) * 10^{-7}} \tag{32}$$

$$E_{cm} = 4700\sqrt{f'_c} \text{ and } (f'_c \text{ and } E_{cm} \text{ in MPa}) \quad \ldots \text{Empirical equation (ACI 1999)} \tag{33}$$

Inelastic strain could also be found using the simplified equation presented by Hafezolghorani (2017) as shown below

$$\varepsilon_c{}^{in} = \varepsilon - \frac{\sigma}{E_{cm}} \tag{34}$$

Where: $\varepsilon_c{}^{in}$: Inelastic hardening strain in compression

II. <u>Second stage:</u> $(\varepsilon_{c,0} \leq \varepsilon \leq \varepsilon_{c,c})$

The second stage is considered as strain increment without stress softening in which the maximum strength of the concrete is sustained. This method is primarily presented by Tao et al. (2013) as "any strength increase of concrete from confinement will be captured in the simulation through the interaction between the steel tube and concrete." Therefore, in this stage, the basic aspect is to determine the maximum strain ($\varepsilon_{c,c}$) at which the ultimate compressive strength of concrete reaches its limit before the stress softening point.

To follow the equation of confined concrete stress under passive confining pressure, it is required to formulate an equation of the corresponding strain. Therefore, based on some numerical assumptions, the equation for strain at ultimate confining stress is proposed as shown below.

In this study, the general equations proposed by Mander et al. (1988) for active confinements are importantly used and it is further modified to represent the passive confinement nature of CFSTs.

Equation (24) can be rearranged as follow

$$f_1 = \frac{f_{c,c} - f'_{co}}{k_1} \tag{35}$$

The peak strain expressed in equation (25) for the extended maximum concrete strength at the ultimate load-carrying capacity of the column can be rearranged as follows using equation (35).

$$\varepsilon_{c,c} = \varepsilon_{co}\left(1 + \frac{k_2}{k_1}\left(\frac{f_{c,c} - f'_c}{f'_c}\right)\right) \tag{36}$$

The lateral confinement of CFSTs is defined and implemented in this paper as gradual confinement resulting in a passive confinement idealization. Therefore, equation (27) as proposed by Lin et al. (2018) through applying load in the whole section of the steel and concrete core is used in this paper.

Substituting, equation (27) into (36) and let the constant for $\frac{k_2}{k_1} = k$, results

$$\varepsilon_{cc} = \varepsilon_{co}\left(1 + k\left(\frac{2.2\lambda {f'_c}^{0.3} f_1^{0.81}}{f'_c}\right)\right) \tag{37}$$

The lateral confining pressure (f_1) is also determined using the equation proposed by Hu et al. (2003)

$$f_1 = \begin{cases} f_y\left(0.043646 - 0.000832\left(\frac{D}{t}\right)\right) \text{for } 21.7 \leq \frac{D}{t} \leq 47 \\ f_y\left(0.006241 - 0.0000357\left(\frac{D}{t}\right)\right) \text{for } 47 \leq \frac{D}{t} \leq 150 \end{cases} \quad (38)$$

In this study for some D/t ratios that are lower than 21.7, similar equations were used as conducted above in equation (38) for the range between 21.7 and 47 to obtain an approximate result under the limit given by Hu et al. (2003).

Solving for ‘k’:

$$k = \frac{\left(\frac{\varepsilon_{cc}}{\varepsilon_c}\right) - 1}{\left(\frac{2.2 * \lambda * {f'_c}^{0.81}}{{f'_c}^{0.7}}\right)} \quad (39)$$

In using twenty-three actively confined concrete experimental tests where the value for ‘λ’equals to 1, the average value of ‘k’ is approximately found to be 3.4156. Therefore, equation (37) can be reduced as shown below:

$$\varepsilon_{cc} = \varepsilon_{co}\left(1 + \left(\frac{7.514\lambda f_1^{0.81}}{{f'_c}^{0.7}}\right)\right) \quad (40)$$

Reference	Experimental Results						Proposed Equation	$\frac{\text{Suggested } \varepsilon_{cc}}{\text{Experimental } \varepsilon_{cc}}$
	Test data of actively confined concrete							
	Dimensions	f_c (MPa)	ε_c (%)	f_1 (MPa)	f_{cc} (MPa)	ε_{cc} (%)	$\varepsilon_{cc} = \varepsilon_c(1 + 7.514(\frac{f_1^{0.81}}{f_c^{0.7}}))$	
Candappa et al. (2001)	Dia=98mm, L=200mm	41.9	0.24	4	66.6	**0.87**	**0.65**	0.74
		41.9	0.24	8	85.1	**1.25**	**0.95**	0.76
		41.9	0.24	8	85.4	**1.05**	**0.95**	0.91
Imran and Pantazopoulou (1996)	Dia=54mm, L=115mm	47.4	0.28	2.15	57.7	**0.43**	**0.54**	1.26
		47.4	0.28	4.3	67.3	**0.69**	**0.74**	1.07
		47.4	0.28	8.6	83.6	**1.46**	**1.09**	0.74
		43.11	0.25	2.15	46	**0.43**	**0.50**	1.16
		43.11	0.25	4.3	53.5	**0.65**	**0.69**	1.06
		43.11	0.25	8.6	73	**1.66**	**1.02**	0.61
		28.62	0.26	1.05	33.6	**0.47**	**0.45**	0.97
		28.62	0.26	2.1	36.4	**0.675**	**0.60**	0.89
		28.62	0.26	4.2	48.1	**1.385**	**0.86**	0.62
		28.62	0.26	8.4	65.2	**2.375**	**1.31**	0.55
Jemet et al. (1984)	Dia=110mm, L=220mm	31.43	0.369	3	45.13	**0.697**	**0.97**	1.40
Sfer et al. (2002)	Dia=150mm, L=300mm	35.8	0.2	1.5	45.5	**0.26**	**0.37**	1.43
		35.8	0.2	1.5	47.8	**0.34**	**0.37**	1.09
		35.8	0.2	4.5	55.3	**0.41**	**0.62**	1.50
		35.8	0.2	4.5	58.2	**0.52**	**0.62**	1.18
		35.8	0.2	9	65.7	**0.83**	**0.93**	1.12
		35.8	0.2	9	66.5	**0.63**	**0.93**	1.47
Smith et al. (1989)	Dia=54mm, L=108mm	34.5	0.351	0.69	41.73	**0.397**	**0.51**	1.30
		34.5	0.351	3.45	57.81	**0.838**	**0.95**	1.14
		34.5	0.351	6.89	78.21	**1.158**	**1.41**	1.22
							Mean	**1.05**
							Standard Deviation	**0.28**

Table 2: Suggested strain equation results and experimental findings on actively confined concrete

III. <u>Third stage:</u> $\varepsilon_{c,c} \leq \varepsilon \leq \varepsilon_{c,x}$

This stage is a softening portion with increased ductility resulting from the confinement effect and the stress equation for this portion formulated by Binici B (2005) as shown in equation (41) and it is directly used in this paper.

$$\sigma = f_r + (f_c' - f_r) * \exp\left(-\left(\frac{\varepsilon - \varepsilon_{c,c}}{\alpha}\right)^{\beta}\right) \quad (41)$$

Tao et al. (2013) also presents an equation for the residual stress and determine parameters of α, β for circular CFSTs columns as follows

$$f_r = 0.7 * \left(1 - e^{-1.38\xi_c}\right) f_c' \leq 0.25 f_c' \quad (42)$$

$$\alpha = 0.04 - \left(\frac{0.036}{1 + e^{6.08\xi_c - 3.49}}\right), \beta = 1.2\, , \xi_c = \frac{As * fy}{Ac * f'_c} \quad (43)$$

3.2.9.3 Proposed CFDCST short column's strain hardening/softening rule under compression

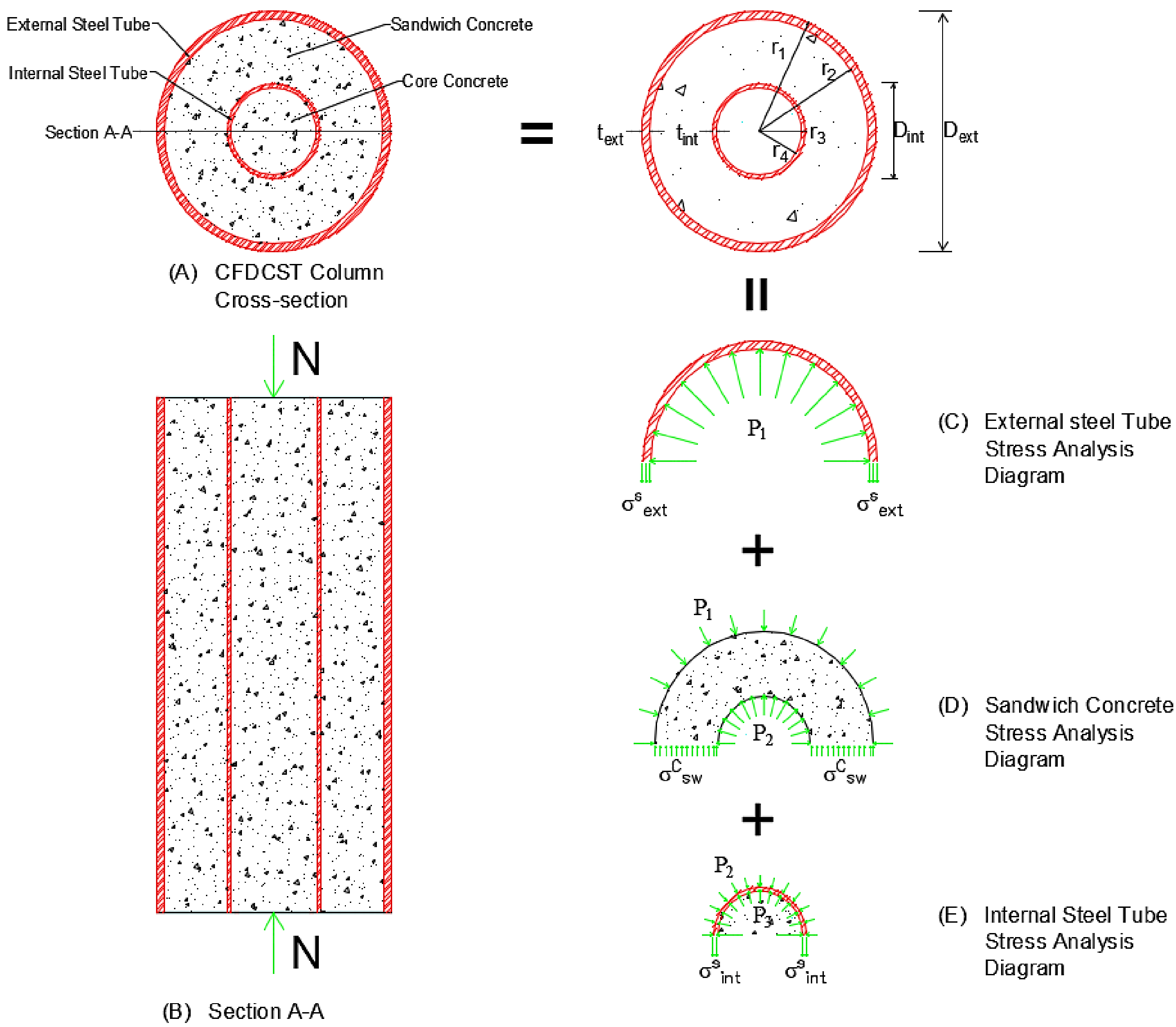

Figure 12: Stress analysis diagram of a CFDCST column

Three mechanical equilibrium equations can be set by taking half-sectional steel tube stress relation as shown below.

- ✓ External steel tube stress equation

$$2\sigma^{s}{}_{ext}(r_1 - r_2) = 2P_1(r_2) \quad \text{…… … Referring to Figure 12: (C)} \tag{44}$$

$$\text{Therefore:} - \; P_1 = \frac{\sigma^{s}{}_{ext}(r_1 - r_2)}{r_2} \tag{45}$$

Where:-

P_1: Lateral pressure of the interface between sandwich concrete and external steel tube

r_1: Outside radius of external steel tube

r_2: Inside radius of external steel tube

$\sigma^s{}_{ext}$: Lateral stress of external steel tube

Similar to the case in CFST columns, the external steel tube lateral confinement (P_1) can be found based on the works of Hu et al. (2003) as shown in equation (38) using the properties of an external steel tube of a CFDCST column.

- ✓ Sandwich concrete stress equation

$$2\sigma^c{}_{sw}(r_2 - r_3) + 2P_2r_3 = 2P_1r_2 \quad \ldots\ldots\ldots \text{ Referring to Figure 12: (D)} \tag{46}$$

$$\therefore\ P_2 = \frac{P_1r_2 - \left(\sigma^c{}_{sw}(r_2 - r_3)\right)}{r_3} \tag{47}$$

Where:-

P_2: Lateral pressure of the interface between sandwich concrete and internal steel tube

r_3: Outside radius of internal steel tube

$\sigma^c{}_{sw}$: Lateral stress of sandwich concrete

But in the consideration of a very small value of annular stress of concrete ($\sigma^c{}_{sw}$) approximated to 0% contribution, equation (47) could be rearranged as follow:

$$P_2 = \frac{P_1r_2}{r_3} \tag{48}$$

- ✓ Internal steel tube stress equation

$$2\sigma^s{}_{int}(r_3 - r_4) + 2P_2r_3 = 2P_3r_4 \quad \ldots\ldots\ldots \text{ Referring to Figure 12: (E)} \tag{49}$$

$$\therefore\ P_3 = \frac{(\sigma^s{}_{int}(r_3 - r_4)) + P_2r_3}{r_4} \tag{50}$$

Where:-

P_3: Lateral pressure of the interface between core concrete and internal steel tube

r_4: Inside radius of internal steel tube

$\sigma^s{}_{int}$: Lateral stress of internal steel tube

$f'_{cc}, P_1, P_2, P_3, f'_c$ are in MPa

Therefore p_3 can be reduced with the replacement of equation (48) in to (50)

$$P_3 = p_3{}' + \frac{P_1 r_2}{r_4} \quad , \text{where } p_3{}' = \frac{(\sigma^{s}{}_{int}(r_3 - r_4))}{r_4} \tag{51}$$

Similar to the external steel tube lateral confinement (P_1), the internal steel tube pure lateral confinement ($p_3{}'$) can be found using the internal steel tube properties.

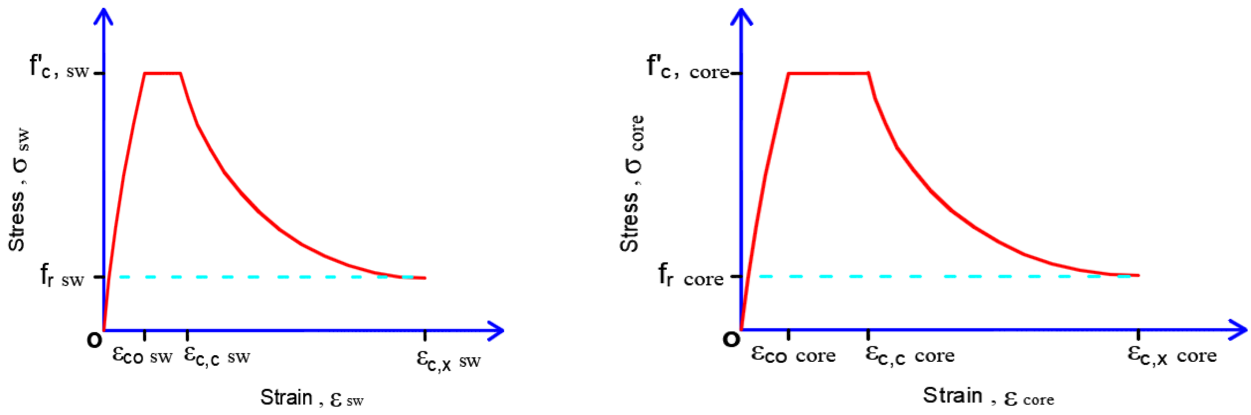

(a). Sandwiched concrete (b). Core concrete

Figure 13: Stress-strain model of confined concrete for CFDCST column

Note: Appendix A and B of this paper may be referred for detailed equations on the three stages of strain hardening/softening rule of sandwiched and core concrete.

CHAPTER-4 Verification Study

Most of the basic FE modeling techniques used in this study were first introduced and verified by different researchers including Hu et al. (2003) and Tao et al. (2013). However, there are some newly suggested and rearranged techniques on both CFST and CFDCST columns, which require further verification. Therefore, eleven test specimens were selected and modeled under concentric axial compression loadings. Seven experimental tests having different D/T ratios were chosen to validate the proposed assumptions made on CFST columns and to examine the proposed FE modeling techniques of CFDCST columns, four experimental tests were selected which are with varied internal steel tube diameter and strength. All of these experimental tests were short columns in which the effect of steel tube confinement is visible and a mode of failure in all such cases was a crushing failure due to the applied axial loading with the expansion of local buckling.

In this FEM based computer simulation, exactly similar techniques were applied for all specimens using the ABAQUS (2018) software program. Axial force resistance and load-displacement curves of selected experimental tests were used to validate the suggestions made in this FE analysis. At each FE model analysis, a point load was exerted at a node on the top reference point. The bottom surface was kept fixed and the top part was restrained in all directions except the translation in the longitudinal direction of the specimen. Instead of plate insertion, the simulations were also carried with restricted boundary conditions. Similarly, the experimental tests were made in a fully restrained condition where plates were used and welded in the top and bottom surfaces of the specimens.

In all cases, force-controlled linear analysis of the external steel tube was primarily simulated and followed by displacement controlled general step non-linear analysis of the whole members. In most cases, the analysis was conducted until the axial displacement reaches 5% of the strain with a rate of 1mm per unit of time.

4.1 Selected experimental tests of CFST and CFDCST short columns

To make this section more convenient, seven experimental tests of CFST columns are chosen from published papers, which were conducted by four different authors. The selected test specimens have a wide range of steel tube diameter to thickness (D/T) ratio between 22 and 150 which means an adequate enclosure of a column size from stocky to slender-sized short columns with geometrical variations in diameter and thickness of the steel tube. In these tests, nominal concrete grade and structural steel strength were used. Most of these experimental tests were also used by researchers like

Hu et al. (2003) and Tao et al (2013) for the approval of their prediction in FEM analysis of CFST columns.

To verify the assumption made about the FE modeling techniques of the CFDCST columns, four experimental tests were selected from the experimental tests of Wan and Zha (2016). These tests possess identical external steel tube property with 1300 mm spacemen height and equal concrete strength for both sandwiched ($f'_{c,sw}$) and core ($f'_{c,core}$) concrete was used with variations in the internal steel tube. Experimentally conducted cubic strength (fcu) equals 30.55 MPa was directly converted to the equivalent cylindrical compressive strength using equation (52) as proposed by Mirza and Lacroix (2004).

$$f'_c = \left[0.76 + 0.2\log_{10}\left(\frac{f_{cu}}{19.6}\right)\right] * f_{cu} \quad \text{,Where } f'_c \text{ and } f_{cu} \text{ are in MPa} \tag{52}$$

ID	Cross Section Dimension: D*T*L (mm)	Concrete strength (f'_c) in (MPa)	Steel Tube yield strength (f_y) in (MPa)	D/T	Collapse Load N_{exp} (KN)	Examiner
CFST-022	140 * 6.5 * 602	23.8	313.0	22	1666.0	Schneider (1998)
CFST-032	114 * 3.6 * 250	44	339	32	1042	Abdalla (2012)
CFST-034	101.8 * 3.03 * 305.4	23.2	371	34	682	Yamamoto et al. (2002)
CFST-040	200 * 5.0 * 840	27.15	265.8	40	2016.9	Huang et al. (2002)
CFST-047	140 * 3.0 * 602	28.18	285	47	893.0	Schneider (1998)
CFST-070	280 * 4.0 * 840	31.15	272.6	70	3025.2	Huang et al. (2002)
CFST-150	300 * 2.0 * 840	27.23	341.7	150	2607.6	Huang et al. (2002)

Table 3: Published experimental tests on CFST columns

ID	External Tube			Internal Tube			Concrete property		Column Length	Collapse Load
	D_{ext} (mm)	t_{ext} (mm)	$f_{y,ext}$ (MPa)	D_{int} (mm)	t_{int} (mm)	$f_{y,int}$ (MPa)	$f'_{c,sw}$ (MPa)	$f'_{c,core}$ (MPa)	L (mm)	N_{exp} (KN)
CFDCST-A1-2	426	7.52	302	219	6.7	316.8	24.36	24.36	1300	9830
CFDCST-A2-2	426	7.52	302	219	6.7	478	24.36	24.36	1300	10025
CFDCST-A1-3	426	7.52	302	273	6.5	322	24.36	24.36	1300	9740
CFDCST-A2-3	426	7.52	302	24.36	273	6.5	447	24.36	1300	10739

Table 4: Published experimental tests on CFDCST columns by Wan and Zha (2016)

4.2 FE Model results and discussion

FE analyses results obtained from this study along with experimentally conducted test results are shown in Table 5. Besides, the estimation of the cross-sectional resistance as depicted by the Eurocode-4 ($N_{E.C}$) is also compared with experimental findings. The partial safety factor of structural steel and concrete materials equal to 1.0 and 1.5 in accord to EN 1993-1-1, 6.1(1), EN 1992-1-1, (2.4.2.4) were used respectively to find EC-4 based estimations.

For a stocky column having no stress descending stage in the stress-strain relation, the ultimate load-carrying capacity was considered at 5% of the longitudinal strain along the loading path similar to the consideration made by Alatshan et al. (2020). However, peak stress values were also obtained at lower strains below 5% like in the case of CFST-032, CFST-034, CFST-070, and CFST-150 columns where the maximum stress values are precisely known due to the presence of stress decrement within the simulation range.

Column ID	**Failure strength comparative summary**					
	Experimental	**FE Analysis**		**Eurocode**	**Variation**	
	Peak Load N_{exp} (KN)	Peak Load N_{FEA} (KN)	Deflection at peak load δ_{FEA} (mm)	N_{EC-4} (KN)	N_{FEA}/N_{exp}	$N_{E.C}/N_{exp}$
CFST-022	1666.0	1654.02	30.1	1128.34	0.99	0.68
CFST-032	1038	989.41	11.11	762.52	0.95	0.73
CFST-034	682	683.26	14.3	510.36	1.00	0.75
CFST-040	2016.9	2045.51	21	1342.63	1.01	0.67
CFST-047	893.0	933.12	30.1	629.31	1.04	0.70
CFST-070	3025.2	2929.4	5.03	2105.80	0.97	0.70
CFST-150	2607.6	2646.77	2.18	1713.74	1.02	0.66
				Mean	**1.0018**	**0.698**
				Standard Deviation	**0.0285**	**0.0318**
CFDCST-A1-2	9830	9221.24	65	6542.87	0.938071	0.67
CFDCST-A2-2	10025	10193.98	65	7229.96	1.016856	0.72
CFDCST-A1-3	9740	9696.23	65	6861.74	0.995506	0.70
CFDCST-A2-3	10739	10630.56	65	7512.34	0.989902	0.70
				Mean	**0.9927**	**0.698**
				Standard Deviation	**0.0289**	**0.0202**

Table 5: FE analysis results of the verification study

As shown in table 5, the proposed FE analysis displays good results in determining the ultimate load-carrying capacity very closer to experimental findings with an average value of 1.00 and 0.993 for CFST and CFDCST columns respectively. This also indicates the possibility to use the proposed techniques for the FE analysis of CFST and CFDCST short columns. All the model results have a percentage error lower than 5% toward the experimentally conducted force resisting capacities, except for the CFDCST-A2-2 column, which has a 6.12% error.

The design resistance computed using Eurocode-4 shows a conservative approach in estimating the experimental test results of both columns with a mean value of 0.698 for both CFST and CFDCST columns. Reduction in plastic resistance due to the slenderness effect was not applied as the specimens were under the category of short columns with a relative slenderness ratio below 0.2. In concern to CFDCST columns, it is also important to remember that the code does not theoretically consider the extra effect of double-tube configuration on the strength enhancement of core concrete whereas the inner steel tube is treated as inner reinforcements.

To validate the methodology used in this study, the Load-displacement relations of FE analyses results were compared with experimental findings. Figure 14 shows axial force resistance and end shortening curves of both experimental tests and FE analysis results of CFST columns. These figures are closely aligned with one another, showing the FE analysis possibly expresses experimentally conducted behaviors of short CFST columns.

In this paper, numerical adjustment on the value of "K_c" was made from the initial work of Tao et al. (2013). This factor is used in the concrete damaged plasticity (CPD) model to describe the concrete's nature and it highly affects the ultimate load-carrying capacity and posts yielding behaviors of a column. In this verification study, it is clearly shown that force-displacement relations of the FE analysis are quite closer to the experimental tests, which indicate the expressivity of the proposed CPD model of the study.

Approximate results of FE analyses and experimental tests in expressing axial force resistances of CFST columns also indicate how the predicted strain equation in the concrete stress-strain model is descriptive of the strain at which the ultimate compressive strength of concrete sustained in its maximum limit before reaching the stress softening point.

In figure 14 the axial force resistance and end shortening of CFST columns are shown in comparing both FE analyses and experimental test results.

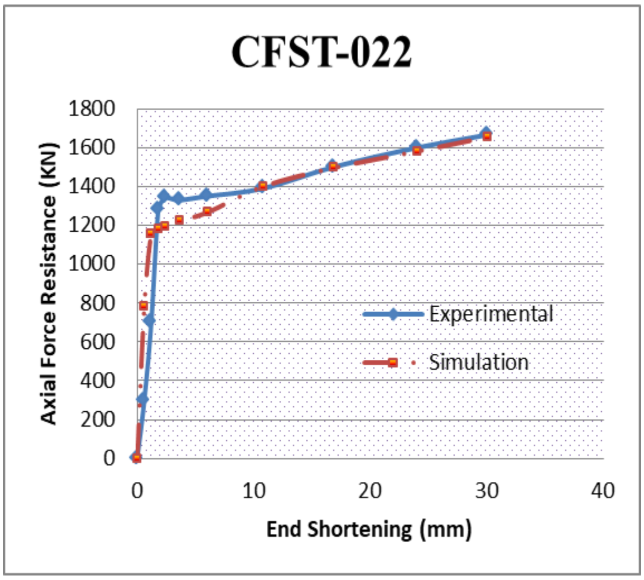
CFST-022
Axial Force Resistance (KN)
1800
1600
1400
1200
1000
800
600
400
200
0
0
10
20
30
40
End Shortening (mm)
Experimental
Simulation

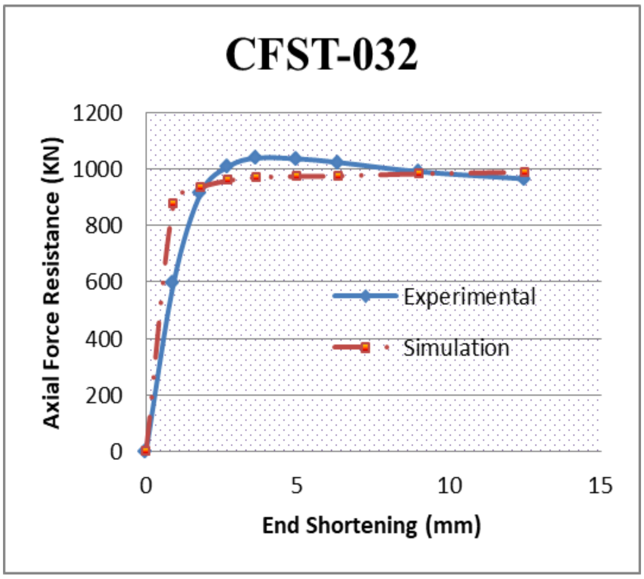
CFST-032
Axial Force Resistance (KN)
1200
1000
800
600
400
200
0
0
5
10
15
End Shortening (mm)
Experimental
Simulation

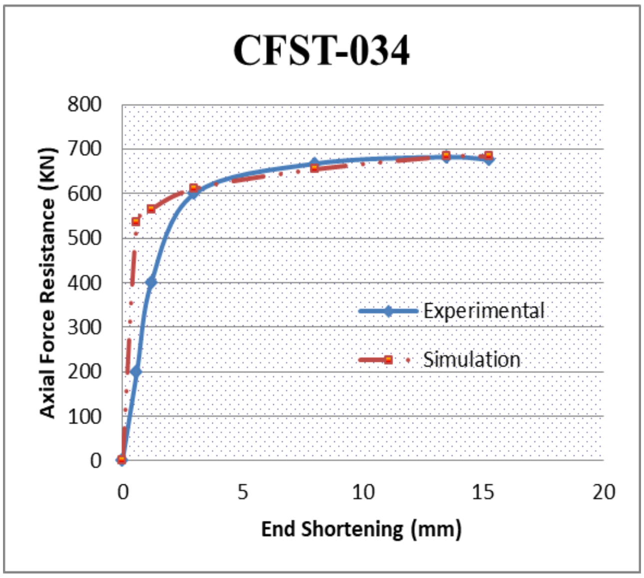
CFST-034
Axial Force Resistance (KN)
800
700
600
500
400
300
200
100
0
0
5
10
15
20
End Shortening (mm)
Experimental
Simulation

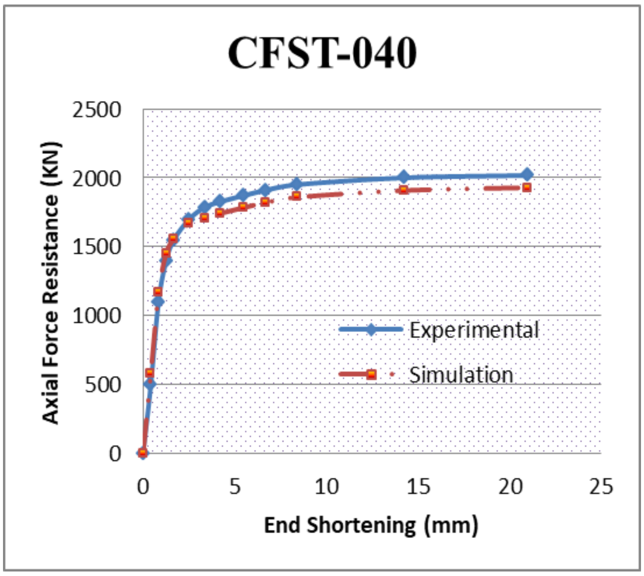
CFST-040
Axial Force Resistance (KN)
2500
2000
1500
1000
500
0
0
5
10
15
20
25
End Shortening (mm)
Experimental
Simulation

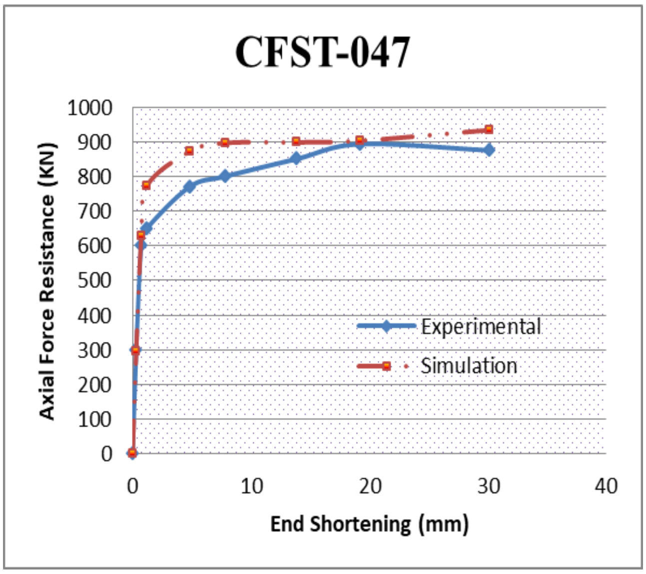
CFST-047
Axial Force Resistance (KN)
1000
900
800
700
600
500
400
300
200
100
0
0
10
20
30
40
End Shortening (mm)
Experimental
Simulation

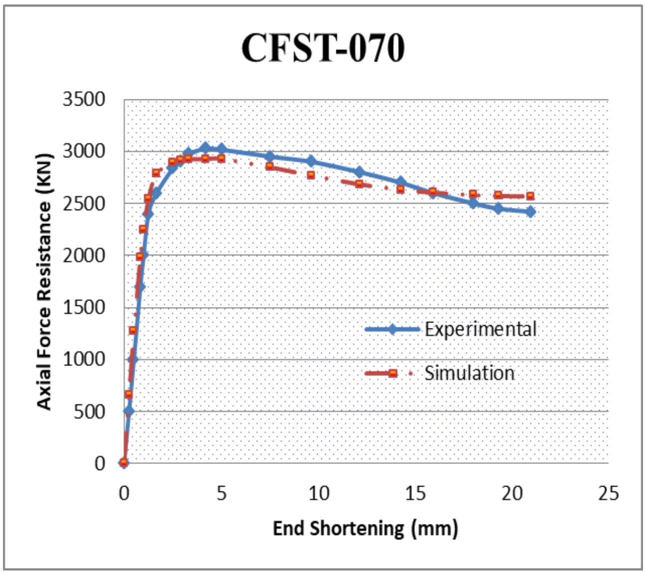
CFST-070
Axial Force Resistance (KN)
3500
3000
2500
2000
1500
1000
500
0
0
5
10
15
20
25
End Shortening (mm)
Experimental
Simulation

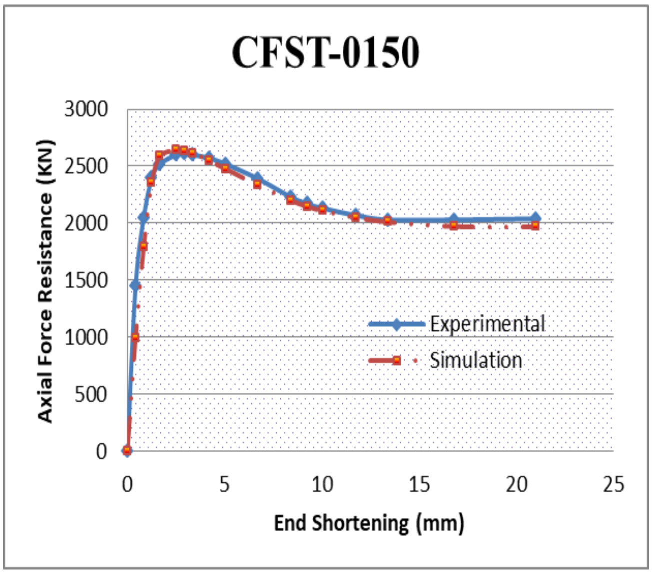

Figure 14: Axial force resistance and axial strain curve of CFST columns

Accurate load-displacement relation between FE analysis and experimental tests assure the applicability of the bilinear stress-strain model of steel tubes. In CFDCST columns, the stress-strain relation of the external steel tube was considered as an elastic-plastic nature with linear strain hardening like that of CFST columns. Whereas the internal steel tube was taken as, elastic-plastic with nominal plateau slope with the assumption that the stress development in the internal steel tube is controlled by the dual action of core and sandwich concrete. For the verification of this prediction, internal steel tubes with variable diameter and strength were simulated on CFDCST columns, and closely related FE analysis results toward experimental tests were obtained as shown in Figure 15.

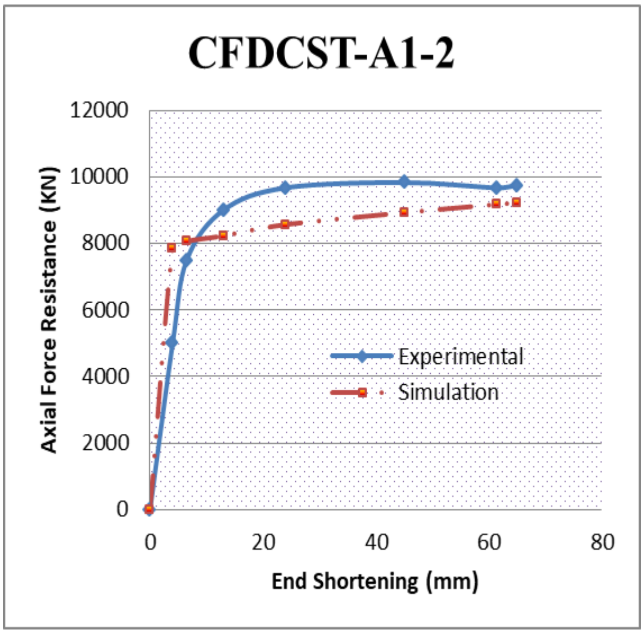

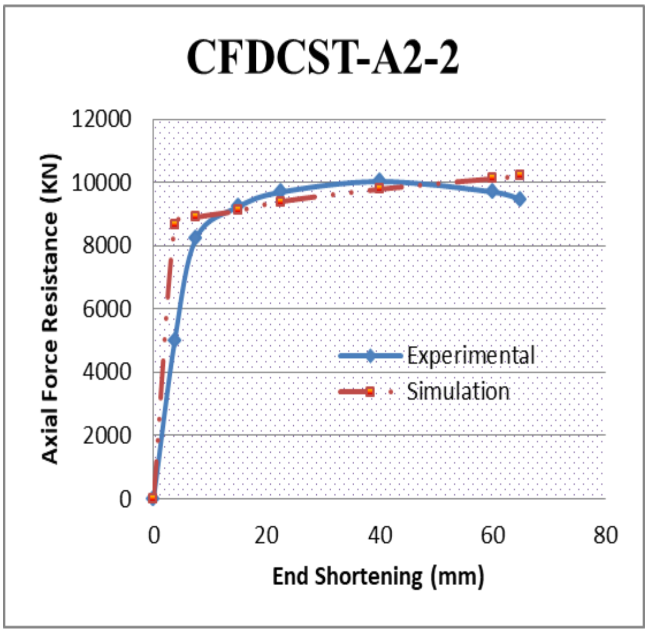

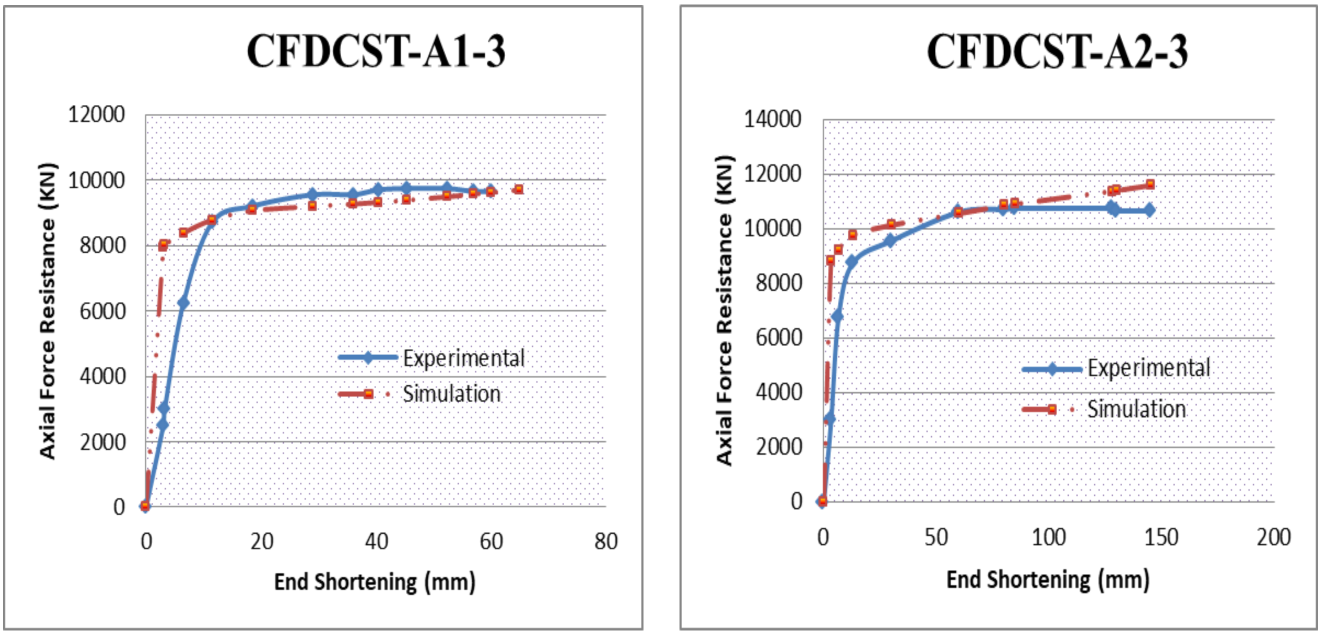

Figure 15: Axial force resistance and axial strain curve of CFDCST columns

The failure mode of the CFDCST A2-3 column is shown in figure 16 and for the experimental test, local buckling was developed in the middle height of the column in which stress was mainly concentrated, and similarly, in the top portion of the column, local buckling was initiated. In the FE analysis, closer to this actual failure mode local buckling was occurred at both ends and mainly appeared along with the mid-height of the column.

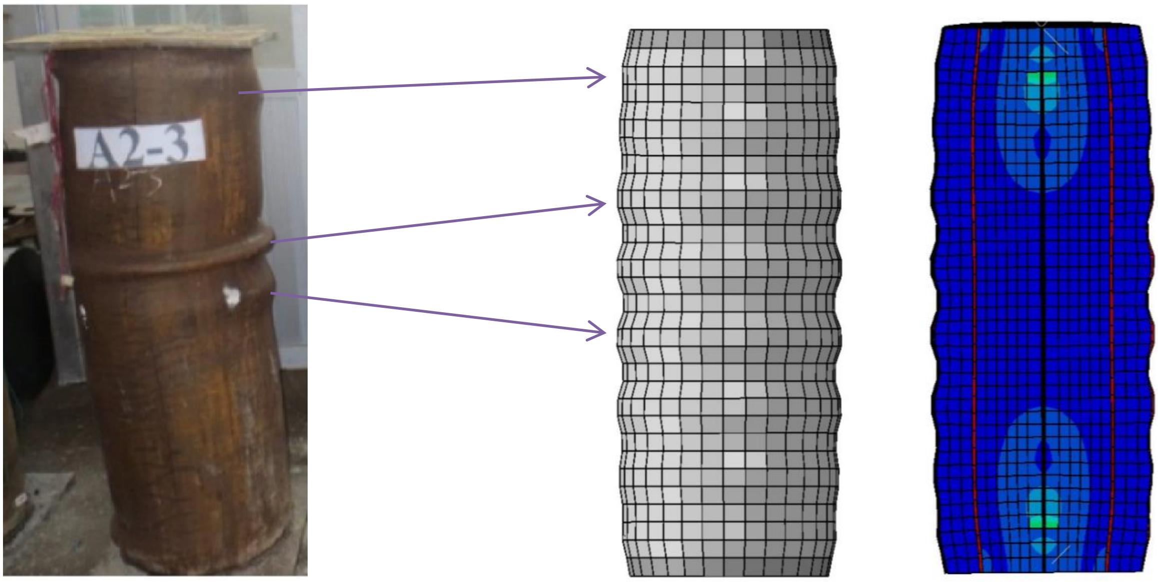

(a). Experimental test result (Wan and Zha, 2016) (b). FE analysis result

Figure 16: Failure mode of CFDCST-A2-3 column

CHAPTER-5 Parametric Study

5.1 FE model specimens

Seven basic sections or groups of model specimens are classified to study the axial load behavior of CFST and CFDCST short columns. Different parameters are also incorporated regarding the change in material strength and geometrical variations and FE analyses of 58 specimens were carried as shown in table 6-8. In all categories, 400mm height of a column was considered except for section-F, which deals with the effect of variation in height. 30MPa and 60MPa concrete strength and steel strength of 235, 275, 300, 355, and 460MPa were used. External steel tubes of 114.3, 139.7, 145, and 177. 8mm diameters were also applied for both CFST and CFDCST columns. For CFDCST columns, internal steel tube diameter of 60.3, 76.1, 88.9, 101.6, 102, 114.3, 139.7, 145mm were considered.

The first section (section-A) includes specimens with different inner steel tube diameters; showing a variety of internal D/t ratios between 20 and 50. Seven CFDCST test specimens were selected to analyze the effect of variation in the internal steel tube diameter with uniform steel tube thickness. A fixed property in the external steel tube was considered for all cases and, a CFST column with a diameter of 177. 8mm was used for a comparison purpose. Nominal concrete strength of 30 MPa and 275MPa steel tube strength were also used.

Effect of external steel tube thickness variation in the performance of CFST and CFDCST columns studied in section two where six specimens for both CFST and CFDCST columns with external steel tube thickness ranging from 1.5 to 9mm were tested. This covers a wider range to study the effect of external steel tube thickness variation in which the external D/t ratio extends from 20 to 120. For CFDCST columns, fixed internal steel tube properties were considered with an internal D/t ratio equals to 33.87. Increased steel tube strength of 355 MPa within the nominal range was used to reveal tiny changes made in the thickness variation of the external steel tube.

Similarly, the third section (C) comprises a variation in the internal steel tube thickness ranging from 1.5mm to 9mm where the internal D/t ratio extended from 11 to 68. The remaining material and geometrical properties were kept the same for all model specimens.

The fourth and fifth sections respectively consisted of models for studying the effect of change in concrete and steel tube material's strength. To analyze the effect of change in materials strength, values having a moderate range within the nominal strength grades were used in both cases.

Details of column Specimens for FE Analysis											
Model ID	D_{ext} (mm)	t_{ext} (mm)	$D/t_{(ext)}$	D_{int} (mm)	t_{int} (mm)	$D/t_{(int)}$	$f'_{c,sw}$ (MPa)	$f'_{c,core}$ (MPa)	$f_{y,ext}$ (MPa)	$f_{y,int}$ (MPa)	Height (mm)
	Section-A (Variation in the internal steel tube diameter)										
CFST-A1	177.8	4.5	39.51	-	-	-	-	30	275	-	400
CFDCST-A1	177.8	4.5	39.51	60.3	3	20.10	30	30	275	275	400
CFDCST-A2	177.8	4.5	39.51	76.1	3	25.37	30	30	275	275	400
CFDCST-A3	177.8	4.5	39.51	88.9	3	29.63	30	30	275	275	400
CFDCST-A4	177.8	4.5	39.51	101.6	3	33.87	30	30	275	275	400
CFDCST-A5	177.8	4.5	39.51	114.3	3	38.10	30	30	275	275	400
CFDCST-A6	177.8	4.5	39.51	139.7	3	46.57	30	30	275	275	400
CFDCST-A7	177.8	4.5	39.51	145	3	48.33	30	30	275	275	400
	Section-B (Variation in the external steel tube thickness)										
CFST-B1	177.8	1.5	118.53	-	-	-	-	30	355	-	400
CFST-B2	177.8	3	59.27	-	-	-	-	30	355	-	400
CFST-B3	177.8	4.5	39.51	-	-	-	-	30	355	-	400
CFST-B4	177.8	6	29.63	-	-	-	-	30	355	-	400
CFST-B5	177.8	7.5	23.71	-	-	-	-	30	355	-	400
CFST-B6	177.8	9	19.76	-	-	-	-	30	355	-	400
CFDCST-B1	177.8	1.5	118.53	101.6	3	33.87	30	30	355	355	400
CFDCST-B2	177.8	3	59.27	101.6	3	33.87	30	30	355	355	400
CFDCST-B3	177.8	4.5	39.51	101.6	3	33.87	30	30	355	355	400
CFDCST-B4	177.8	6	29.63	101.6	3	33.87	30	30	355	355	400
CFDCST-B5	177.8	7.5	23.71	101.6	3	33.87	30	30	355	355	400
CFDCST-B6	177.8	9	19.76	101.6	3	33.87	30	30	355	355	400
	Section-C (Variation in the internal steel tube thickness)										
CFST-C1 Alike to CFST-B3	177.8	4.5	39.51	-	-	-	-	30	355	-	400
CFDCST-C1	177.8	4.5	39.51	101.6	1.5	67.73	30	30	355	355	400
CFDCST-C2 Alike to CFDCST-B3	177.8	4.5	39.51	101.6	3	33.87	30	30	355	355	400
CFDCST-C3	177.8	4.5	39.51	101.6	4.5	22.58	30	30	355	355	400
CFDCST-C4	177.8	4.5	39.51	101.6	6	16.93	30	30	355	355	400
CFDCST-C5	177.8	4.5	39.51	101.6	7.5	13.55	30	30	355	355	400
CFDCST-C6	177.8	4.5	39.51	101.6	9	11.29	30	30	355	355	400
	Section-D (Variation in concrete strength)										
CFST-D1	139.7	3.6	38.81	-	-	-	-	30	275	-	400
CFST-D2	139.7	3.6	38.81	-	-	-	-	60	275	-	400
CFDCST-D1	139.7	3.6	38.81	76.1	3	25.37	30	30	275	275	400
CFDCST-D2	139.7	3.6	38.81	76.1	3	25.37	30	60	275	275	400
CFDCST-D3	139.7	3.6	38.81	76.1	3	25.37	60	30	275	275	400
CFDCST-D4	139.7	3.6	38.81	76.1	3	25.37	60	60	275	275	400
	Section-E (Variation in steel strength)										
CFST-E1	139.7	3.2	43.66	-	-	-	-	30	275	-	400
CFST-E2	139.7	3.2	43.66	-	-	-	-	30	460	-	400
CFDCST-E1	139.7	3.2	43.66	76.1	3	25.37	30	30	275	275	400
CFDCST-E2	139.7	3.2	43.66	76.1	3	25.37	30	30	275	460	400
CFDCST-E3	139.7	3.2	43.66	76.1	3	25.37	30	30	460	275	400
CFDCST-E34	139.7	3.2	43.66	76.1	3	25.37	30	30	460	460	400

Table 6: Model specimens for the assessment of a particular variation impact

In section-F, four CFST and CFDCST columns are considered to evaluate the effect of change in the height of the column within the range of short columns. Similar cross-sectional properties and material grades were used in all cases and relative slenderness ratios below 0.3 were considered.

Model ID	D_{ext} (mm)	t_{ext} (mm)	$D/t_{(ext)}$	D_{int} (mm)	t_{int} (mm)	$D/t_{(int)}$	$f'_{c,sw}$ (MPa)	$f'_{c,core}$ (MPa)	$f_{y,ext}$ (MPa)	$f_{y,int}$ (MPa)	Height (mm)	Slenderness $\bar{\lambda}$
	Section-F (Variation in the height of the column)											
CFST-F1	114.3	3.6	31.75	-	-	-	-	30	355	-	238	0.086
CFST-F2	114.3	3.6	31.75	-	-	-	-	30	355	-	357	0.129
CFST-F3	114.3	3.6	31.75	-	-	-	-	30	355	-	476	0.171
CFST-F4	114.3	3.6	31.75	-	-	-	-	30	355	-	714	0.257
CFDCST-F1	114.3	3.6	31.75	76.1	3	25.37	30	30	355	355	238	0.092
CFDCST-F2	114.3	3.6	31.75	76.1	3	25.37	30	30	355	355	357	0.139
CFDCST-F3	114.3	3.6	31.75	76.1	3	25.37	30	30	355	355	476	0.185
CFDCST-F4	114.3	3.6	31.75	76.1	3	25.37	30	30	355	355	714	0.277

Table 7: Model specimens for the assessment of variation in column height

In section-G, variations on different parameters were considered to study the cross-linked effect of change in material strength and geometrical property. Thirteen models were also selected and analyzed as shown in table 8.

Model ID	D_{ext} (mm)	t_{ext} (mm)	$D/t_{(ext)}$	D_{int} (mm)	t_{int} (mm)	$D/t_{(int)}$	$f'_{c,sw}$ (MPa)	$f'_{c,core}$ (MPa)	$f_{y,ext}$ (MPa)	$f_{y,int}$ (MPa)	Height (mm)
	Section-G (Variation in the internal steel tube D/t ratio and materials strength)										
	Part-1 Strength enhancement of CFDCSTs with a reduced internal steel tube diameter										
CFDCST-G1	177.8	4.5	39.51	139.7	3	46.57	30	30	300	235	400
CFDCST-G2	177.8	4.5	39.51	101.6	3	33.87	30	30	300	235	400
CFDCST-G3	177.8	4.5	39.51	101.6	3	33.87	30	30	300	355	400
CFDCST-G4	177.8	4.5	39.51	101.6	3	33.87	30	60	300	235	400
CFDCST-G5	177.8	4.5	39.51	101.6	4.5	22.58	30	30	300	235	400
CFDCST-G6	177.8	4.5	39.51	60.3	3	20.10	30	30	300	460	400
CFDCST-G7	177.8	4.5	39.51	60.3	4.5	13.4	30	30	300	460	400
	Part-2 Distinct impact of a similar area covering constituent materials of a CFDCST column										
CFDCST-G8	145	3.2	45.31	102	4.7	21.70	30	60	355	355	400
CFDCST-G9	145	3.2	45.31	102	4.7	21.70	60	30	355	355	400
CFDCST-G10	145	3.2	45.31	102	4.7	21.70	30	30	355	460	400
CFDCST-G11	145	3.2	45.31	102	4.7	21.70	30	30	460	355	400
CFDCST-G12	145	3.2	45.31	102	4.7	21.70	60	30	235	460	400
CFDCST-G13	145	3.2	45.31	102	4.7	21.70	30	60	460	235	400

Table 8: Model specimens for the assessment of combined variations impact

This section could be classified into two parts; CFDCST-G1 to G7 can be categorized in one part in which the variation in the internal steel tube D/t ratio, core concrete, and internal steel tube strength was studied. The basic target of the first part of this section is to identify how CFDCST columns with a lower internal steel tube diameter could have a maximized axial load carrying capacity. For this reason, CFDCST-G1 had set to have sandwich concrete, which is half of the area of core concrete, and for CFDCST-G2 to G5 50% reduction in the internal steel tube diameter was made to make the sandwiched concrete twice the area of core concrete. In the case of CFDCST-G6 and G7 columns, an internal steel tube was reduced to be 66% of the external steel tube diameter.

CFDCST-G8 to G13 are classified in the second part where variations in concrete and steel material's strength were made with a controlled cross-sectional area of the constituent materials. An approximated area of external and internal steel tubes with closely equivalent areas of core and sandwiched concrete were used to differentiate the material's particular contribution and the effect of double confinement in CFDCST columns.

5.2 Simulation program

This study adopted an ABAQUS software program to perform finite element analyses of both CFST and CFDCST columns. Two analysis steps were involved; the first analysis was conducted to include geometrical imperfection in the system. From this step, possible failure modes of the structure were attained and the nodal displacements were further used to apply imperfection in the second stage analysis. However, in the case of short columns, the effect of geometrical imperfection is not a serious issue but to get more precisions, this effect is considered under this paper. The analyses were also conducted on the external steel tubes only. Internal steel tubes in CFDCST columns were not included in the first analysis step as the tube exhibit a failure mode pattern guided by the external steel tube due to the presence of concrete materials.

The linear perpetuation step was also used and three eigenvalues were arranged in all cases. For axially loaded short members there is no such tremendous difference among failure modes that further influence the response of the structure, therefore the first Mode was used by default to introduce imperfection in the system. Force controlled method with a unit load application at the geometrical center of the steel tube was implemented. To apply restrictions on edge faces, two boundaries on the top and bottom surface were assigned in the sets of assembly and constrained in the type of rigid body within the top and bottom reference points along the centroid axis. The nodal displacement files (U) were also saved through editing the program's keyword. The sample analysis result of the first linear step on an arbitrary external steel tube is shown in figure 17.

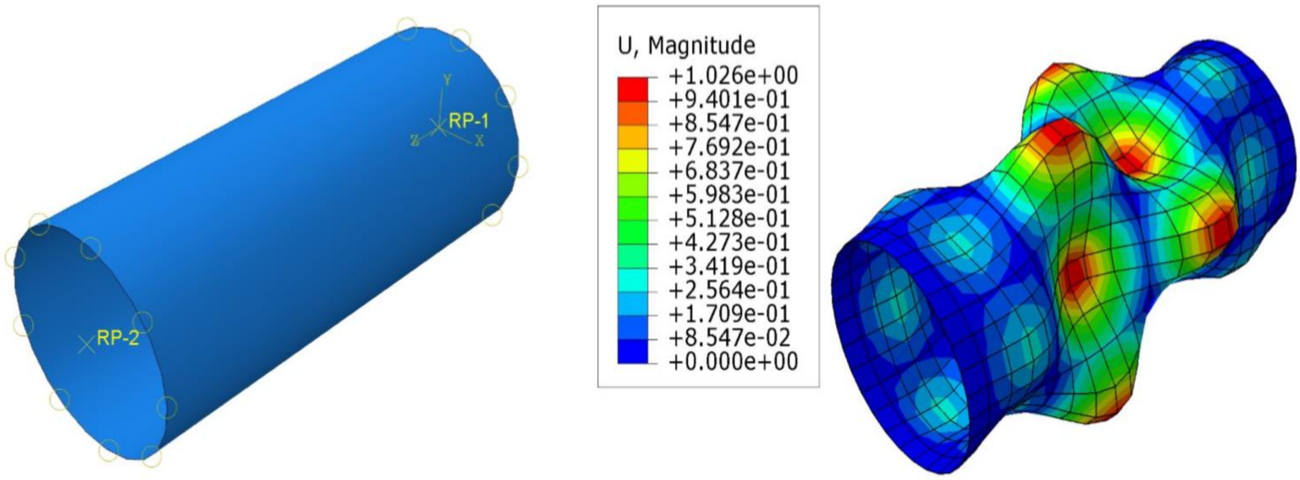

(a). FE model sample (b). Possible deformed shape of the analysis

Figure 17: Sample failure mode of the external steel tube from the first step analysis

After the first step analyses, nonlinear analyses were conducted on the overall structural members of the column. This displacement controlled analysis was simulated in static general step and geometric nonlinearity was included. Similar to the first step, the top and bottom surfaces of the column were constrained at reference points, which were fixed except in the direction of the applied displacement. In CFDCST columns, three surfaces to surface interactions were defined:

- ✓ The inner surface of the external steel tube and the outer surface of the sandwich concrete
- ✓ The outer surface of the internal steel tube and the inner surface of the sandwich concrete
- ✓ The inner surface of the internal steel tube and the outer surface of the core concrete

However, for CFST columns only one interaction was used between the external steel tube and core concrete. Interactions were defined by hard contacts and a penalty form of friction was used in the normal tangential column's behavior. In all interactions, steel tubes were used as a master surface with a relatively increased mesh size while the concrete was defined as a slave surface. Furthermore, the external steel tube was considered as a shell element for both CFST and CFDCST columns. However, in CFDCST columns the internal steel tube was modeled as a solid element for creating accurate interaction toward the core and sandwich concrete. For the application of geometric imperfection, displacement files registered in the first step analysis of the external steel tube were called on the nonlinear step using the edited keyword format of the program.

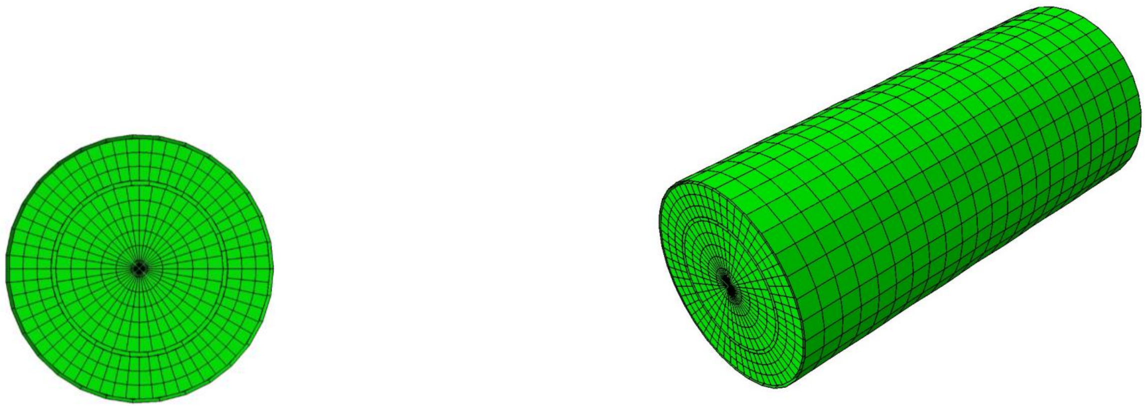

(a). Cross-sectional View (b). 3D View

Figure 18: Mesh sample of a CFDCST column

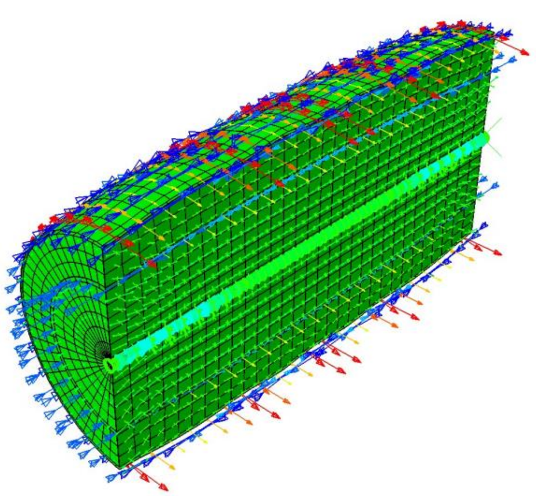

(a) Principal stresses on deformed shape

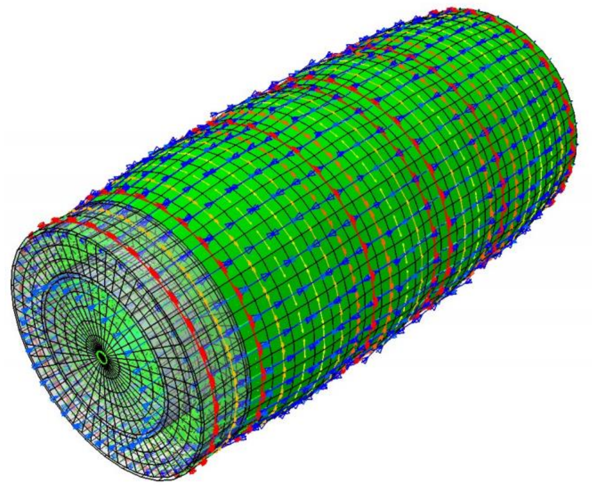

(b) Principal stresses on deformed and undeformed shapes

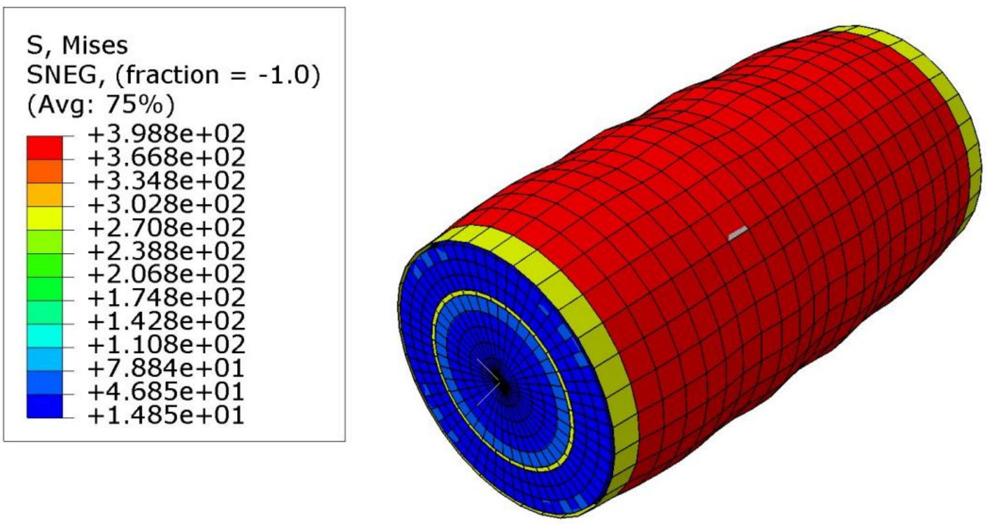

(c) Analysis results of stress components

Figure 19: Nonlinear FE analysis result of an arbitrary CFDCST column

5.3 Analyses results and discussions

5.3.1 Section-A (Variation in the internal steel tube diameter)

The basic aspect of this section is to generalize the effect of change in the internal steel tube diameter of a CFDCST column. Maximum and minimum limits of D_{ext}/D_{int} ratios are required to allow a proper gap for concrete placement between steel tubes. In this study, the ratio of the external steel tube diameter to an internal steel tube diameter is approximately chosen between 1.2 and 3. A fixed thickness of 4.5 and 3mm was used for external and internal steel tubes respectively. As shown in table 9, it is also possible to express the decrement of the internal steel tube diameter in percentage; the cross-sectional diameter decrement of the external steel tube toward the internal steel tube extends from 66.09% to 18.45%. Following this, CFDCST columns develop percentage load increments ranging from 9.86% to 23.77% relative to the ultimate load-carrying capacity of CFST-A1. CFDCST-A7 with an internal steel tube diameter of 145mm also shows a 12.67% load increment from that of CFDCST-A1 having a 60.3mm internal tube diameter. Increasing the internal steel tube diameter to a certain extent has a vital advantage in modifying the ultimate load-bearing capacity of CFDCST columns due to the increment of steel contributions and improvements in the effective area coverage of the dual confinement.

Model Column ID	FE Model: $-\ t_{ext} = 4.5\text{mm},\ t_{int} = 3\text{mm}, f'_{c,sw} = f'_{c,core} = 30\text{MPa},\ f_{y,ext} = f_{y,int} = 275\text{MPa}$				FE Analysis Result	
	D_{ext} (mm)	D_{int} (mm)	$\frac{D_{ext}}{D_{int}}$	External to internal steel tubes decrement	Peak Load N_{FEA} (KN)	Load Increment of CFDCSTs over CFST-A1
CFST-A1	177.8	-	-	-	1702.72	<Reference Load>
CFDCST-A1	177.8	60.3	2.95	66.09%	1870.53	9.86%
CFDCST-A2	177.8	76.1	2.34	57.20%	1909.48	12.14%
CFDCST-A3	177.8	88.9	2.00	50.00%	1954.13	14.77%
CFDCST-A4	177.8	101.6	1.75	42.86%	1993.39	17.07%
CFDCST-A5	177.8	114.3	1.56	35.71%	2038.05	19.69%
CFDCST-A6	177.8	139.7	1.27	21.43%	2098.70	23.26%
CFDCST-A7	177.8	145	1.23	18.45%	2107.49	23.77%

Table 9: Analysis result of section-A specimens

Axial force resistance and end shortening curves of section-A specimens are given in figure 20. These curves show a regular increment in strength depending on the internal steel tube diameter, but no visible change was seen in the linear elastic properties of each column.

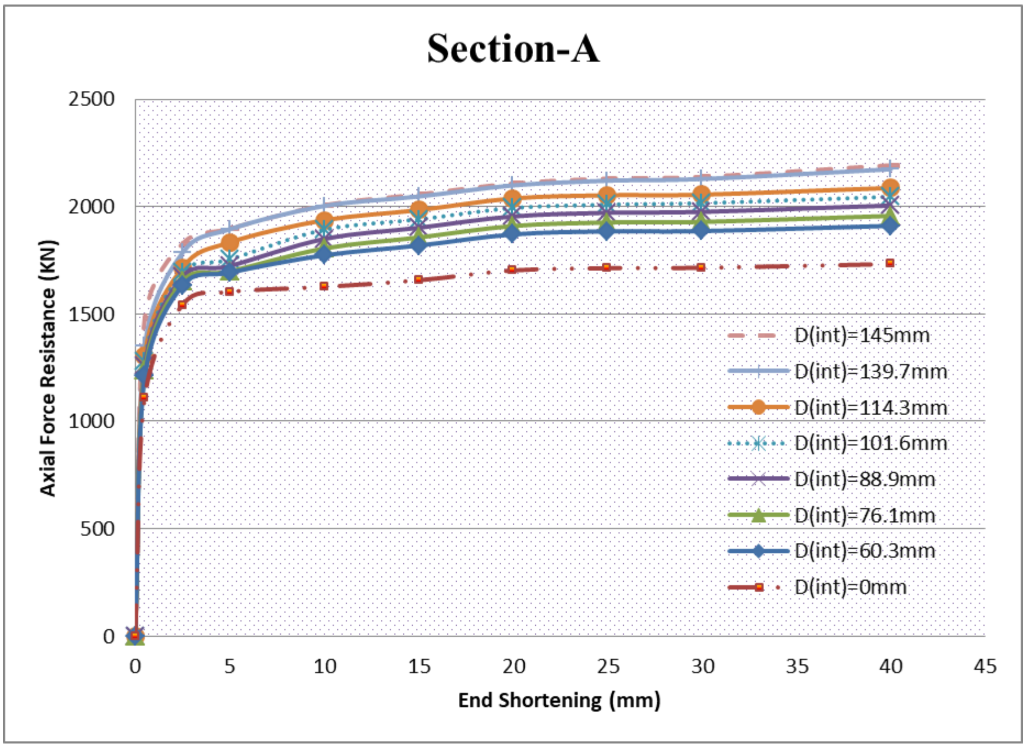

Figure 20: Effect of variation in the internal steel tube diameter

In referring to the external to internal steel tubes diameter percentage decrement and axial force resistance, the percentage decrement between the ranges 30-45% approximately shows better applicability and axial force resistance.

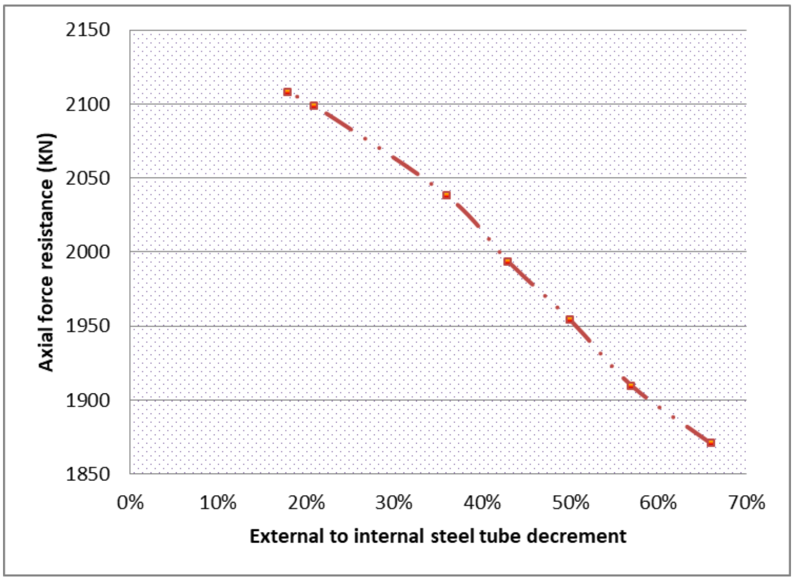

Figure 21: Percentage decrement of external to internal steel tubes diameter and axial force resistance

5.3.2 Section-B (Variation in the external steel tube thickness)

To investigate the effect of external steel tube thickness variation on the axial load performance of a column, six models of CFST and CFDCST columns were simulated under this section. Variation in tube thickness is related to the change in D/t ratios and it affects the load-carrying capacity of CFST or CFDCST columns. Change in D/t ratio with variation in diameter could be possible, but in finite element analysis, increasing the diameter results to have a large number of meshed elements that further increases the computation time of the analysis. Therefore, in this study, the variation in the external D/t ratio achieved using the change in the steel tube thickness only.

The structural response of CFST and CFDCST columns under the alteration in the external steel tube thickness is shown in table 10. This effect was examined using a uniform internal D/t ratio equals to 33.87 for CFDCST columns. The reduction in diameter of the internal steel tube from that of external tubes is 43.86% in which external D/t ratios studied within the range of 20 to 120. External steel tube thicknesses of 1.5, 3, 4.5, 6, 7.5, and 9mm were used.

Analyses results show the axial load carrying capacity of CFST and CFDCST column approximately extended in 196 % and 146% respectively as the external steel tube thickness increases from 1.5mm to 9mm for each type of columns. This also indicates CFST columns' dependability on the external steel tube property is very higher than that of CFDCST columns.

In these analyses, it is clearly seen that the load increment of CFDCSTs over their corresponding CFST columns decreases with increasing external steel tube thickness due to the suppressed influence of the internal steel tube with the enlarged size of the external steel tube. This condition is clearly shown in table 10, for external steel tube thickness ranging from 1.5 to 9mm the increment in CFDCST columns over their corresponding CFST columns diminished from 31.14% to 8.83%.

For both CFST and CFDCST columns, a wide range of D/t ratios extending from 20 to 120 were used to evaluate the effect of external D/t ratios. In confined concrete consideration of these varied ratios is highly important, especially in short columns where the effect of confinement is an important issue. Relatively lower values of D/t ratios represent a greater improvement in the load resisting performance of a column. In former research conducted by Yadav and Chen (2017), it is conducted that, the increase in D/t ratio of a CFST column from 15 to 125 decreases its ultimate load-carrying capacity by 67.9%. Similarly, in this study, for CFST columns 66.24% reduction in load resistance is shown as the D/t ratio increased approximately from 20 to 120. In concerning CFDCST columns, the reduction in the ultimate load-carrying capacity extended to 59.32% as the D/t ratio increased from 20 to 120. This indicates that the insertion of an internal steel tube has a great influence to tolerate the reduction due to the variation in the external D/t ratios, which can be seen as a measure to enhance the capacity of a CFST column.

Model Column ID	FE Model: $-\ D_{int} = 101.6mm,\ t_{int} = 3mm, f'_{c,sw} = f'_{c,core} = 30MPa,\ f_{y,ext} = f_{y,int} = 355MPa$			FE Analysis Result	
	D_{ext} (mm)	t_{ext} (mm)	$\frac{D_{ext}}{t_{ext}}$	Peak Load N_{FEA} (KN)	Load Increment of CFDCSTs over CFST
CFST-B1	177.8	1.5	118.53	1078.64	<Ref. Load>
CFDCST-B1	177.8	1.5	118.53	1414.55	31.14%
CFST-B2	177.8	3	59.27	1470.73	<Ref. Load>
CFDCST-B2	177.8	3	59.27	1849.83	25.78%
CFST-B3	177.8	4.5	39.51	1929.49	<Ref. Load>
CFDCST-B3	177.8	4.5	39.51	2290.50	18.71%
CFST-B4	177.8	6	29.63	2349.79	<Ref. Load>
CFDCST-B4	177.8	6	29.63	2725.38	15.98%
CFST-B5	177.8	7.5	23.71	2800.73	<Ref. Load>
CFDCST-B5	177.8	7.5	23.71	3074.90	9.79%
CFST-B6	177.8	9	19.76	3194.88	<Ref. Load>
CFDCST-B6	177.8	9	19.76	3476.98	8.83%

Table 10: Analysis result of Section-B specimens

Figure 22 graphically presents the change in the axial force resistance of CFST columns due to variation in the external steel tube thickness. Different kinds of load vs. axial deflections are shown, CFST-B1 reaches its maximum capacity very near from the yielding point of the column, and it develops a sudden decrement in its load resisting capacity due to the formation of weak confinement in the external steel tube of 1.5mm thickness. Similarly, CFST-B2 reaches its ultimate load-carrying capacity in the early stage, but unlike CFST-B1, it exhibits a gradual decrement in strength due to the increased confinement in the external steel tube of 3mm thickness. However, the analyses of the remaining three columns generally maintain strain hardening until the simulation terminates in reaching 5% axial shortening of the column’s length.

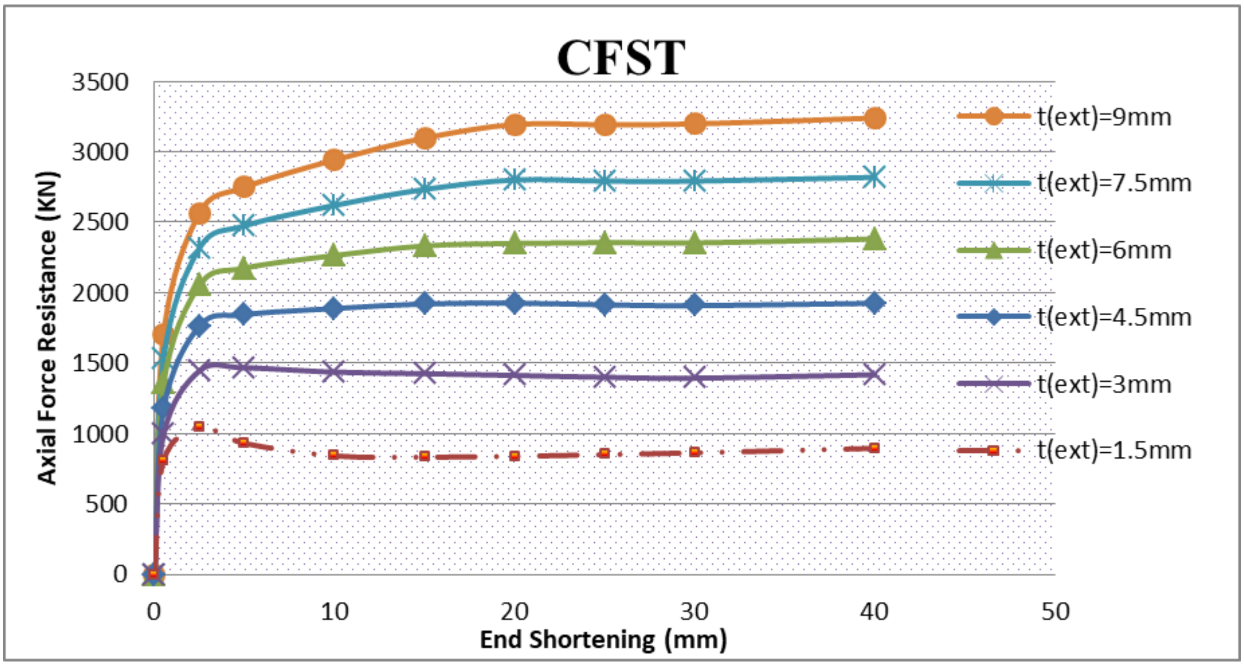

Figure 22: Effect of external steel tube thickness variation in CFST columns

In the model analyses conducted for CFDCST columns, only CFDCST-B1 shows a slight gradual decrement after attaining its maximum capacity, whereas the remaining other specimens develop rapid strain hardening as shown in figure 23.

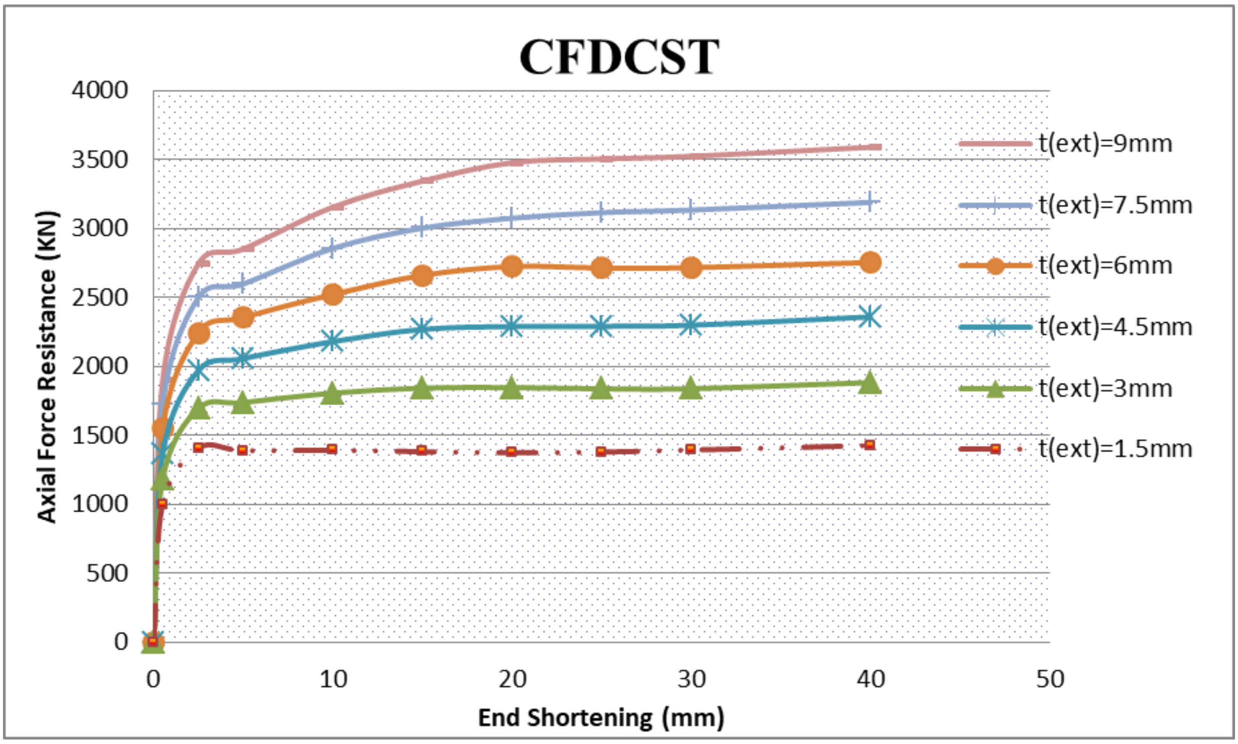

Figure 23: Effect of external steel tube thickness variation in CFDCST columns

For detailed comparison in the post yielding behaviors, change in the structural response of the CFDCST columns relative to their corresponding CFST columns is shown in figure 24.

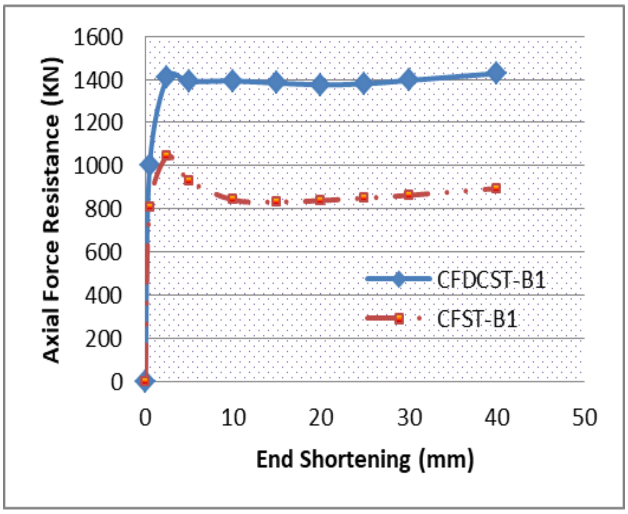

(a). Load Increment (31%):- t_{ext}: 1.5mm

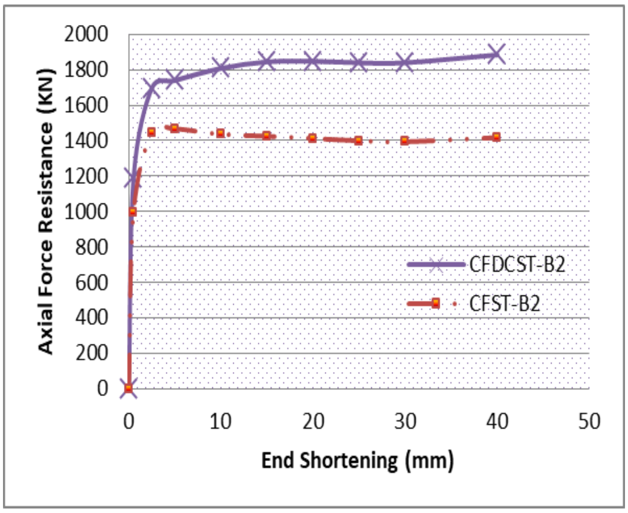

(b). Load Increment (26%):- t_{ext}: 3.0mm

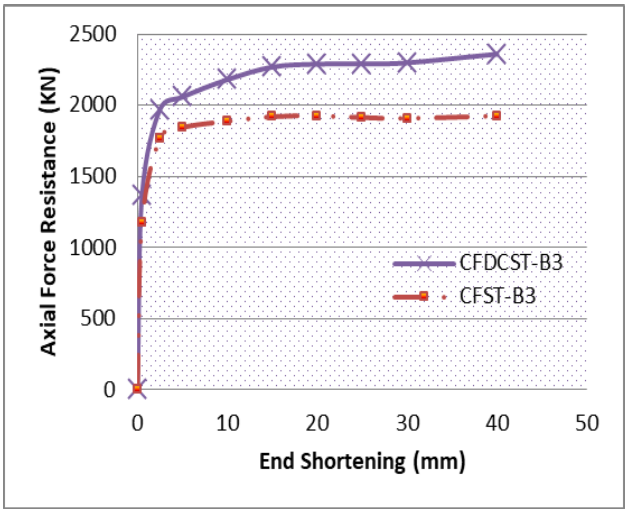

(c). Load Increment (19%):- t_{ext}: 4.5mm

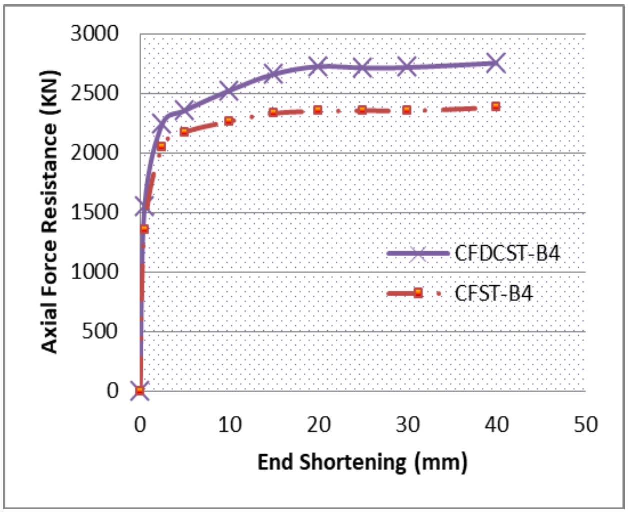

(d). Load Increment (16%):- t_{ext}: 6.0mm

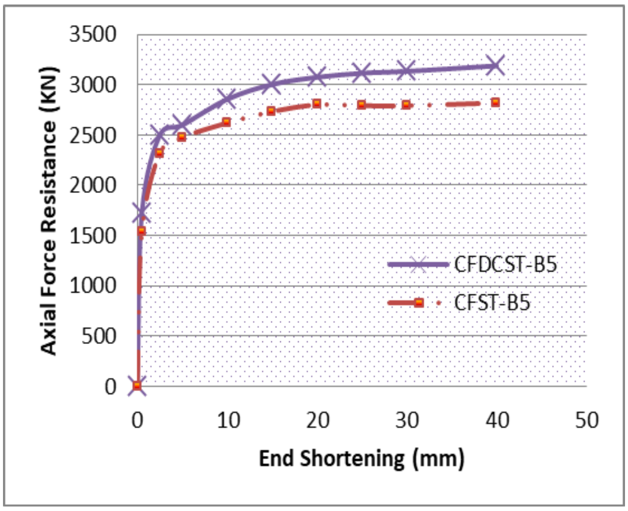

(e). Load Increment (10%):- t_{ext}: 7.5mm

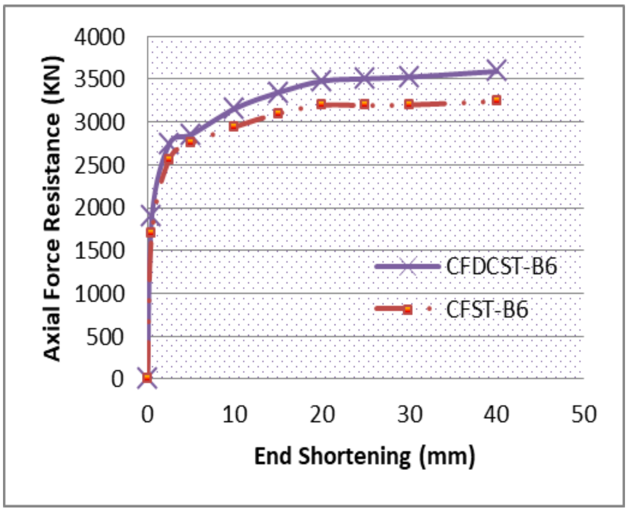

(f). Load Increment (9%):- t_{ext}: 9.0mm

Figure 24: Load increment of CFDCSTs over CFSTs for the variation in external steel tube thickness

In figure 25, the effect of the external steel tube D/t ratio is shown for both CFST and CFDCST columns. The axial load resistance of columns increases with decreasing in the external steel D/t ratios and for smaller ratios, curves of both column types slightly approach one another.

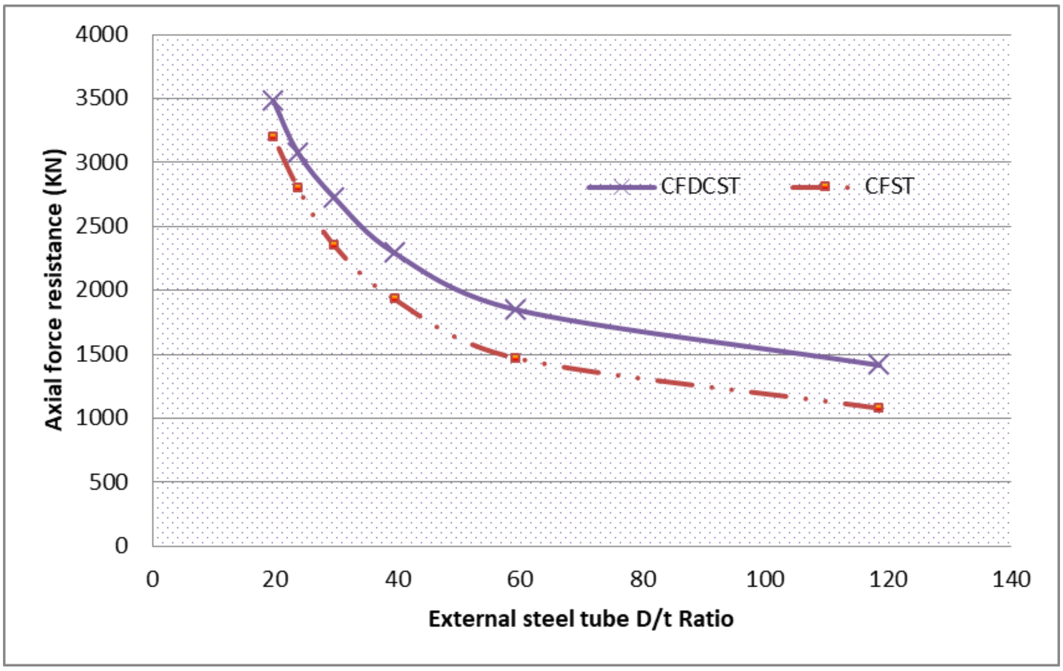

Figure 25: Effect of variation in the external steel tube D/t ratios

5.3.3 Section-C (Variation in the internal steel tube thickness)

Six models were analyzed to investigate the effect of internal steel tube thickness variation on the axial load performance of a CFDCST column. The internal D/t ratio ranges from 11 to 68, which cover a moderate range to evaluate the effect of D/t ratios and a constant external D/t ratio equals to 40 was implemented

In this section, the external steel tube dimension and thickness were kept constant. Internal tube thicknesses of 1.5, 3, 4.5, 6, 7.5, 9mm were used and the load increment of CFDCST columns appeared to rise from 9.78% to 49.15% in comparison with the CFST-C1 column as the internal steel tube thickness increased from 1.5mm to 9mm.

Model Column ID	FE Model: $D_{ext} = 177.8mm,\ t_{ext} = 4.5mm,\ f'_{c,sw} = f'_{c,core} = 30MPa,\ f_{y,ext} = f_{y,int} = 355MPa$			FE Analysis Result	
	D_{int} (mm)	t_{int} (mm)	$\frac{D_{int}}{t_{int}}$	Peak Load N_{FEA} (KN)	Load Increment of CFDCSTs over CFST-C1
CFST-C1	-	-	-	1929.49	<Ref. Load>
CFDCST-C1	101.6	1.5	67.73	2118.1	9.78%
CFDCST-C2	101.6	3	33.87	2290.50	18.71%
CFDCST-C3	101.6	4.5	22.58	2514.12	30.30%
CFDCST-C4	101.6	6	16.93	2614.66	35.51%
CFDCST-C5	101.6	7.5	13.55	2757.12	42.89%
CFDCST-C6	101.6	9	11.29	2877.82	49.15%

Table 11: Analysis result of section-C specimens

Modifications in the internal steel tube D/t ratios with increment in tube thickness influence the cross-sectional capacity of the CFDCST columns with a change in confinement distribution through developing a higher dual confinement effect on the core concrete. In this study, the ultimate load-carrying capacity of CFDCST columns increased by 35.87% as the internal D/t ratio reduced from 67.73 to 11.29.

Figure 26 also shows a graphical representation of the change in the axial load resistance of CFDCST columns with variation in the internal steel tube thickness.

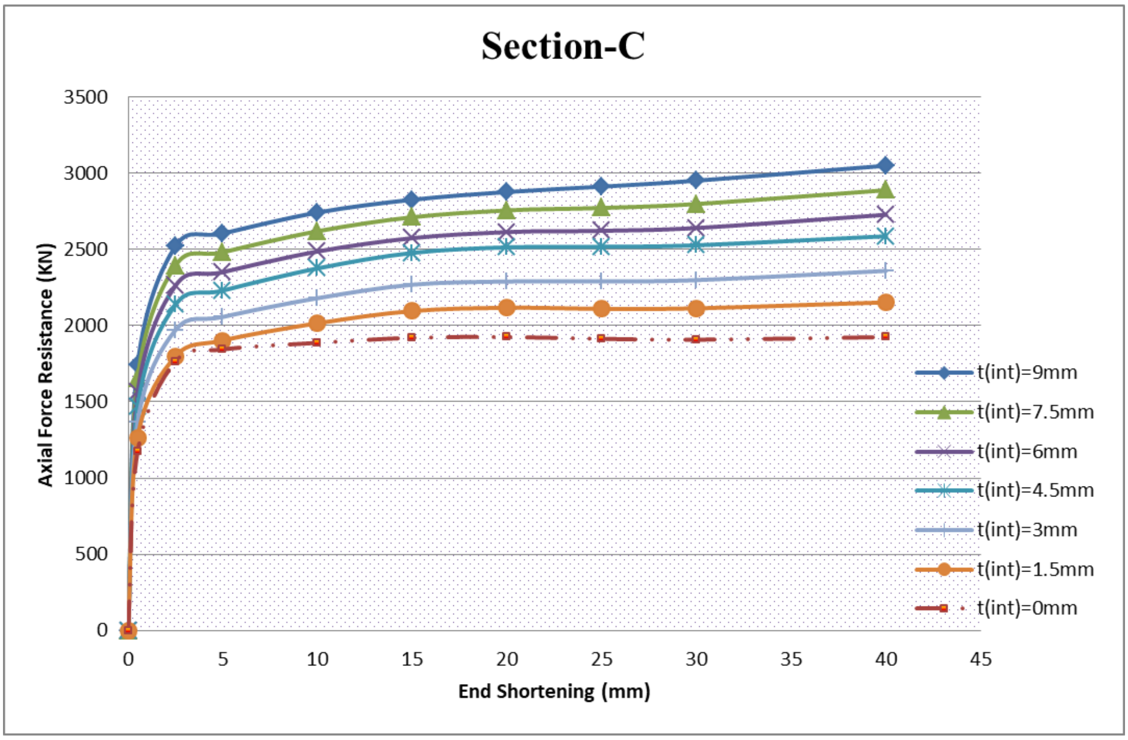

Figure 26: Effect of internal steel tube thickness variation

The decrement in the ultimate load-carrying capacity of CFDCST columns due to the increment in internal steel tube D/t ratio is also shown in figure 27.

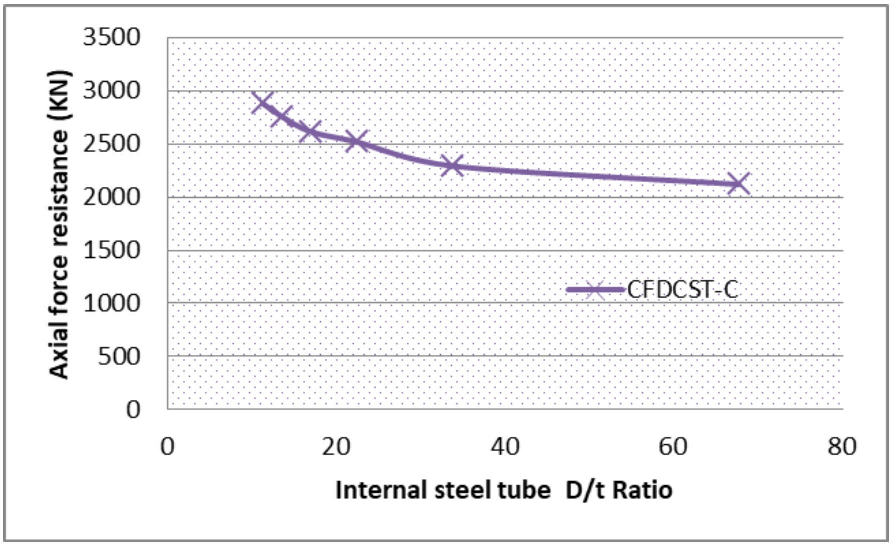

Figure 27: Internal steel tube D/t ratios and axial force resistance of CFDCST columns

5.3.4 Section-D (Variation in concrete strength)

To study the effect of change in the concrete strength, the nominal concrete strength grades of 30 and 60 MPa were used. However, this effect is not highly influential in CFST and CFDCST columns in comparison with steel tube geometrical and materials' property. CFST columns tend to develop a 24.66% increment in their axial load behavior as the concrete core strength increased from 30 to 60MPa. Similarly, in consideration of similar concrete stiffening CFDCST column shows a 16.15% increment in the ultimate load-carrying capacity as the concrete strength for sandwiches and core concrete increased from 30 to 60MPa.

In this section, fixed steel tube thickness and diameter were considered. Internal steel tube diameter reduced to be 45.53% of the external steel tube diameter. In CFDCST columns, the difference in the area of the core and sandwiched concrete has an effect. In this section, a fixed area of 3859.45mm^2 and 9240.24mm^2 of core and sandwich concrete were used for all models in which the core concrete area is 41.77% of the sandwich concrete. However, the effect of using high concrete strength in the sandwich concrete as in the case of CFDCST-D3 has little improvement in the ultimate load-carrying capacity, which is only a 2.39% increment from the stiffened core concrete column of CFDCST-D2.

Model Column ID	FE Model: $-$ $D_{ext} = 139.7mm, t_{ext} = 3.6mm,\ D_{int} = 76.1mm, t_{int} = 3mm,\ f_{y,ext} = f_{y,int} = 275MPa$		FE Analysis Result	
	$f'_{c,sw}$ (MPa)	$f'_{c,core}$ (MPa)	Peak Load N_{FEA} (KN)	Deflection at peak load δ_{FEA} (mm)
CFST-D1	-	30	1061.44	20
CFST-D2	-	60	1323.17	2.44
CFDCST-D1	30	30	1276.67	20
CFDCST-D2	30	60	1350.98	20
CFDCST-D3	60	30	1383.29	4.2
CFDCST-D4	60	60	1482.89	3.59

Table 12: Analysis result of section-D specimens

The deflection at which maximum load-bearing capacity was registered is indicated in table 12. For a column with high concrete strength, the peak load occurred closer to the initial loading stage. In this case, the concrete sustains a higher load with little strain development in which the steel-concrete interaction goes slowly until the concrete gets its maximum capacity and there will be a sudden failure in the system as the confining capacity of the steel tube would not be relatively stronger to resist the elevated higher load. However, to some extent later the axial behavior starts to rise following the steel-concrete interaction. This phenomenon is clearly shown in CFST-D2 in which the concrete strength was 60MPa. Conversely, column model type CFST-D1 with concrete strength of 30MPa sustain stress hardening throughout the analysis due to the reason that the maximum load-carrying capacity of the concrete core possibly prolonged within the confining tendency of the steel tube. However, the fall in the strength of CFDCST columns which are with high concrete grade greatly reduced by the dual confinement effect of the steel tubes; in reasoning to this CFDCST-D4 column with 60MPa grade in its core and sandwich concrete shows very gradual load decrement after the ultimate load-bearing capacity of the column.

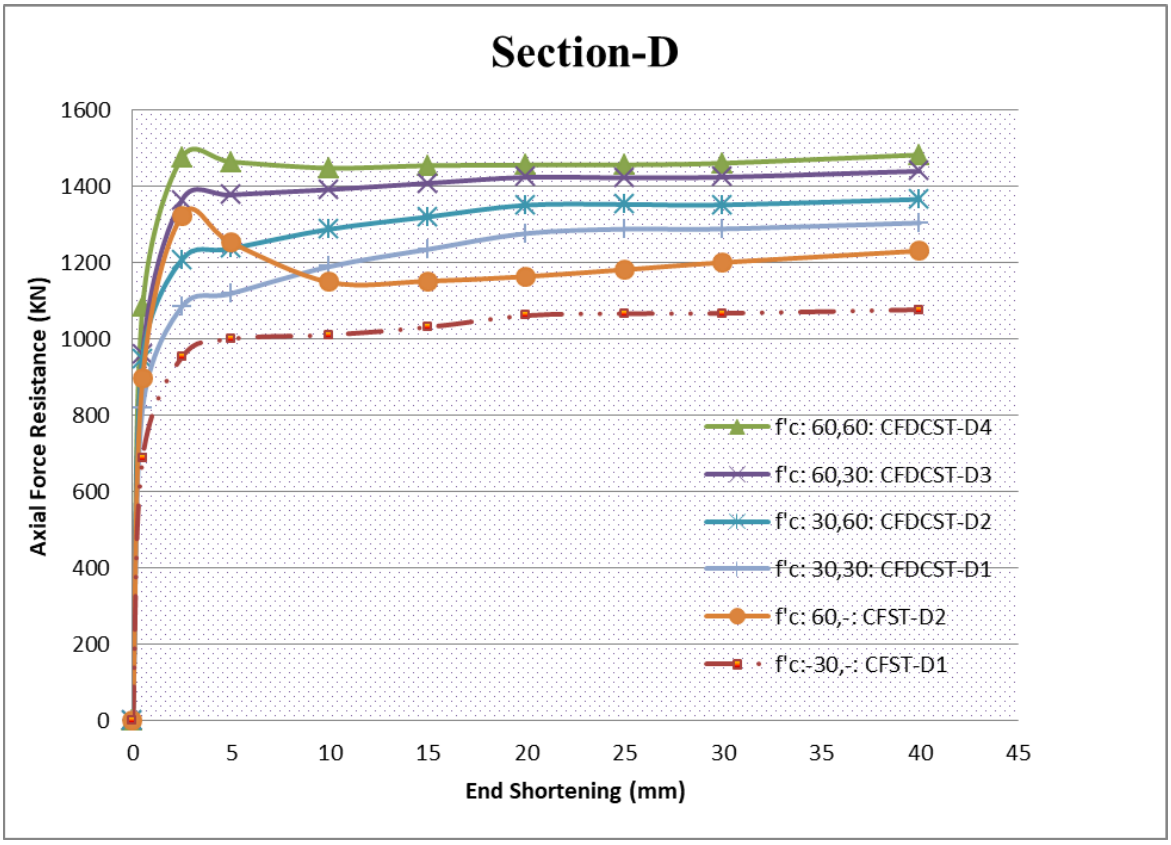

Figure 28: Effect of concrete strength variation

Increasing the concrete strength of the core and sandwich concrete increases the strength of a CFDCST column where the changes in the concrete strength alter the cross-sectional stiffness of the member and in turn, shifts the structural response and failure mode of the column as shown in figure 28.

Figure 29 selectively shows the load-displacement curve under the effect of variation in the core concrete grade of CFDCST columns with high sandwich concrete strength and improvement in the core concrete strength from 30 to 60 MPa results in a 7.2% increment in the load-carrying capacity of CFDCST-D4 from that of CFDCST-D3. CFST-D2 also sustains higher stiffness and shows a brittle behavior that develops a sudden fall due to the crushing of concrete. However, in the case of CFDCST-D4, this brittle effect is highly reduced by the dual confining effect resulted in the core concrete.

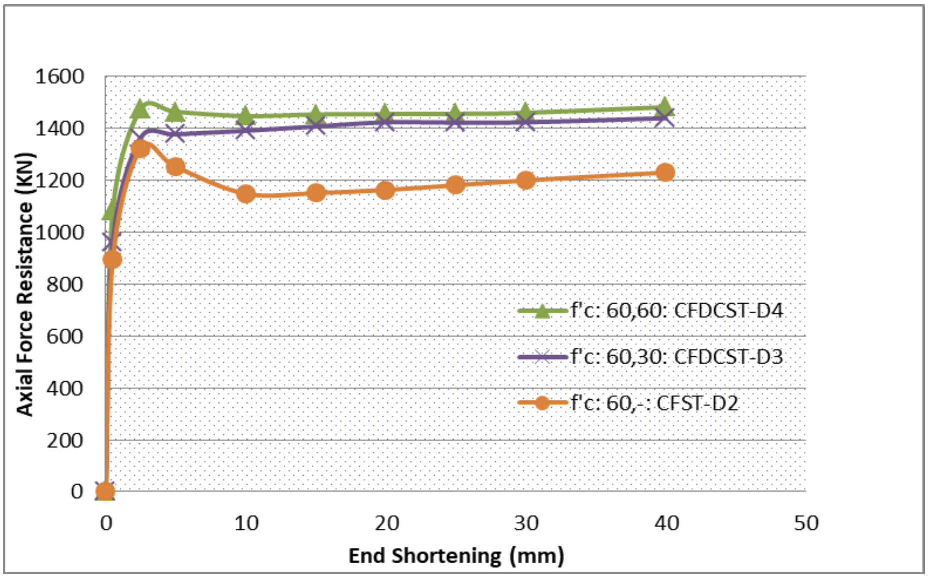

Figure 29: Effect of core concrete strength variation with high strength sandwich concrete

Figure 30 also shows the load-displacement curve under the effect of variation in the core concrete grade of CFDCST columns with low sandwich concrete strength. Improvement in the core concrete strength results in a 5.82% increment in the load-carrying capacity of CFDCST-D2 from that of the CFDCST-D1 column.

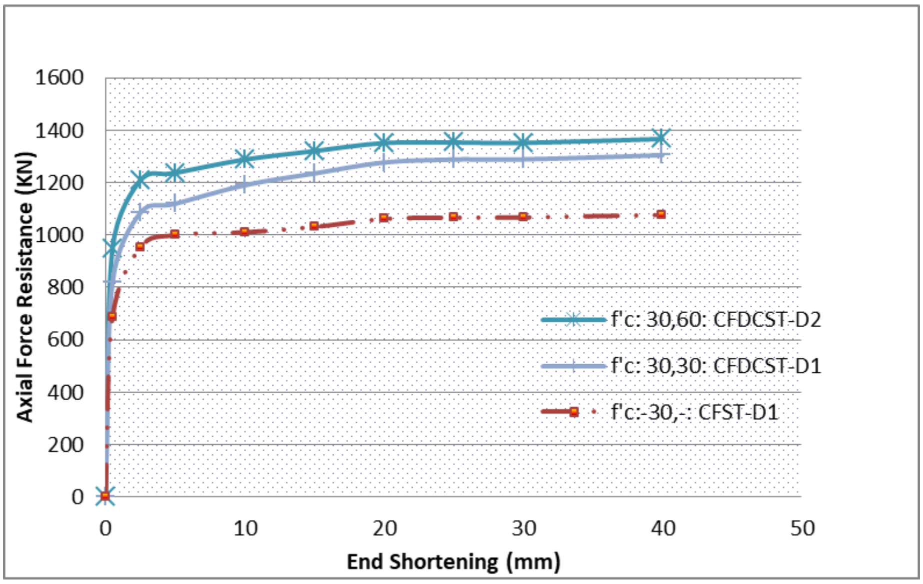

Figure 30: Effect of core concrete strength variation with low strength sandwich concrete

Change in the concrete grade of CFST and CFDCST columns from 30 MPa to 60 MPa shows parallel translation except for its closeness on high strength concrete grades. As the concrete strength becomes very higher and if there is a relatively weaker dual confinement effect, then the ultimate load-carrying capacity of the CFDCST columns shows little difference from the corresponding CFST columns. However, there will be no immediate failure in CFDCSTs due to the presence of an internal steel tube. Therefore, the strength of material selection in structural designs has to consider the dual interaction of both steel tubes and concrete strength.

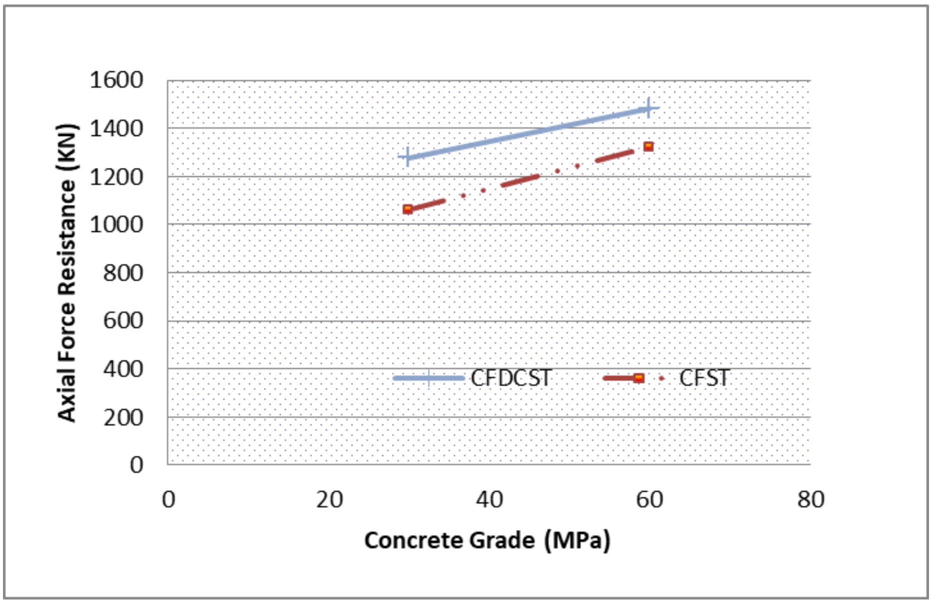

Figure 31: Concrete grade versus axial force resistance of CFST and CFDCST columns

CFST column failure mode tends to develop greater lateral displacement at an average height of the column relative to the corresponding CFDCST column. The presence of an internal steel tube in the CFDCST columns restricts lateral expansion of the concrete as shown in figure 32.

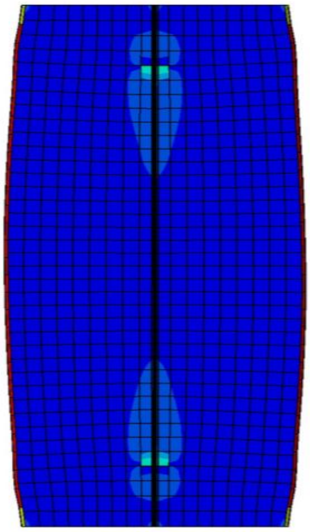

(a). CFST-D2 column

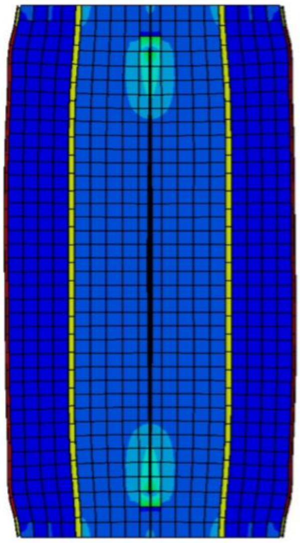

(b). CFDCST-D2 column

Figure 32: Failure mode of CFST-D2 and CFDCST-D2 columns

In figure 33, axial and lateral displacement of CFST-D2 and CFDCST-D2 columns is shown and in the mid height of the columns, lateral displacement of 5.7mm and 3.02mm were recorded respectively for CFST-D2 and CFDCST-D2 columns at 40mm axial displacement.

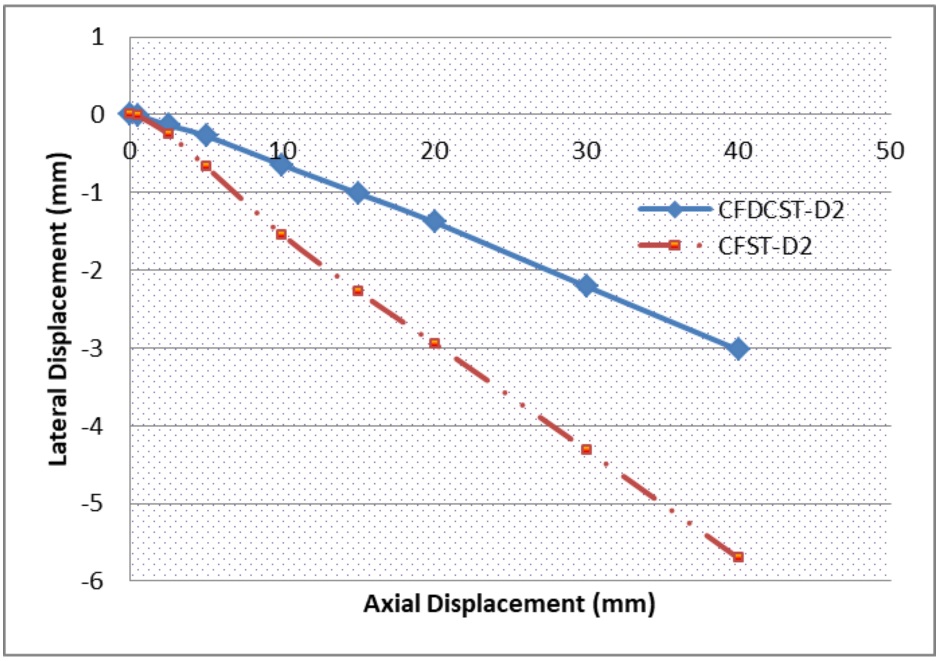

Figure 33: Axial displacement versus lateral expansion

5.3.5 Section-E (Variation in steel strength)

Steel tube yield strength of 275 and 460 MPa were used to study the change in the structural response of CFST and CFDCST columns where concrete strength and other geometrical properties were kept fixed. To magnify the effect of steel tube strength, external steel tube thickness was limited to a smaller value of 3.2mm. FE analyses of CFST columns show that increasing the external steel tube strength from 275 MPa to 460 MPa results in a 31.03% improvement in the peak load resistance. Similarly, on CFDCST columns, 35.64% load increment is shown with strengthening both external and internal steel tubes from 275 to 460MPa.

Model Column ID	FE Model: $-\ D_{ext} = 139.7mm, t_{ext} = 3.2mm,\ D_{int} = 76.1mm, t_{int} = 3mm,\ f'_{c,sw} = f'_{c,core} = 30MPa$		FE Analysis Result	
	$f_{y,ext}$ (MPa)	$f_{y,int}$ (MPa)	Peak Load N_{FEA} (KN)	Deflection at peak load δ_{FEA} (mm)
CFST-E1	275	-	969.25	20
CFST-E2	460	-	1270.02	13.26
CFDCST-E1	275	275	1191.40	20
CFDCST-E2	275	460	1349.43	20
CFDCST-E3	460	275	1457.37	20
CFDCST-E4	460	460	1616.07	20

Table 13: Analysis result of section-E specimens

Results from Table 13 show that the ultimate load-carrying capacity of both CFST and CFDCST columns highly increases with an increase in the yield strength of steel tubes. CFDCST-E1 and CFDCST-E2 can be seen as modified categories of CFST-E1 column with the insertion of 275 and 460 MPa internal steel tubes and results in 22.92% and 39.22% load increment. Similarly CFDCST-E3 and CFDCST-E4 shows 14.75% and 27.25% load increment from their corresponding column CFST-E2. This clearly shows how the internal steel tube behaves or interacts with different external steel tube strengths; for reduced external steel tube strength, the influence of the internal steel tube becomes more visible.

In figure 34, the load vs. axial deflection curves of all specimens shows continuous stress hardenings except CFST-E2 column in which relatively higher strength of steel (460MPa) was used and results in attaining peak load early at 13.26mm axial displacement and develops gradual decrement in its load-displacement response.

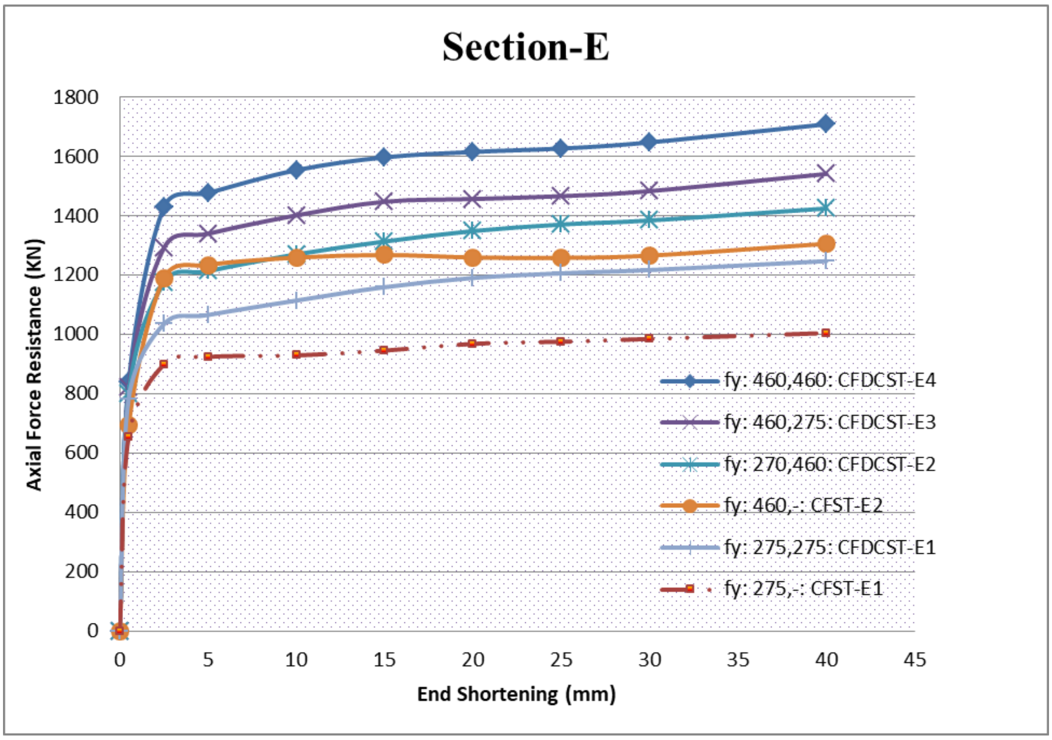

Figure 34: Effect of variation in steel-grades

Alteration of steel tube's strength from 275 MPa to 460 MPa shows a parallel translation between CFST and CFDCST columns except for their closeness for lower strength steel tubes as shown in figure 35. This directive also indicates the dual confinement effect in CFDCSTs becomes larger for high strength steel tubes. Moreover, it shows that within the interaction of low strength steel tubes and relatively high strength concrete, the effect of concrete strength becomes vital in determining the ultimate load-carrying capacity, which may result in a closer outcome between CFST and CFDCST column's resistance.

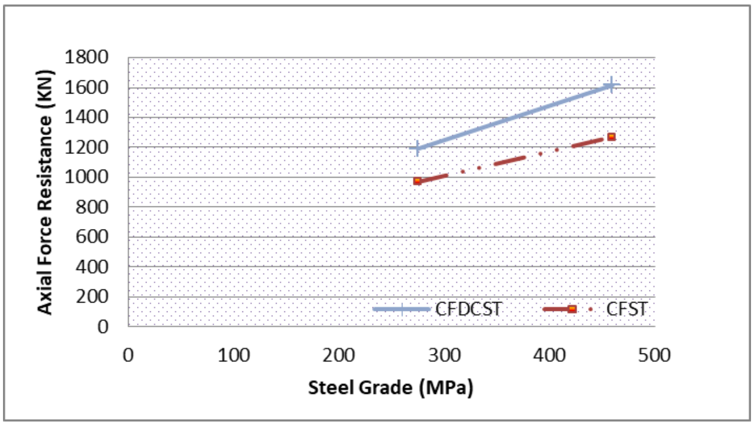

Figure 35: Steel grade versus axial force resistance of CFST and CFDCST columns

5.3.6 Section-F (Variation in the height of the column)

The effect of variation in height also referred to the effect of relative slenderness in the case of CFST and CFDCST columns. This effect is not crucial in the case of short columns or even the effect can be ignored. For example, Eurocode-4 ignores the effect for columns having relative slenderness lower than 0.2; but for higher slenderness ratios, the code recommends a reduction in the plastic resistance of the cross-sections to be considered in referring to the European buckling curves. In this section, the basic concept is to check short CFDCST columns if the effect of change in relative slenderness could have a serious effect on their ultimate load-bearing capacity in comparison with CFST columns. Therefore, relative slenderness lowers than 0.3 was used and simulated with similar cross-sectional properties.

Model Column ID	FE Model: $- D_{ext} = 114.3mm, t_{ext} = 3.6mm,\ D_{int} = 76.1mm, t_{int} = 3mm,\ f'_{c,sw} = f'_{c,core} = 30MPa\ f_{y,ext} = f_{y,int} = 355MPa$		FE Analysis Result	
	Height (mm)	Relative Slenderness $(\bar{\lambda})$	Peak Load N_{FEA} (KN)	Deflection at peak load: δ_{FEA} (mm)
CFST-F1	238	0.086	935.13	11.41
CFST-F2	357	0.129	928.47	17.62
CFST-F3	476	0.171	927.82	22.68
CFST-F4	714	0.257	852.10	18.65
CFDCST-F1	238	0.092	1195.57	10.95
CFDCST-F2	357	0.139	1188.38	18.03
CFDCST-F3	476	0.185	1166.18	20.78
CFDCST-F4	714	0.277	996.71	20.9

Table 14: Analysis result of section-F specimens

Specimen's height of both CFST and CFDCST columns were taken to be the same. However, relative slenderness values of CFDCST columns are slightly higher due to the increased cross-sectional resistance ($N_{pl,Rk}$) of the columns following the replacement of some concrete portions with an internal steel tube. Therefore, CFDCST columns tend to be more influenced by the effect of relative slenderness. As shown in table 14, the reduction in the plastic resistance of CFDCST columns becomes 16.63% as the specimen height stretched from 238mm to 714mm; for the same material property and diminished heights, CFST columns only possess an 8.88 % reduction in their plastic resistance which is comparatively very small. It also has to be noted that this difference closely relates to the steel contribution ratio (δ), for example: - $\delta_{CFST-F4} = 0.74$ and $\delta_{CFDCST-F4} = 0.85$; the larger the steel's contribution, the more it becomes susceptible to the effect of relative slenderness ratio.

Note: - steel contribution ratio (δ) calculated as per the Eurocode-4 using partial safety factors of 1.0 and 1.5 for steel and concrete materials respectively.

Figures 36 and 37 also show the effect of the short column's relative slenderness ratio in the axial load-bearing capacity of CFST and CFDCST columns respectively.

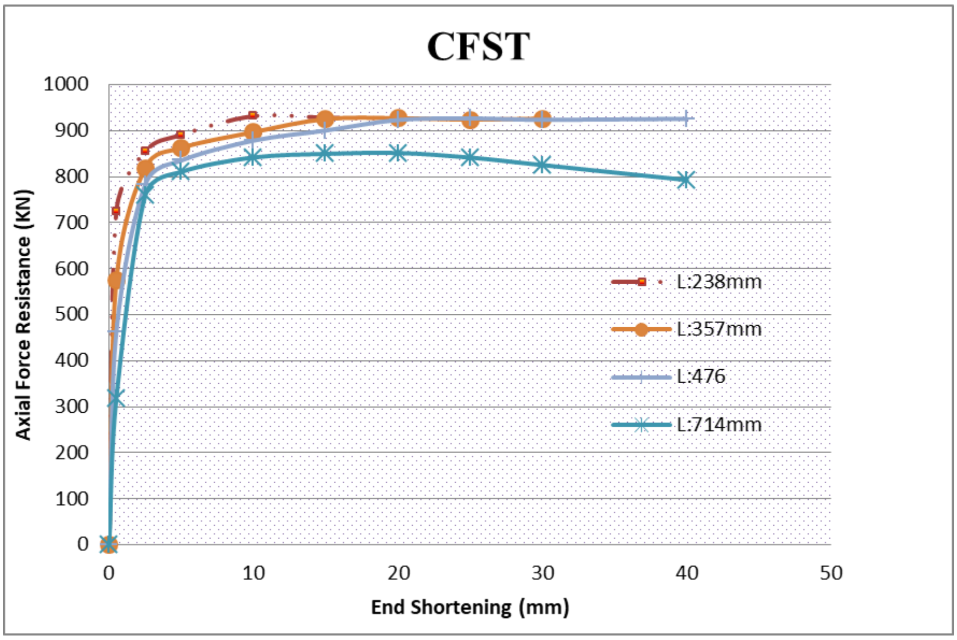

Figure 36: Effect of change in column Length on CFST short columns

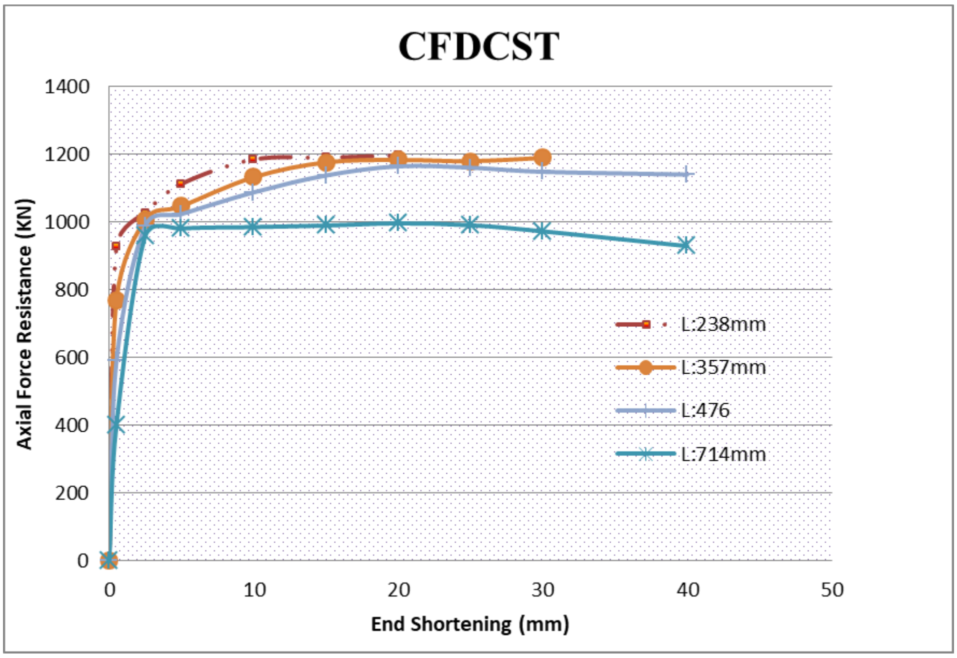

Figure 37: Effect of change in column Length on CFDCST short columns

From figure 38, it is possible to realize how short columns are less affected by the change in the relative slenderness ratios; but CFST columns develop a gradual fall in their load-bearing capacity for the increased relative slenderness ratio after the value of 0.2 in comparison with CFDCST columns. Similarly, Eurocode-4 recommends the effect of the column's relative slenderness to be considered only for ratios beyond 0.2.

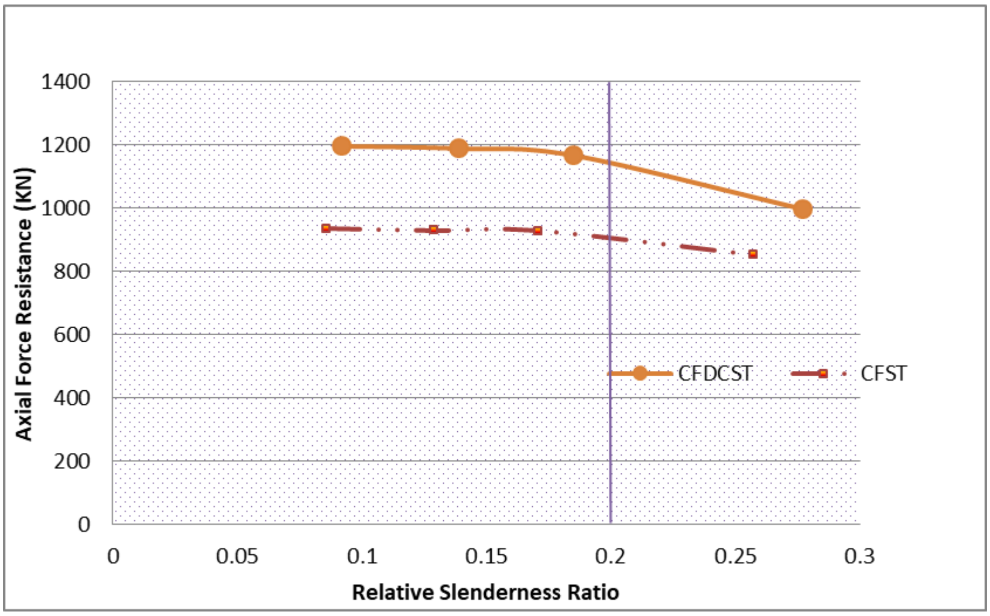

Figure 38: Effect of relative slenderness on axial force resistance of CFST and CFDCST columns

5.3.7 Section-G (Variation in the internal steel tube D/t ratio and materials strength)

The effect of variation in the internal steel tube D/t ratio together with the change in the material's strength was studied under this section including the application of controlled steel and concrete cross-sectional areas. As conducted in the above test results; for fixed tube thicknesses, the increase in the internal steel tube diameter is clearly shown to have a positive influence on the axial load carrying capacity of a short column, this is because for large internal steel tube diameter the area coverage of the dual confinement increases in shielding larger cross-sectional areas. However, concerning its application, increased diameters of internal steel tubes create difficulties during sandwich concrete placement, as the two steel tubes get closer to each other. Therefore, there must be a minimum space to permit easy placement and compaction. Internal steel tubes of larger diameter also have higher costs in comparison with smaller diameter steel tubes, thus it is required to exploit how to enhance the capacity of CFDCST columns with the use of lower internal steel tube diameters, and it is discussed in the first part of this section. However, this study has to be limited to short columns study only, in the case of slender sections; different analogy regarding the moment of inertia has to be studied.

Similar cross-sectional areas of external and internal steel tubes that confines nearly equal areas of sandwich and core concrete with the change in material’s strength are also discussed in the second part of this section to recognize individual materials response of a CFDCST column.

5.3.7.1 Part-one (Strength enhancement of CFDCSTs with a reduced internal steel tube diameter)

CFDST Column ID (Part-1)	FE Model: $-$ $D_{ext} = 177.8mm, t_{ext} = 4.5mm, f'_{c,sw} = 30MPa,\ f_{y,ext} = 300MPa$				FE Analysis Result
	D_{int} (mm)	t_{int} (mm)	$f'_{c,core}$ (MPa)	$f_{y,int}$ (MPa)	Peak Load N_{FEA} (KN)
CFDCST-G1	139.7	3	30	235	2100.81
CFDCST-G2	101.6	3	30	235	2022.39
CFDCST-G3	101.6	3	30	355	2167.21
CFDCST-G4	101.6	3	60	235	2147.37
CFDCST-G5	101.6	4.5	30	235	2123.96
CFDCST-G6	60.3	3	30	460	2061.24
CFDCST-G7	60.3	4.5	30	460	2174.41

Table 15: Analysis result of section-G (part-1) specimens

Note: - Peak loads of section-G (part-1) FE analyses were taken at 5% strain.

In section-G (part 1), three improvement techniques were chosen, the first is to increase the internal steel tube strength, the second focused only on maximizing the core concrete strength and the last is to increase the internal steel tube thickness. In all three cases, the area of core concrete enclosed with 60.3 mm and 101.6 mm internal steel tube diameter compared with CFDCST-G1 column specimen having internal steel tube diameter equals 139. 7 mm. It can also be expressed as 66.09%, 42.86%, and 21.43% reduction in the external to internal steel tube diameter were considered with varied material's strength and tube thicknesses. And it is found that increasing the ultimate load-carrying capacity of the CFDCST column is easily possible with lower diameter steel tubes through increasing internal steel tube strength, thickness, or core concrete strength.

In comparing CFDCST-G1 with CFDCST-G2, a 3.73% ultimate load-carrying capacity decrement observed in CFDCST-G2 due to a 27.27% reduction in the internal steel tube diameter from 139.7mm to 101.6 mm where the external steel tube remains the same ($D_{ext} = 177.8mm$). Therefore, with such decrements in the inner steel tube diameter, CFDCST-G3 were treated with increased steel tube strength ($f_{y,int} = 355MPa$), which is 51.06% strength modification from the reference model CFDCST-G1 and the result shows a 3.16% increment in the load-carrying capacity. Similarly, in CFDCST-G4 core concrete strength was twice the capacity of the reference model and results to have 2.22% axial load increment. Thicker internal steel tube section with 50% increment as in the case of CFDCST-G5 also shows a 1.1% modification in the load-carrying capacity. Therefore, it can be concluded that 51.06% increments in the internal steel tube strength most effectively compensate for the 27.27% reduction in the internal steel tube diameter.

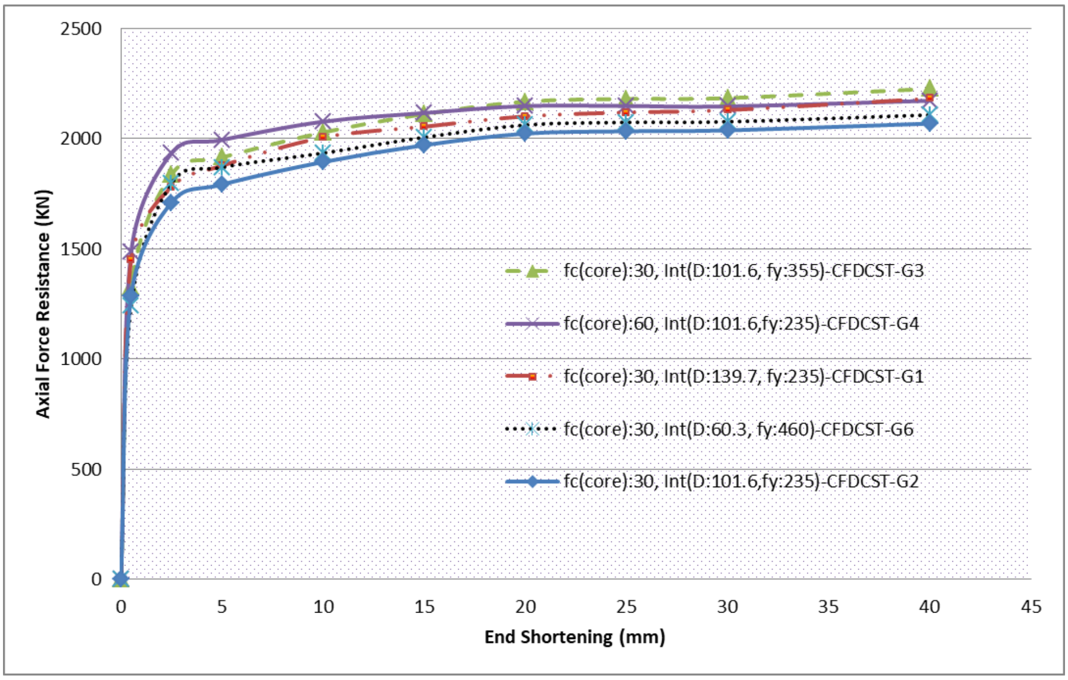

Figure 39: Effect of variation in internal steel tube and core concrete properties

In figure 39, it is clearly shown that increasing the core concrete strength develops very efficient early post yielding behaviors. For comparison, at 1.25% of axial strain (5mm axial displacement), the increase in load-carrying capacity of CFDCST-G4 with higher core concrete strength shows a 4% increment than the CFDCST-G3 column which was with a modification in the internal steel tube strength. However, in the late response CFDCST-G3 column develops an exceeding load increment from that of the CFDCST-G4 column. This occurrence effectively expresses how the confinement in short columns works; the encased concrete predominantly resists the upcoming axial load in its full capacity until it reaches its limit, and beyond its ultimate load-carrying capacity the performance of the column becomes dependent on the steel tube properties. This is clearly shown in figure 39, as most of the stress-strain diagrams show a linear increment until reaching a 5% strain, and it follows an extended strain before developing the stage of stress hardening due to the effect of confinement. This is also an important instance to show how the existence of an internal steel tube alters the axial performance of a CFDCST column not just like the way the internal longitudinal and transversal reinforcements act as considered in the Eurocodes-4, but it is in the form of creating a dual confinement effect on the encased core concrete.

Further CFDCST-G6 and G7 were simulated with a 56.84% reduction in the internal steel tube diameter from that of the reference column CFDCST-G1. However, CFDCST-G6 could not be effective with the 95.74% increment in the internal steel tube strength from 235 MPa to 460 MPa. Increasing both thickness and strength of the internal steel tube as in the case of column CFDCST-G7 develop a maximum increment of 3.5% in the load-carrying capacity while CFDCST-G5 which was with thickness improvement only shows 1.1% increment as compared with CFDCST-G1. These also indicate that very small internal steel tubes with higher material strength and thickness (lower D/t ratio) could replace the use of larger diameter internal steel tubes.

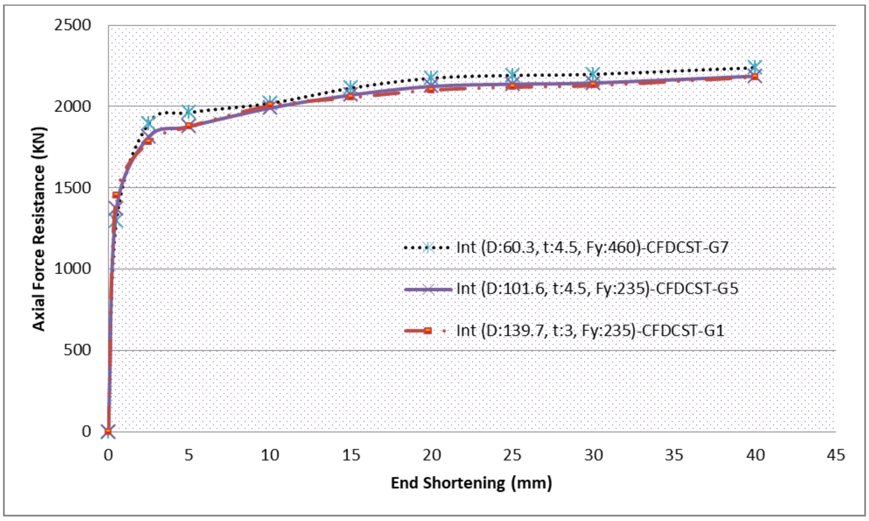

Figure 40: Effect of variation in the internal steel tube properties

5.3.7.2 Part-Two (Distinct impact of a similar area covering constituent materials of a CFDCST column)

CFDST Column ID (Part-2)	FE Model: $-$ $D_{ext} = 145mm, t_{ext} = 3.2mm, D_{int} = 102mm, t_{int} = 4.7mm$				Peak Load N_{FEA} (KN)
	$f'_{c,sw}$ (MPa)	$f'_{c,core}$ (MPa)	$f_{y,ext}$ (MPa)	$f_{y,int}$ (MPa)	
CFDCST-G8	30	60	355	355	1881.84
CFDCST-G9	60	30	355	355	1876.10
CFDCST-G10	30	30	355	460	1919.28
CFDCST-G11	30	30	460	355	1891.58
CFDCST-G12	60	30	235	460	1874.16
CFDCST-G13	30	60	460	235	1812.79

Table 16: Analysis result of section-G (part-2) specimens

In this second part of section-G, variation in materials strength was studied with an approximately comparable cross-sectional area of sandwich and core concrete equals 6916 mm^2 and 6735 mm^2 respectively and the cross-sectional area of core concrete only reduced by 181 mm^2 from the area covered by sandwich concrete. A similar area of external and internal steel tubes equivalent to 1426 mm^2 and 1437 mm^2 were considered correspondingly through rearranging the diameter and thickness of steel tubes.

Relatively higher core concrete and weaker sandwiched concrete strength contained in the CFDCST-G8 model specimen. However, CFDCST-G9 constituted with reversed concrete grades. The results of both models show a very close response in which the peak load for higher core concrete exceeds only 0.31%.

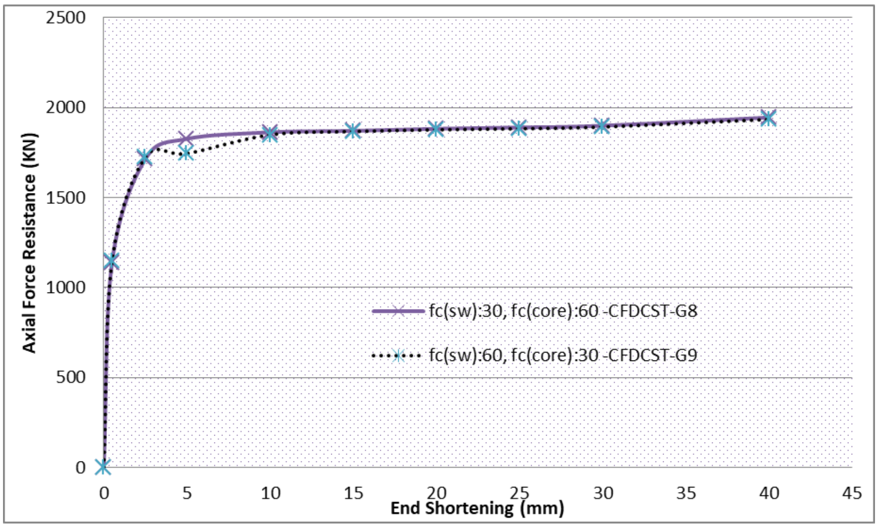

Figure 41: Effect of variation in the sandwiched and core concrete grades

Effect of variation in the strength of steel tubes having very similar areas of external and internal steel tubes analyzed in CFDCST-G10 and CFDCST-G11 columns. Analyses results of both models show approximately similar responses only with a 1.5% increment in the peak load of the model with higher internal steel tube strength.

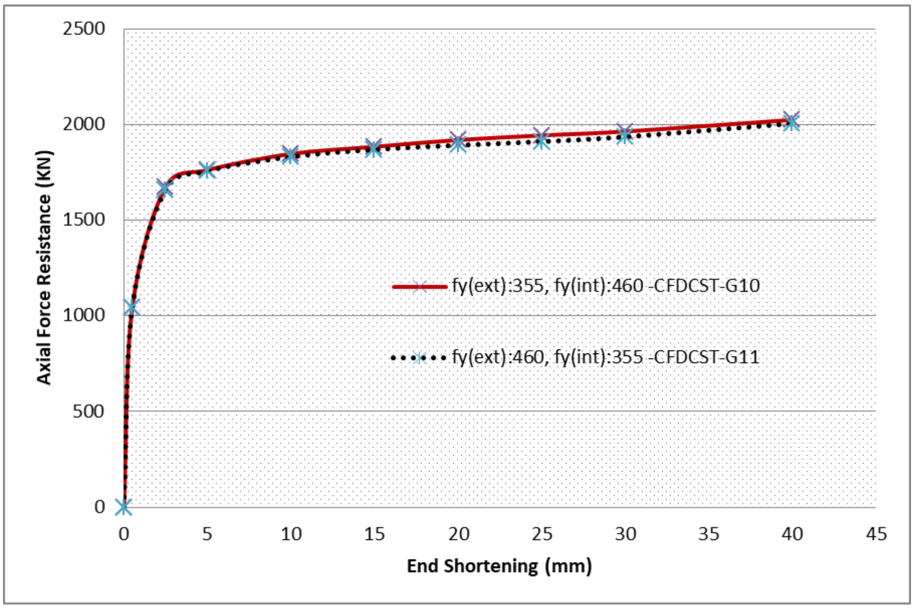

Figure 42: Effect of variation in the external and internal steel tube grades

In column models of CFDCST-G12, higher sandwich concrete and internal steel tube grade were constituted whereas in CFDCST-G13 higher core concrete and external steel tube strength were adopted. The result shows a 3.4% increment in the peak load of the CFDCST-G12 column specimen and it is graphically represented in figure 43.

In the above comparison of CFDCST-G8 and G9, it is possible to conclude that higher core concrete strength shows extra performance in axial load capacity than stiffened sandwich concrete of similar area. Similarly, from CFDCST-G10 and G11 columns, it is shown that stiffened internal steel tubes somehow develop additional axial resistance. CFDCST-G12 column with higher internal steel tube strength and stiffer sandwich concrete also shows a better performance than that of the CFDCST-G13 column. This increment in the force-resisting tendency may develop from the stiff surrounding actions of internal steel tube and sandwich concrete toward the core concrete of a CFDCST column.

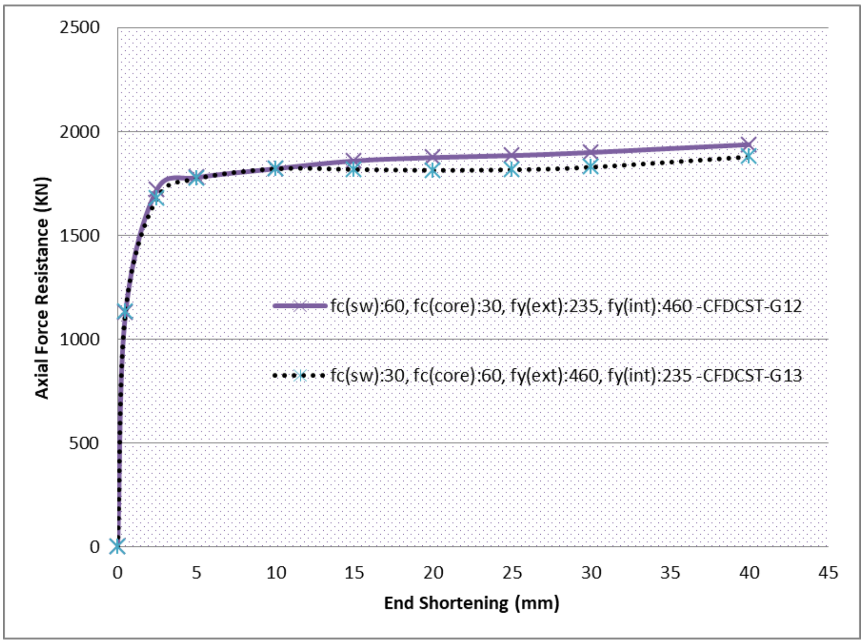

Figure 43: Effect of strength grade variations on concrete and steel tubes

5.4 Eurocode-4 based numerical estimations and FE analyses results

In this section, the cross-sectional resistance obtained from the Eurocode-4 (N_{EC-4}) is compared with the FE analysis result of 58 model specimens. Steel and concrete material's partial safety factors equal to 1.0 and 1.5 were used respectively in accordance with EN 1993-1-1, 6.1(1), and EN 1992-1-1, (2.4.2.4).

The design resistance computed using Eurocode-4 somehow shows a conservative approach in estimating the finite element analysis results of both columns; however, the code's estimation made for CFDCST columns has a mean value slightly better than the CFSTs and comparably less variance is shown. This in general assures the code's formulation procedure for CFST column's design does not have an extreme gap in determining the design tendencies of CFDCSTs. However, the clear gap in the code for excluding the double confinement effect is shown in table 17 of section-G columns (CFDCST-G8 and CFDCST-G9). In these columns, an approximately comparable cross-sectional area of sandwich and core concrete equals 6916 mm^2 and 6735 mm^2 respectively were used with a similar area of external and internal steel tubes equivalent to 1426 mm^2 and 1437 mm^2 as shown in section 5.3.7.8 of this paper. Here the peak load obtained from the Eurocode-4 shows that CFDCST-G9 with a higher sandwich and lower core concrete strength possess better tendency than the CFDCST-G8 column which is with a lower sandwich and higher core concrete strength through following the cross-sectional area to strength distribution of short columns. However, the FE analysis shows a reverse outcome due to the effect of double confinement resulted in increasing the core concrete strength of the CFDCST-G8 column.

Model Column ID	**Peak Load Result**		**Variation**	**Model Column ID**	**Peak Load Result**		**Variation**
	Peak Load N_{FEA} (KN)	N_{EC-4} (KN)	$\frac{N_{EC-4}}{N_{FEA}}$		Peak Load N_{FEA} (KN)	N_{EC-4} (KN)	$\frac{N_{EC-4}}{N_{FEA}}$
CFST-A1	1702.72	1219.50	0.72	CFDCST-D2	1350.98	980.25	0.73
CFDCST-A1	1870.53	1346.31	0.72	CFDCST-D3	1383.29	1083.64	0.78
CFDCST-A2	1909.48	1382.09	0.72	CFDCST-D4	1482.89	1156.95	0.78
CFDCST-A3	1954.13	1411.44	0.72	CFST-E1	969.25	688.71	0.71
CFDCST-A4	1993.39	1440.92	0.72	CFST-E2	1270.02	993.71	0.78
CFDCST-A5	2038.05	1470.78	0.72	CFDCST-E1	1191.40	854.18	0.72
CFDCST-A6	2098.70	1531.59	0.73	CFDCST-E2	1349.43	976.49	0.72
CFDCST-A7	2107.49	1544.45	0.73	CFDCST-E3	1457.37	1154.04	0.79
CFST-B1	1078.64	745.26	0.69	CFDCST-E4	1616.07	1274.24	0.79
CFST-B2	1470.73	1113.54	0.76	CFST-F1	935.13	715.50	0.77
CFST-B3	1929.49	1467.44	0.76	CFST-F2	928.47	682.28	0.73
CFST-B4	2349.79	1806.81	0.77	CFST-F3	927.82	653.25	0.70
CFST-B5	2800.73	2131.81	0.76	CFST-F4	852.10	600.06	0.70
CFST-B6	3194.88	2442.73	0.76	CFDCST-F1	1195.57	927.35	0.78
CFDCST-B1	1414.55	1050.23	0.74	CFDCST-F2	1188.38	895.86	0.75
CFDCST-B2	1849.83	1409.61	0.76	CFDCST-F3	1166.18	868.88	0.75
CFDCST-B3	2290.50	1755.83	0.77	CFDCST-F4	996.71	814.13	0.82
CFDCST-B4	2725.38	2088.19	0.77	CFDCST-G1	2100.81	1558.59	0.74
CFDCST-B5	3074.90	2406.61	0.78	CFDCST-G2	2022.39	1481.90	0.73
CFDCST-B6	3476.98	2711.23	0.78	CFDCST-G3	2167.21	1588.87	0.73
CFST-C1	1929.49	1467.44	0.76	CFDCST-G4	2147.37	1617.26	0.75
CFDCST-C1	2118.1	1613.51	0.76	CFDCST-G5	2123.96	1570.18	0.74
CFDCST-C2	2290.50	1755.83	0.77	CFDCST-G6	2061.24	1518.81	0.74
CFDCST-C3	2514.12	1894.26	0.75	CFDCST-G7	2174.41	1621.35	0.75
CFDCST-C4	2614.66	2028.66	0.78	CFDCST-G8	1881.84	1452.88	0.77
CFDCST-C5	2757.12	2158.97	0.78	CFDCST-G9	1876.10	1457.71	0.78
CFDCST-C6	2877.82	2285.09	0.79	CFDCST-G10	1919.28	1470.18	0.77
CFST-D1	1061.44	743.75	0.70	CFDCST-G11	1891.58	1499.53	0.79
CFST-D2	1323.17	1002.58	0.76	CFDCST-G12	1874.16	1403.09	0.75
CFDCST-D1	1276.67	907.81	0.71	CFDCST-G13	1812.79	1461.26	0.81
Peak load result variation of Eurocode-4 based computations and FE analyses of CFST columns							
				Mean value	0.74		
				Standard deviation	0.029		
Peak load result variation of Eurocode-4 based computations and FE analyses of CFDCST columns							
				Mean value	0.76		
				Standard deviation	0.027		

Table 17: FE analyses and Eurocode-4 based ultimate axial strength estimations

CHAPTER-6 Conclusion and Recommendation

6.1 Conclusion

This research targets to exploit the axial load performance of short CFDCST columns in relation to CFST columns. The effect of cross-sectional and materials' strength variation primarily investigated using finite element modeling and the following fundamental aspects are concluded.

- The influence and effect of the external steel tube and the core concrete strength of a CFST column tremendously diminished by the actions of the internal steel tube in the CFDCST column. The insertion of an internal steel tube has a great influence to tolerate the reduction in the load response due to the variation in the external D/t ratios. Furthermore, increasing the internal steel tube diameter to a certain extent has an advantage in modifying the ultimate load-bearing capacity of CFDCST columns due to the increment of steel contributions and improvements in the effective area coverage of the dual confinement.

- To utilize the most structural benefits of CFDCSTs, it is importantly required to enhance the confinement tendency of the columns through the modification in the steel tubes' property. However, increment in steel strength has to be within the recommended range according to EC-4 (S6.7.1) and the cross-sectional diameter and thickness arrangement should favor the increment in confinement tendencies with overcoming local buckling effects.

- The strength of materials selection in the structural design of CFDCST short columns has to consider the interaction compatibility of both steel tubes and concrete strengths. The dual confinement effect in CFDCSTs becomes larger for high strength steel tubes and come to be a governing factor for providing the highest contribution in the system's response. On the other hand, within the interaction of low strength steel tubes and relatively high strength concrete, the effect of concrete strength on the system's response becomes vital that results in a closer outcome between CFST and CFDCST columns.

6.2 Recommendation

The technique developed as part of this study may further be improved with the fulfillment of the following requirements.

- A variety of experimentally conducted short CFDCST columns may further be used to rearrange and extend the methods developed under this study.
- The FE analysis could be advanced in using highly refined models that precisely express the material's combined plastic nature.

This research may also be extended to understand the full axial nature of the CFDCST columns in terms of the following two basic aspects.

- This FE modeling technique could be rearranged and developed to analyze intermediate and slender CFDCST columns.
- It is also important to extend this research in conducting the CFDCST column's fire resistance tendency.

REFERENCE

Abbas, Y.R. (2017). Nonlinear finite element analysis to the circular CFST stub columns. Procedia engineering, 173, pp.1692-1699.

Abdalla, S.H. (2012). Behavior of Concrete Filled Steel Tube (CFST) Under Different Loading Conditions (Doctoral dissertation).

ACI. (1999). Building code requirements for structural concrete and commentary. ACI 318-99, Detroit.

Alatshan, F., Osman, S. A., Mashiri, F., and Hamid, R. (2020). Explicit Simulation of circular CFST stub columns with external steel confinement under axial compression. Materials, 13(1), 23.

Alejano, L.R. and Bobet, A. (2012). Drucker–prager criterion. In The ISRM Suggested Methods for Rock Characterization, Testing and Monitoring: 2007-2014 (pp. 247-252). Springer, Cham.

Bathe, Klaus-Jürgen. (1996). Finite Element Procedures, 2nd ed. Pearson Education, New Jersey, US.

Binici, B. (2005). An analytical model for stress–strain behavior of confined concrete. Engineering structures, 27(7), pp.1040-1051.

Candappa, D.C., Sanjayan, J.G. and Setunge, S. (2001). Complete triaxial stress-strain curves of high-strength concrete. Journal of Materials in Civil Engineering, 13(3), pp.209-215.

De Nicolo, B., Pani, L. and Pozzo, E. (1994). Strain of concrete at peak compressive stress for a wide range of compressive strengths. Materials and Structures, 27(4), pp.206-210.

Dere, Y. and Koroglu, M.A. (2017). Nonlinear FE modeling of reinforced concrete. International Journal of Structural and Civil Engineering Research, 6(1), pp.71-74.

Du, G., Andjelic, A., Li, Z., Lei, Z. and Bie, X. (2018). Residual axial bearing capacity of concrete-filled circular steel tubular columns (CFCSTCs) after transverse impact. Applied Sciences, 8(5), p.793.

Ekmekyapar, T. and Al-Eliwi, B.J. (2017). Concrete filled double circular steel tube (CFDCST) stub columns. Engineering Structures, 135, pp.68-80.

Ellobody, E. and Young, B. (2011). Numerical simulation of concrete encased steel composite columns. Journal of Constructional Steel Research, 67(2), pp.211-222.

EN 1993-1-5:2006 Eurocode 3-Design of Steel Structures, Part 1.5: Plated structural elements, CEN - European committee for Standardization, Brussels (Belgium).

EN, B. (2008). 1090-2 (2008): Execution of Steel Structures and Aluminum Structures – Part 2:2. Technical Requirements for Steel Structures.

Espinos, A., Romero, M.L. and Hospitaler, A. (2012). Finite element analysis of fire behavior of concrete filled circular hollow section columns. Technical sheet 1 European Project FRISCC–Fire Resistance of Innovative and Slender Concrete Filled Tubular Composite Columns.

Eurocode 2. (2004): Design of concrete structures - Part 1-1: General rules and rules for buildings. BS EN 1992-1-1, British Standards Institution, London, UK.

Eurocode 3 (2004): Design of steel structures- Part 1-5: Plated structural elements. BS EN 1993-1-5, British Standards Institution, London, UK.

Eurocode 3 (2005): Design of steel structures- Part 1-1: General rules and rules for buildings. BS EN 1993-1-1, British Standards Institution, London, UK.

Eurocode 4 (2004): Design of composite steel and concrete structures. Part 1.1, General rules and rules for buildings. BS EN 1994-1-1, British Standards Institution, London, UK.

Furlong, R.W. (1967). Strength of steel-encased concrete beam columns. Journal of the Structural Division, 93(5), pp.113-124.

Giakoumelis, G. and Lam, D. (2004). Axial capacity of circular concrete-filled tube columns. Journal of Constructional Steel Research, 60(7), pp.1049-1068.

Goel, T. and Tiwary, A.K.. (2018). Finite element modelling of circular concrete filled steel tube (CFST). Indian Journal of Science and Technology, 11, p.34.

Hafezolghorani, M., Hejazi, F., Vaghei, R., Jaafar, M. S. B., and Karimzade, K. (2017). Simplified damage plasticity model for Concrete. Structural Engineering International, 27(1), 68-78.

He, L., Lin, S. and Jiang, H. (2019). Confinement effect of concrete-filled steel tube columns with infill concrete of different strength grades. Frontiers in Materials, 6, p.71.

Hu, H.T., Huang, C.S., Wu, M.H. and Wu, Y.M. (2003). Nonlinear analysis of axially loaded concrete-filled tube columns with confinement effect. Journal of Structural Engineering, 129(10), pp.1322-1329.

Huang, C.S., Yeh, Y.K., Liu, G.Y., Hu, H.T., Tsai, K.C., Weng, Y.T., Wang, S.H. and Wu, M.H. (2002). Axial load behavior of stiffened concrete-filled steel columns. Journal of Structural Engineering, 128(9), pp.1222-1230.

Imran, I. and Pantazopoulou, S.J. (1996). Experimental study of plain concrete under triaxial stress. ACI Materials Journal-American Concrete Institute, 93(6), pp.589-601.

Jamet, P., Millard, A. and Nahas, G. (1984). Triaxial behaviour of a micro-concrete complete stress-strain curves for confining pressures ranging from 0 to 100 MPa (No. CEA-CONF--7303). CEA Centre d'Etudes Nucleaires de Saclay.

Ji, J., Yu, D., Jiang, L., Zhang, S., and Yang, M. (2018). Numerical Analysis of Axial Compression Performance of Concrete Filled Double Steel Tube Short Columns. MS and E, 439(4), 042058.

Jönsson, J. and Stan, T.C. (2017). European column buckling curves and finite element modelling including high strength steels. Journal of Constructional Steel Research, 128, pp.136-151.

Laim, L.M.S., Rodrigues, J.P., Correia, A.M. and Pires, T.A. (2012). Numerical analysis of composite steel columns under fire conditions. Technical sheet 4 European Project FRISCC–Fire Resistance of Innovative and Slender Concrete Filled Tubular Composite Columns.

Lam, D., Dai, X.H., Han, L.H., Ren, Q.X. and Li, W. (2012). Behaviour of inclined, tapered and STS square CFST stub columns subjected to axial load. Thin-walled structures, 54, pp.94-105.

Lin, S., Zhao, Y.G. and He, L. (2018). Stress paths of confined concrete in axially loaded circular concrete-filled steel tube stub columns. Engineering Structures, 173, pp.1019-1028.

Mander, J.B., Priestley, M.J. and Park, R. (1988). Theoretical stress-strain model for confined concrete. Journal of structural engineering, 114(8), pp.1804-1826.

Michał, S. and Andrzej, W. (2015). Calibration of the CDP model parameters in Abaqus. In THE 2015 WOURLD CONGRESS ON ADVANCES IN STRUCTURAL ENGINEERING AND MECHANICS (ASEM15).

Mirza, S.A. and Lacroix, E.A. (2004). Comparative strength analyses of concrete-encased steel composite columns. Journal of Structural Engineering, 130(12), pp.1941-1953.

Musthafa, L., Rani, S. and KK, S. (2016). Study of Material Property of Concrete Filled Steel Tubular Columns. International Research Journal of Engineering and Technology, 3(9), pp. 189–195.

Pagoulatou, M., Sheehan, T., Dai, X. H., and Lam, D. (2014). Finite element analysis on the capacity of circular concrete-filled double-skin steel tubular (CFDST) stub columns. Engineering Structures, 72, 102-112.

Richart, F.E., Brandtzæg, A. and Brown, R.L. (1928). A study of the failure of concrete under combined compressive stresses. University of Illinois at Urbana Champaign, College of Engineering. Engineering Experiment Station.

Romero, M.L., Espinós, A., Portolés, J.M., Hospitaler, A. and Ibañez, C. (2015). Slender double-tube ultra-high strength concrete-filled tubular columns under ambient temperature and fire. Engineering Structures, 99, pp.536-545.

Saenz, L.P. (1964). Discussion of Equation for the Stress-Strain Curve of Concrete by Desayi and Krishnan. Journal of the American Concrete Institute, 61, pp.1229-1235.

Sakino, K., Nakahara, H., Morino, S. and Nishiyama, I. (2004). Behavior of centrally loaded concrete-filled steel-tube short columns. Journal of structural engineering, 130(2), pp.180-188.

Schaumann, P. and Kleiboemer, I. (2012). 3D-modelling of concrete-filled circular composite columns with embedded steel core in case of fire. Technical sheet 2 European Project FRISCC–Fire Resistance of Innovative and Slender Concrete Filled Tubular Composite Columns.

Schneider, S.P. (1998). Axially loaded concrete-filled steel tubes. Journal of structural Engineering, 124(10), pp.1125-1138.

Sfer, D., Carol, I., Gettu, R. and Etse, G. (2002). Study of the behavior of concrete under triaxial compression. Journal of engineering mechanics, 128(2), pp.156-163.

SIMULIA, 2018. ABAQUS/Standard Version 6.18 Analysis User’s Manual.

Smith, S.S., Willam, K.J., Gerstle, K.H. and Sture, S. (1989). Concrete over the top--or, is there life after peak?. Materials Journal, 86(5), pp.491-497.

Tao, Z., Wang, Z.B. and Yu, Q. (2013). Finite element modelling of concrete-filled steel stub columns under axial compression. Journal of Constructional Steel Research, 89, pp.121-131.

Wan, C.Y. and Zha, X.X. (2016). Nonlinear analysis and design of concrete-filled dual steel tubular columns under axial loading. Steel and Composite Structures, 20(3), pp.571-597.

Wang, W., Tang, Z., Li, Z. and Ma, H. (2016). Bearing capacities of different-diameter concrete-filled steel tubes under axial compression. Advances in Materials Science and Engineering, 2016.

Yadav, R. and Chen, B. (2017). Parametric Study on the Axial Behaviour of Concrete Filled Steel Tube (CFST) Columns. American Journal of Applied Scientific Research, 3(4), pp.37-41.

Yamamoto, T., Kawaguchi, J. and Morino, S. (2002). Experimental study of the size effect on the behavior of concrete filled circular steel tube columns under axial compression. Journal of Structural and Construction Engineering, (561), pp.237-244.

Zhao, Y.G., Lin, S., Lu, Z.H., Saito, T. and He, L. (2018). Loading paths of confined concrete in circular concrete loaded CFT stub columns subjected to axial compression. Engineering Structures, 156, pp.21-31.

APPENDIX A: Sandwich concrete strain hardening/softening rule

The stress-strain relationship of sandwich concrete can be classified into three stages and equations are provided based on the basic concept and formulation conducted in the CFST column's concrete property:

I. <u>First stage:</u> $(0 \le \varepsilon_{sw} \le \varepsilon_{\mathrm{co,sw}})$

$$\sigma_{sw} = \mathrm{f'}_{\mathrm{c,sw}}\left(\frac{\mathrm{k}_{sw} * \eta_{sw} - \eta_{sw}{}^{2}}{1 + (\mathrm{k}_{sw} - 2) * \eta_{sw}}\right) \tag{A.1}$$

$$\eta_{sw} = \varepsilon_{sw}/\varepsilon_{\mathrm{co,sw}} \tag{A.2}$$

$$\mathrm{k}_{sw} = 1.05 * \mathrm{E}_{\mathrm{cm,sw}} * \frac{\varepsilon_{\mathrm{co,sw}}}{\mathrm{f}'_{\mathrm{c,sw}}} \tag{A.3}$$

$$\varepsilon_{\mathrm{co,sw}} = 0.00076 + \sqrt{\left(0.626\mathrm{f'}_{\mathrm{c,sw}} - 4.33\right) * 10^{-7}}, \mathrm{E}_{\mathrm{cm.sw}} = 4700\sqrt{\mathrm{f'}_{\mathrm{c,sw}}} \tag{A.4}$$

($\mathrm{f}'_{\mathrm{c,sw}}$ and $\mathrm{E}_{\mathrm{cm,sw}}$ are in MPa)

II. <u>Second stage:</u> $(\varepsilon_{\mathrm{co,sw}} \le \varepsilon_{sw} \le \varepsilon_{\mathrm{cc\ sw}})$

The strain equation proposed for CFST short column is used to determine the corresponding strain in CFDCST columns.

$$\varepsilon_{\mathrm{cc,sw}} = \varepsilon_{\mathrm{co,sw}}\left(1 + \left(\frac{7.514\lambda_{\mathrm{sw}}\mathrm{P}_1^{0.81}}{\mathrm{f}'^{\,0.7}_{\mathrm{c,sw}}}\right)\right) \tag{A.5}$$

$$\mathrm{P}_1 = \frac{\sigma^{\mathrm{s}}{}_{\mathrm{ext}}(\mathrm{r}_1 - \mathrm{r}_2)}{\mathrm{r}_2} \tag{A.6}$$

$$\varepsilon_{\mathrm{c,sw}} = 0.00076 + \sqrt{\left(0.626\mathrm{f'}_{\mathrm{c,sw}} - 4.33\right) * 10^{-7}} \tag{A.7}$$

$$\lambda_{\mathrm{sw}} = \begin{cases} 0.66\eta'_{\mathrm{sw}}{}^{0.52} & , 0 \le \eta'_{\mathrm{sw}} \le 2.223 \\ 1.0, & , \eta'_{\mathrm{sw}} \ge 2.223 \end{cases} \tag{A.8}$$

External steel tube confinement coefficient:

$$\eta'_{\mathrm{sw}} = \frac{\left(2 * \mathrm{t}_{\mathrm{ext}} * \mathrm{f}_{\mathrm{y,ext}}\right)}{\left((\mathrm{D}_{\mathrm{ext}} - \mathrm{D}_{\mathrm{int}} - 2\mathrm{t}_{\mathrm{ext}}) * \mathrm{f'}_{\mathrm{c,sw}}\right) + \left((\mathrm{D}_{\mathrm{int}} - 2\mathrm{t}_{\mathrm{int}}) * \mathrm{f'}_{\mathrm{c,core}}\right)} \tag{A.9}$$

Based on the works of Hu et al. (2003) the equation for P_1 can be found using the following equations

$$P_1 = \begin{cases} f_{y,ext}\left(0.043646 - 0.000832\left(\frac{D_{ext}}{t_{ext}}\right)\right) \text{for } 21.7 \le \frac{D_{ext}}{t_{ext}} \le 47 \\ f_{y,ext}\left(0.006241 - 0.0000357\left(\frac{D_{ext}}{t_{ext}}\right)\right) \text{for } 47 \le \frac{D_{ext}}{t_{ext}} \le 150 \end{cases} \quad (A.10)$$

III. <u>Third stage:</u> $\varepsilon_{cc,sw} \le \varepsilon_{sw} \le \varepsilon_{cx,sw}$

$$\sigma_{sw} = f_{r,sw} + \left(f'_{c,sw} - f_{r,sw}\right) * \exp\left(-\left(\frac{\varepsilon_{sw} - \varepsilon_{cc,sw}}{\alpha}\right)^{\beta}\right) \quad (A.11)$$

$$f_{r,sw} = 0.7 * \left(1 - e^{-1.38\xi_{c,eqv}}\right) * f'_{c,sw} \le 0.25 f'_{c,sw} \quad (A.12)$$

Where:-

$$\alpha = 0.04 - \left(\frac{0.036}{1 + e^{6.08\xi_{c,eqv} - 3.49}}\right), \beta = 1.2\ , \xi_{c,eqv} = \frac{(A_{s,ext} * f_{y,ext}) + (A_{s,int} * f_{y,int})}{(A_{c,sw}\ f'_{c,sw}) + (A_{c,core}\ f'_{c,core})} \quad (A.13)$$

APPENDIX B: Core concrete strain hardening/softening rule

The stress-strain relationship of core concrete can be described as follows:-

I. <u>First stage:</u> $(0 \leq \varepsilon_{core} \leq \varepsilon_{co,core})$

$$\sigma_{core} = f'_{c,core}\left(\frac{k_{core} * \eta_{core} - \eta_{core}^{2}}{1 + (k_{core} - 2) * \eta_{core}}\right) \quad (B.1)$$

$$\eta_{core} = \frac{\varepsilon_{core}}{\varepsilon_{co,core}} \quad (B.2)$$

$$k_{core} = 1.05 * E_{cm,core} * \frac{\varepsilon_{co,core}}{f'_{c,core}} \quad (B.3)$$

$$\varepsilon_{co,core} = 0.00076 + \sqrt{(0.626f'_{c,core} - 4.33) * 10^{-7}}, \quad E_{cm.core} = 4700\sqrt{f'_{c,core}} \quad (B.4)$$

($f'_{c,core}$ and $E_{cm,core}$ are in MPa)

II. <u>Second stage:</u> $(\varepsilon_{co,core} \leq \varepsilon_{core} \leq \varepsilon_{cc\ core})$

Procedures used in the stress-strain relationship of sandwiched concrete are applied for the core concrete except for the formulations in the lateral pressure and confinement coefficient.

$$\varepsilon_{cc,core} = \varepsilon_{co,core}\left(1 + \left(\frac{7.514\lambda_{core}P_3^{0.81}}{f'^{\,0.7}_{c,core}}\right)\right) \quad (B.5)$$

$$\varepsilon_{co,core} = 0.00076 + \sqrt{(0.626f'_{c,core} - 4.33) * 10^{-7}} \quad (B.6)$$

$$\lambda_{core} = \begin{cases} 0.66\eta'^{\,0.52}_{core} & , 0 \leq \eta'_{core} \leq 2.223 \\ 1.0, & , \eta'_{core} \geq 2.223 \end{cases} \quad (B.7)$$

$$\eta'_{core} = \frac{(2t_{int} * f_{y,int})}{((D_{int} - 2t_{int}) * f'_{c,core})} \quad \text{(Internal steel tube confinement coefficient)} \quad (B.8)$$

$$P_3 = p_3' + \frac{P_1 r_2}{r_4} \quad (B.9)$$

Pure lateral confinement part (p_3') of the internal steel tube can be found using the expression suggested by Hu et al. (2003) similar to the external steel tube lateral confinement (p_1).

$$p_3' = \begin{cases} f_{y,int}\left(0.043646 - 0.000832\left(\frac{D_{int}}{t_{int}}\right)\right) \text{for } 21.7 \leq \frac{D_{int}}{t_{int}} \leq 47 \\ f_{y,int}\left(0.006241 - 0.0000357\left(\frac{D_{int}}{t_{int}}\right)\right) \text{for } 47 \leq \frac{D_{int}}{t_{int}} \leq 150 \end{cases} \quad (B.10)$$

III. <u>Third stage:</u> $\varepsilon_{\mathrm{cc,core}} \leq \varepsilon_{core} \leq \varepsilon_{\mathrm{cx,core}}$

$$\sigma_{core} = \mathrm{f_{r,core}} + \left(\mathrm{f'_{c,core}} - \mathrm{f_{r,core}}\right) * \exp\left(-\left(\frac{\varepsilon_{core} - \varepsilon_{\mathrm{cc,core}}}{\alpha}\right)^{\beta}\right) \quad (B.11)$$

$$\mathrm{f_{r,core}} = 0.7 * \left(1 - \mathrm{e}^{-1.38\xi_{\mathrm{c,eqv}}}\right) * \mathrm{f'_{c,core}} \leq 0.25\mathrm{f'_{c,core}} \quad (B.12)$$

Where:-

$$\alpha = 0.04 - \left(\frac{0.036}{1 + \mathrm{e}^{6.08\xi_{\mathrm{c,eqv}} - 3.49}}\right), \beta = 1.2 \text{ and } \xi_{\mathrm{c,eqv}} = \frac{(\mathrm{A_{s,ext}} * \mathrm{f_{y,ext}}) + (\mathrm{A_{s,int}} * \mathrm{f_{y,int}})}{(\mathrm{A_{c,sw}}\ \mathrm{f'_{c,sw}}) + (\mathrm{A_{c,core}}\ \mathrm{f'_{c,core}})} \quad (B.13)$$

APPENDIX C: FE analysis based stress-strain computations for steel and concrete

C.1 Sample calculation for Model CFST-022

C.1.1 Geometrical and material's strength property

Cross Section Dimension: D*T*L (mm)	Concrete strength (f'_c) in (MPa)	Steel Tube yield strength (f_y) in (MPa)
140 * 6.5 * 602	23.8	313.0

C.1.2 Stress-strain relationship of steel

The bilinear elastic-plastic stress-strain curve with strain hardening for the external steel tube of a CFST column could be calculated as follow.

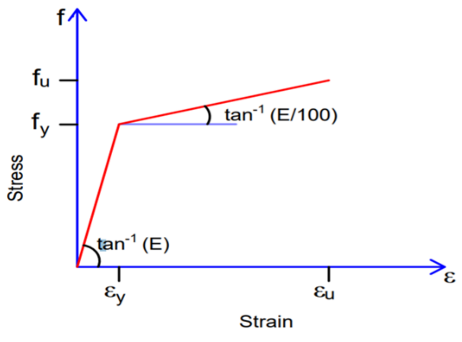

For 200MPa $\leq f_y \leq$ 400MPa could be calculated as follow.

$$f_u = \left(1.6 - 2 * 10^{-3}(f_y - 200)\right) f_y = \left(1.6 - 2 * 10^{-3}(313 - 200)\right) * 313 = 430.062 \text{ MPa}$$

$$\varepsilon_y = \frac{f_y}{E} = \frac{313.0\text{MPa}}{200000\text{MPa}} = 0.001565$$

$$\varepsilon_u = \varepsilon_y + \left(\frac{f_u - f_y}{\frac{E}{100}}\right) = 0.001565 + \left(\frac{430.062 - 313.0}{2000}\right) = 0.060096$$

$\varepsilon^{pl} = \varepsilon^t - \varepsilon^{el} = \varepsilon^{pl} = \varepsilon^t - \frac{\sigma}{E}$ (According to the ABAQUS documentation)

Where: $-\ \varepsilon^{pl}$ and ε^{el} represent plastic and elastic parts at total stress (ε^t)

Summary:-

Stress (MPa)	Strain (Total strain)	Plastic Strain
0	0	0
313.00	0.001565	0
430.062	0.060096	0.05794569

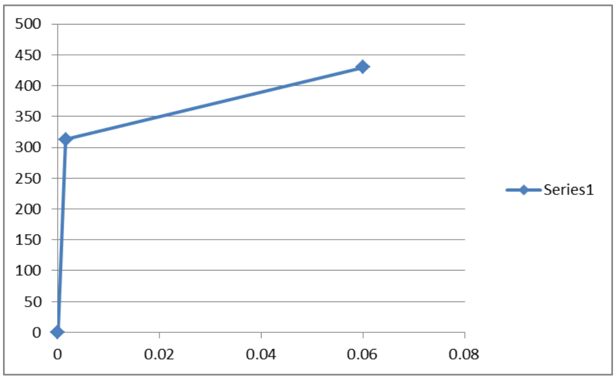

C.1.3 Stress-strain relationship of concrete in compression

- First stage: $(0 \le \varepsilon \le \varepsilon_{co})$

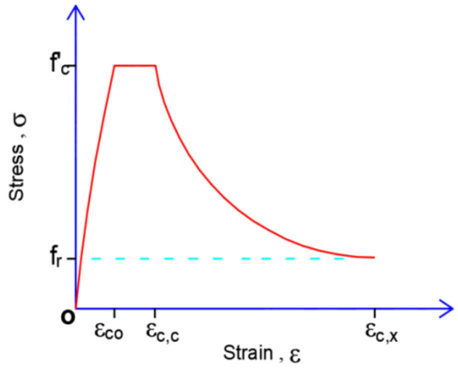

$$E_{cm}(\mathrm{MPa}) = 4700\sqrt{f'_c} = 4700 * \sqrt{23.8} = 22929.064\mathrm{MPa}$$

$$\varepsilon_{c0} = 0.00076 + \sqrt{(0.626f'_c - 4.33) * 10^{-7}}$$

$$= 0.00076 + \sqrt{\left((0.626 * 23.8) - 4.33\right) * 10^{-7}} = 0.001788$$

$$k = 1.05 * E_{cm} * \frac{\varepsilon_{c0}}{f'_c} = 1.05 * 22929.064 * \frac{0.001788}{23.8} = 1.808746$$

$$\eta = \frac{\varepsilon}{\varepsilon_{c0}}$$

$$\sigma = f'_c\left(\frac{k * \eta - \eta^2}{1 + (k-2) * \eta}\right)$$

Strain	η	Stress (MPa)
0	0	0
0.000415194	0.232205101	9.52
0.000758407	0.424153826	15.21121565
0.00110162	0.616102551	19.82390995
0.001444833	0.808051275	22.76281554
0.001788	1	23.8

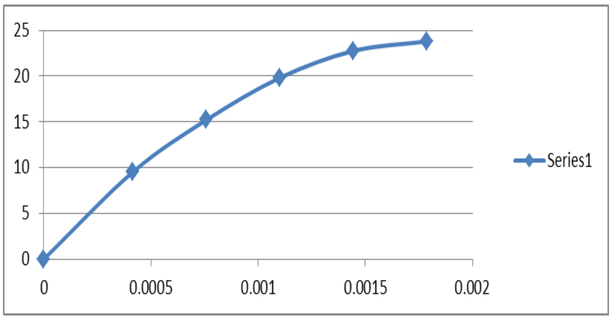

- Second stage: $(\varepsilon_{c,0} \le \varepsilon \le \varepsilon_{c,c})$

$$\eta' = \frac{2t * f_y}{(D-2t) * f'_c} = \frac{2 * 6.5 * 313}{(140 - 2 * 6.5) * 23.8} = 1.3462$$

$$\lambda = \begin{cases} 0.66\eta'^{0.52} & ,0 \le \eta' < 2.223 \\ 1.0 & ,\eta' \ge 2.223 \end{cases} = 0.66 * 0.007885^{0.52}$$

$$= 0.770335$$

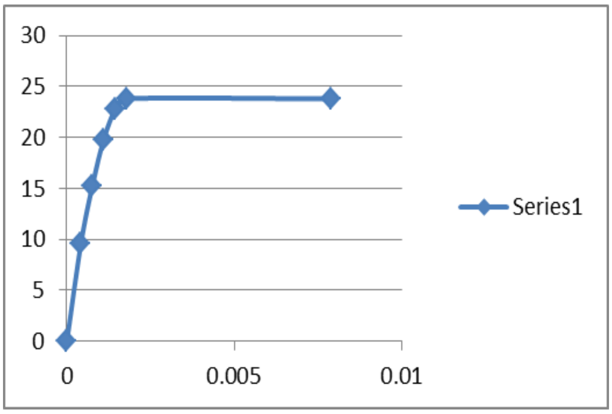

$$f_1 = \begin{cases} f_y\left(0.043646 - 0.000832\left(\frac{D}{t}\right)\right) \text{for } 21.7 \le \frac{D}{t} \le 47 \\ f_y\left(0.006241 - 0.0000357\left(\frac{D}{t}\right)\right) \text{for } 47 \le \frac{D}{t} \le 150 \end{cases} = 313(0.043646 - 0.000832 * \left(\frac{140}{6.5}\right)$$

$$= 8.05224$$

$$\varepsilon_{cc} = \varepsilon_{co}\left(1 + \left(\frac{7.514\lambda f_1^{0.81}}{f_c'^{\,0.7}}\right)\right) = 0.001788 * \left(1 + \left(\frac{7.514 * 0.770335 * 8.05224^{0.81}}{23.8^{0.7}}\right)\right) = 0.007885075$$

- <u>Third stage:</u> $\varepsilon_{c,c} \leq \varepsilon \leq \varepsilon_{c,x}$

$$A_s = \frac{\pi}{4}(D^2 - (D - 2 * t)^2) = \frac{\pi}{4}(140^2 - (140 - 2 * 6.5)^2) = 2{,}726.117\text{mm}^2$$

$$A_c = \frac{\pi}{4}(D - 2 * t)^2 = \frac{\pi}{4}(140 - 2 * 6.5)^2 = 12{,}667.69\text{mm}^2$$

$$\xi_c = \frac{As * fy}{Ac * f'_c} = \frac{2726.117 * 313}{12667.69 * 23.8} = 2.83$$

$\beta = 1.2$

$$f_r = 0.7 * \left(1 - e^{-1.38\xi_c}\right)f_c' = 0.7 * (1 - e^{-1.38*2.83}) * 23.8 = 16.325$$

$f_r = 16.325 \leq 0.25f_c' = 0.25 * 23.8 = 5.95$ .... Not Satisfied; use $f_r = 5.95$

$$\alpha = 0.04 - \left(\frac{0.036}{1 + e^{6.08\xi_c - 3.49}}\right) = 0.04 - \left(\frac{0.036}{1 + e^{6.08*2.83-3.49}}\right) = 0.03999996$$

$$\sigma = f_r + (f_c' - f_r) * \exp\left(-\left(\frac{\varepsilon - \varepsilon_{c,c}}{\alpha}\right)^{\beta}\right)$$

$\varepsilon_c{}^{in} = \varepsilon - \frac{\sigma}{E_{cm}}$ … For the determination of inelastic strain

Stress-strain summary for concrete in compression:

Strain (ε)	**Stress** (σ)	**Inelastic Strain** ($\varepsilon_c{}^{in}$)
0.000415	9.52	0
0.000758	15.2112	9.5E-05
0.001102	19.8239	0.00024
0.001445	22.7628	0.00045
0.001788	23.8	0.00075
0.007885	23.8	0.00685
0.017885	20.7191	0.01698
0.027885	17.5005	0.02712
0.037885	14.7428	0.03724
0.057885	10.7805	0.05741
0.077885	8.47125	0.07752
0.097885	7.21595	0.09757
0.167885	6.04108	0.16762
0.217885	5.96188	0.21763
0.303885	5.95029	0.30363

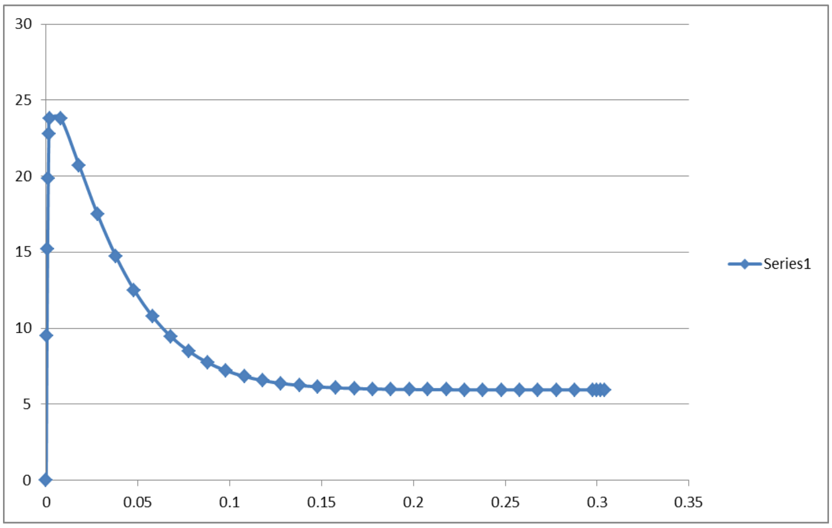

C.1.4 Stress-strain relationship of concrete in tension

$$f_t = 0.3 * (f'_c)^{\frac{2}{3}} = 0.3 * (23.8)^{\frac{2}{3}} = 2.4822\text{MPa}$$

$$\varepsilon_t = \frac{f_t}{E_{cm}} = \frac{2.4822}{22929.064} = 0.000108256$$

$$\sigma = f_t \left(\frac{\varepsilon_t}{\varepsilon}\right)^{0.7+1000\varepsilon} , \sigma \text{ in MPa}$$

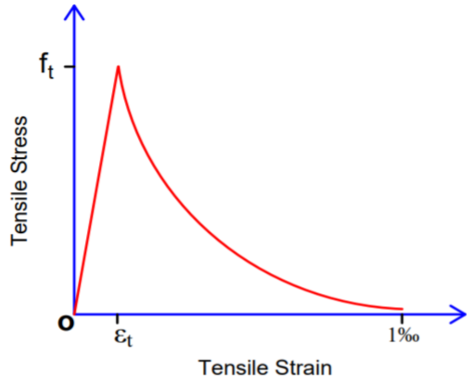

Strain (ε)	Stress (σ)	Cracking Strain
0	0	0
0.00010826	2.48221403	0
0.00021972	1.294473051	0.000163269
0.00033119	0.783545622	0.00029702
0.00044266	0.496556021	0.000421004
0.00055413	0.320232293	0.000540162
0.0006656	0.207833029	0.000656532
0.00077706	0.135041293	0.000771175
0.00088853	0.087613526	0.000884711
0.001	0.056677298	0.000997528

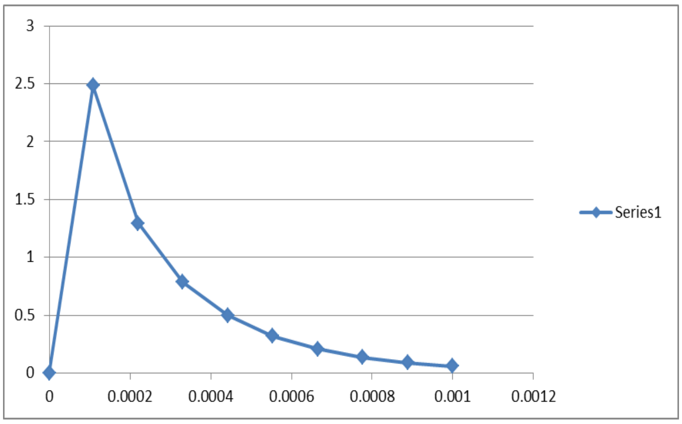

C.2 Sample calculation for Model CFDCST-A-1-2

C.2.1 Geometrical and material's strength property

External Tube				Internal Tube				Column Length
D_{ext} (mm)	t_{ext} (mm)	$f_{y,ext}$ (MPa)	$f'_{c,sw}$ (MPa)	D_{int} (mm)	t_{int} (mm)	$f_{y,int}$ (MPa)	$f'_{c,core}$ (MPa)	L (mm)
426	7.52	302	24.36	219	6.7	316.8	24.36	1300

C.2.2 Stress-strain relationship of steel

For external steel tube:

$$f_{u,ext} = \left(1.6 - 2 * 10^{-3}\left(f_{y,ext} - 200\right)\right) f_{y,ext} = \left(1.6 - 2 * 10^{-3}(302 - 200)\right) * 302 = 421.592\ \text{MPa}$$

$$\varepsilon_{y,ext} = \frac{f_{y,ext}}{E} = 0.00151,$$

$$\varepsilon_{u,ext} = \varepsilon_{y,ext} + \left(\frac{f_{u,ext} - f_{y,ext}}{\frac{200000}{100}}\right) = 0.061306$$

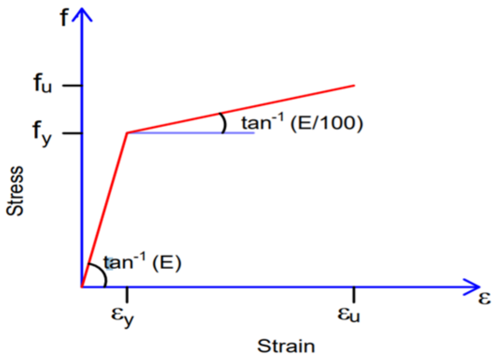

Summary:-

Stress (MPa)	Strain	Plastic Strain
0	0	0
302.0	0.00151	0
421.592	0.061306	0.05919804

For internal steel tube:

$$f_{u,int} = \left(1.6 - 2 * 10^{-3}\left(f_{y,int} - 200\right)\right) f_{y,int} = 432.87552\ \text{MPa}$$

$$\varepsilon_{y,int} = \frac{f_{y,int}}{E} = 0.001584$$

$$\varepsilon_{u,int} = \varepsilon_{y,int} + \left(\frac{f_{u,int} - f_{y,int}}{\frac{200000}{10000}}\right) = 5.80536$$

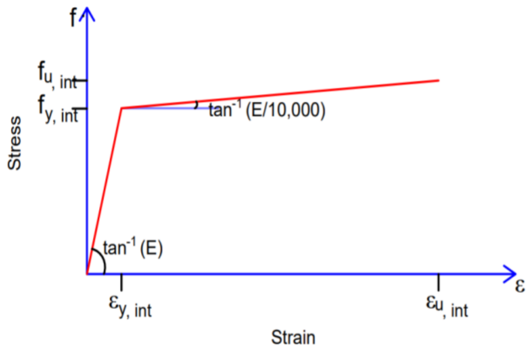

Summary:-

Stress (MPa)	Strain	Plastic Strain
0	0	0
316.8	0.001584	0
432.87552	5.80536	5.803195622

C.2.3 Stress-strain relationship of sandwiched concrete in compression

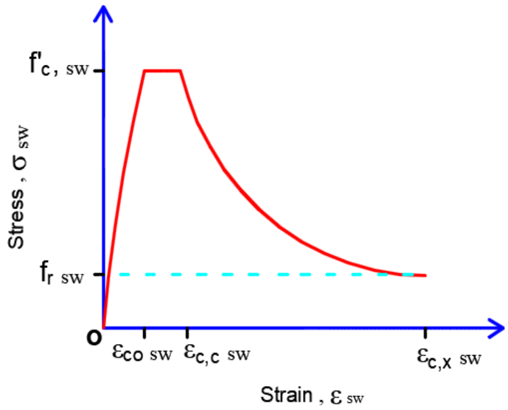

- First stage: $(0 \le \varepsilon_{sw} \le \varepsilon_{co,sw})$

$$E_{cm,sw}(MPa) = 4700\sqrt{f'_{c,sw}} = 23197.402MPa$$

$$\varepsilon_{co,sw} = 0.00076 + \sqrt{(0.626f'_{c,sw} - 4.33) * 10^{-7}} = 0.001805$$

$$k_{sw} = 1.05 * E_{cm,sw} * \frac{\varepsilon_{c0,sw}}{f'_{c,sw}} = 1.8047412$$

$$\eta_{sw} = \frac{\varepsilon_{sw}}{\varepsilon_{c0,sw}}$$

$$\sigma_{sw} = f'_{c,sw}\left(\frac{k_{sw} * \eta_{sw} - \eta_{sw}{}^2}{1 + (k_{sw} - 2) * \eta_{sw}}\right)$$

Strain (ε_{sw})	η_{sw}	Stress (σ_{sw})
0	0	0
0.00042	0.23272	9.744128
0.000766	0.42454	15.56414
0.001113	0.61636	20.28445
0.001459	0.80818	23.29604
0.001805	1	24.36032

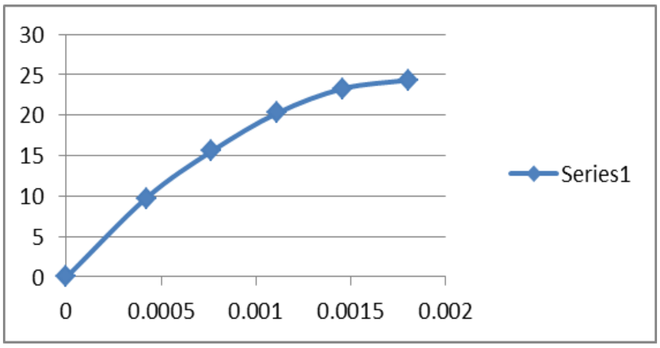

- Second stage: $(\varepsilon_{co,sw} \le \varepsilon_{sw} \le \varepsilon_{cc,sw})$

$$\eta'_{sw} = \frac{(2t * f_{y,ext})}{\left((D_{ext} - D_{int} - 2t_{ext}) * f'_{c,sw}\right) + \left((D_{int} - 2t_{int}) * f'_{c,sw}\right)} = 0.469$$

$$\lambda_{sw} = \{0.66\eta'_{sw}{}^{0.52} \quad , 0 \le '\eta_{sw} < 2.223 \quad = 0.66 * 0.469^{0.52} = 0.4452$$

$$p_1 = \left\{f_{y,ext}\left(0.006241 - 0.0000357\left(\frac{D_{ext}}{t_{ext}}\right)\right)\right. \quad = 1.274$$

$$\varepsilon_{cc,sw} = \varepsilon_{co,sw}\left(1 + \left(\frac{7.514\lambda_{sw}p_1^{0.81}}{f'^{\,0.7}_{c,sw}}\right)\right) = 0.00259$$

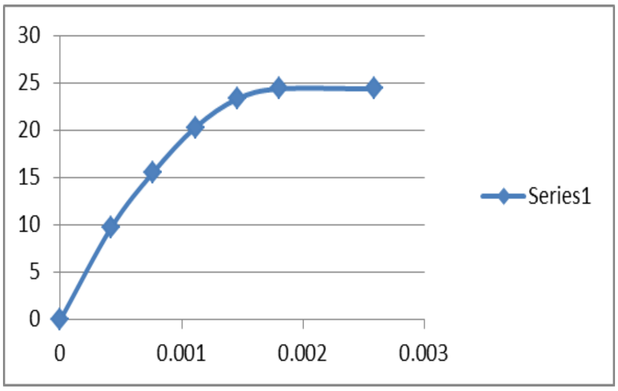

- Third stage: $\varepsilon_{c,c} \le \varepsilon \le \varepsilon_{c,x}$

$$A_{s,ext} = \frac{\pi}{4}\left(D_{ext}{}^2 - (D_{ext} - 2 * t_{ext})^2\right)$$

$$= \frac{\pi}{4}(426^2 - (426 - 2 * 7.52)^2)$$

$$= 9{,}886.497mm^2$$

$$A_{s,int} = \frac{\pi}{4}\left(D_{int}{}^{2} - (D_{int} - 2 * t_{int})^{2}\right) = \frac{\pi}{4}\left(219^{2} - (219 - 2 * 6.7)^{2}\right) = 4{,}468.633\text{mm}^{2}$$

$$A_{c,sw} = \frac{\pi}{4}(D_{ext} - 2 * t_{ext})^{2} - A_{s,int} - A_{c,core} = \frac{\pi}{4}(426 - 2 * 7.52)^{2} - 4{,}468.633\text{mm}^{2} - 33{,}199.85\text{mm}^{2}$$

$$= 94{,}975.94\text{mm}^{2}$$

$$A_{c,core} = \frac{\pi}{4}(D_{int} - 2 * t_{int})^{2} = \frac{\pi}{4}(219 - 2 * 6.7)^{2} = 33{,}199.85\text{mm}^{2}$$

$$\xi_{c,eqv} = \frac{(A_{s,ext} * f_{y,ext}) + (A_{s,int} * f_{y,int})}{(A_{c,sw}\, f'_{c,sw}) + (A_{c,core}\, f'_{c,core})} = 1.4096$$

$$\beta = 1.2$$

$$f_{r,sw} = 0.7 * \left(1 - e^{-1.38\xi_{c,eqv}}\right)f'_{c,sw} = 14.615 \text{ MPa}$$

$$f_{r,sw} = 14.615 \leq 0.25f'_{c,sw} = 0.25 * 24.36 = 6.09 \text{ MPa} \ldots\text{. Not Satisfied; use } f_{r,sw} = 6.09 \text{ MPa}$$

$$\alpha = 0.04 - \left(\frac{0.036}{1 + e^{(6.08*\xi_{c,eqv}) - 3.49}}\right) = 0.03978$$

$$\sigma_{sw} = f_{r,sw} + \left(f'_{c,sw} - f_{r,sw}\right) * \exp\left(-\left(\frac{\varepsilon_{sw} - \varepsilon_{cc,sw}}{\alpha}\right)^{\beta}\right), \sigma_{sw} \text{ in MPa}$$

Stress-strain summary for sandwich concrete in compression:

Strain (ε_{sw})	**Stress** (σ_{sw})	**Inelastic Strain** ($\varepsilon_{c,sw}{}^{in}$)
0.00042	9.744128	0
0.000766	15.56414	9.53E-05
0.001113	20.28445	0.000238
0.001459	23.29604	0.000454
0.001805	24.36032	0.000755
0.002591	24.36032	0.001541
0.012591	21.1877	0.011678
0.032591	15.04725	0.031942
0.052591	10.99113	0.052117
0.072591	8.637002	0.072219
0.092591	7.36302	0.092274
0.142591	6.287684	0.14232
0.212591	6.10166	0.212328
0.322591	6.090171	0.322328
0.412591	6.090081	0.412328
0.432591	6.09008	0.432328

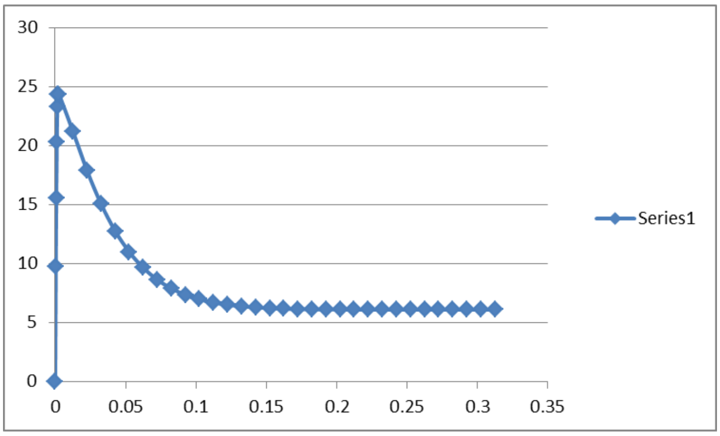

C.2.4 Stress-strain relationship of core concrete in compression

- First stage: $(0 \leq \varepsilon_{core} \leq \varepsilon_{co,core})$

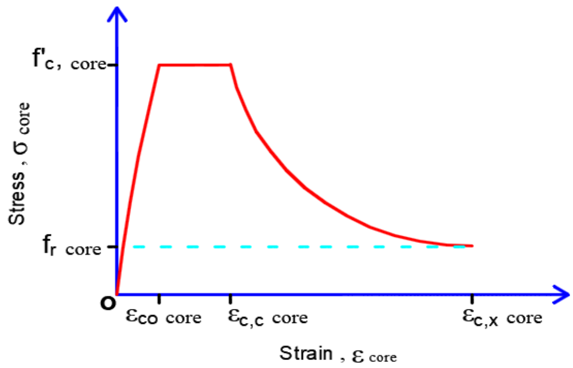

$$E_{cm,core}(MPa) = 4700\sqrt{f'_{c,core}} = 23197.402MPa$$

$$\varepsilon_{co,core} = 0.00076 + \sqrt{(0.626f'_{c,core} - 4.33) * 10^{-7}}$$

$$= 0.001805$$

$$k_{core} = 1.05 * E_{cm,core} * \frac{\varepsilon_{co,core}}{f'_{c,core}} = 1.8047412$$

$$\eta_{core} = \frac{\varepsilon_{core}}{\varepsilon_{co,core}}$$

$$\sigma_{core} = f'_{c,core}\left(\frac{k_{core} * \eta_{core} - \eta_{core}^{2}}{1 + (k_{core} - 2) * \eta_{core}}\right), \sigma_{core} \text{ in MPa}$$

Strain (ε_{core})	η_{core}	Stress (σ_{core})
0	0	0
0.00042	0.23272	9.744128
0.000766	0.42454	15.56414
0.001113	0.61636	20.28445
0.001459	0.80818	23.29604
0.001805	1	24.36032

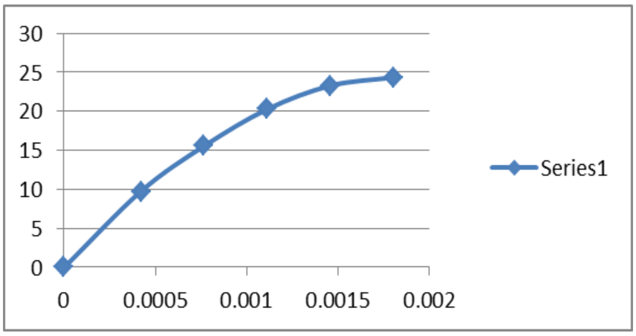

- Second stage: $(\varepsilon_{co,core} \leq \varepsilon_{core} \leq \varepsilon_{cc,core})$

$$\eta'_{core} = \frac{(2t_{int} * f_{y,int})}{((D_{int} - 2t_{int}) * f'_{c,core})} = 0.84759$$

$$\lambda_{core} = \{0.66\eta'^{\,0.52}_{core} \quad , 0 \leq '\eta_{core} < 2.223$$

$$= 0.66 * 0.84759^{0.52} = 0.6056$$

$$p_1 = \left\{f_{y,ext}\left(0.006241 - 0.0000357\left(\frac{D_{ext}}{t_{ext}}\right)\right) = 1.274\right.$$

$$p'_3 = \left\{f_{y,int}\left(0.043646 - 0.000832\left(\frac{D_{int}}{t_{int}}\right)\right) = 5.212\right.$$

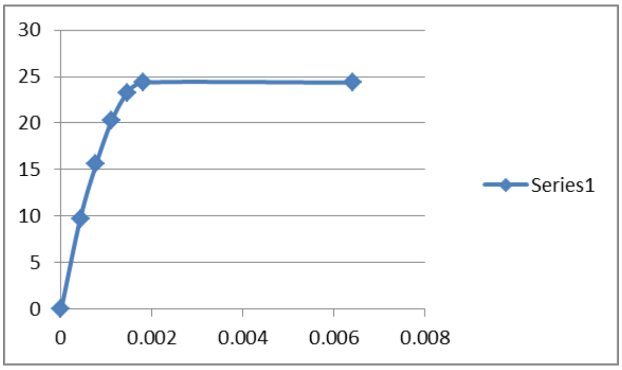

$$P_3 = p_3' + \frac{P_1 r_2}{r_4} = 5.212 + \frac{1.274 * 205.48}{102.8} = 7.7582$$

r_2: Inside radius of External steel tube And r_4: Inside radius of internal steel tube

$$\varepsilon_{cc,core} = \varepsilon_{co,core}\left(1 + \left(\frac{7.514\lambda_{core}p_3^{0.81}}{f'^{\,0.7}_{c,core}}\right)\right) = 0.0064242$$

- Third stage: $\varepsilon_{cc,core} \leq \varepsilon_{core} \leq \varepsilon_{cx,core}$

$$\xi_{c,eqv} = \frac{(A_{s,ext} * f_{y,ext}) + (A_{s,int} * f_{y,int})}{(A_{c,sw}\, f'_{c,sw}) + (A_{c,core}\, f'_{c,core})} = 1.4096$$

$\beta = 1.2$

$$f_{r,core} = 0.7 * \left(1 - e^{-1.38\xi_{c,eqv}}\right) f'_{c,core} = 14.615 \text{ MPa}$$

$$f_{r,core} = 14.615 \leq 0.25 f'_{c,core} = 0.25 * 24.36 = 6.09 \text{ MPa} \ldots \text{Not Satisfied; use } f_r = 6.09 \text{ MPa}$$

$$\alpha = 0.04 - \left(\frac{0.036}{1 + e^{6.08\xi_{c,eqv} - 3.49}}\right) = 0.03978$$

$$\sigma_{core} = f_{r,core} + \left(f'_{c,core} - f_{r,core}\right) * \exp\left(-\left(\frac{\varepsilon_{core} - \varepsilon_{cc,core}}{\alpha}\right)^{\beta}\right), \sigma_{core}\ in\ \text{MPa}$$

Stress-strain summary for core concrete in compression:

Strain (ε_{core})	**Stress** (σ_{core})	**Inelastic Strain** ($\varepsilon_{c,core}{}^{in}$)
0.00042	9.744128	0
0.000766	15.56414	9.53E-05
0.001113	20.28445	0.000238
0.001459	23.29604	0.000454
0.001805	24.36032	0.000755
0.002591	24.36032	0.001541
0.012591	21.1877	0.011678
0.032591	15.04725	0.031942
0.052591	10.99113	0.052117
0.072591	8.637002	0.072219
0.092591	7.36302	0.092274
0.142591	6.287684	0.14232
0.212591	6.10166	0.212328
0.322591	6.090171	0.322328
0.412591	6.090081	0.412328
0.432591	6.09008	0.432328

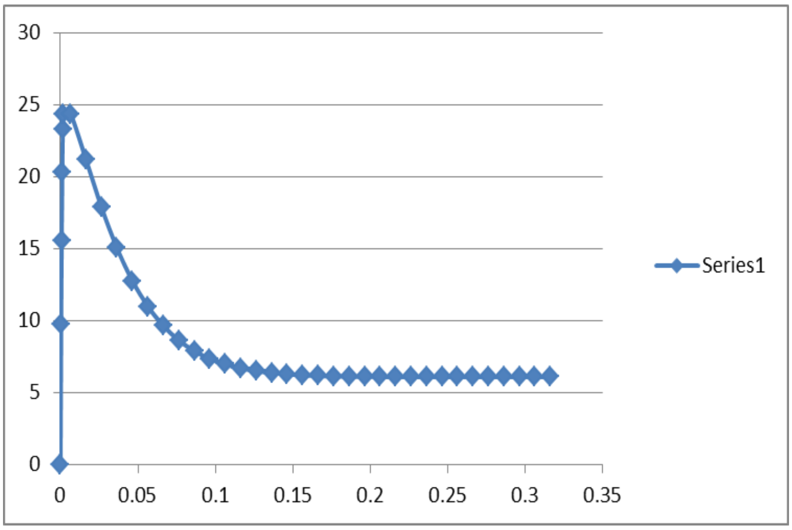

C.2.5 Stress-strain relationship of sandwiched concrete in tension

$$f_{t,sw} = 0.3 * (f'_{c,sw})^{\frac{2}{3}} = 0.3 * (24.36)^{\frac{2}{3}} = 2.521 \text{ MPa}$$

$$\varepsilon_{t,sw} = \frac{f_{t,sw}}{E_{cm,sw}} = \frac{2.521}{23197.4} = 0.0001087$$

$$\sigma_{sw} = f_{t,sw}\left(\frac{\varepsilon_{t,sw}}{\varepsilon_{sw}}\right)^{0.7+1000\varepsilon_{sw}}, \sigma_{sw} \text{ in MPa}$$

Summary:

Strain (ε_{sw})	**Stress (σ_{sw})**	**Cracking Strain**
0	0	0
0.00010868	2.521021668	0
0.00022009	1.317037415	0.000163317
0.00033151	0.797919871	0.000297111
0.00044292	0.506028689	0.000421109
0.00055434	0.326557236	0.000540261
0.00066575	0.212073948	0.000656612
0.00077717	0.137884405	0.000771225
0.00088858	0.089514899	0.000884726
0.001	0.057944186	0.000997502

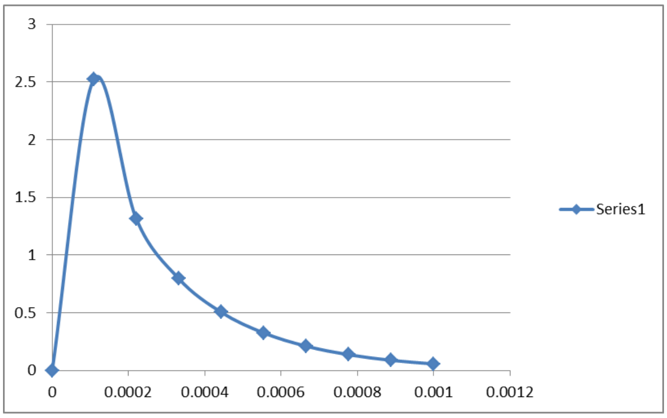

C.2.6 Stress-strain relationship of core concrete in tension

$$f_{t,core} = 0.3 * (f'_{c,core})^{\frac{2}{3}} = 2.521$$

$$\varepsilon_{t,core} = \frac{f_{t,core}}{E_{cm,core}} = 0.0001087$$

$$\sigma_{core} = f_{t,core}\left(\frac{\varepsilon_{t,core}}{\varepsilon_{core}}\right)^{0.7+1000\varepsilon_{core}}$$

Strain (ε_{sw})	**Stress (σ_{sw})**	**Cracking Strain**
0	0	0
0.00010868	2.521021668	0
0.00022009	1.317037415	0.000163317
0.00033151	0.797919871	0.000297111
0.00044292	0.506028689	0.000421109
0.00055434	0.326557236	0.000540261
0.00066575	0.212073948	0.000656612
0.00077717	0.137884405	0.000771225
0.00088858	0.089514899	0.000884726
0.001	0.057944186	0.000997502

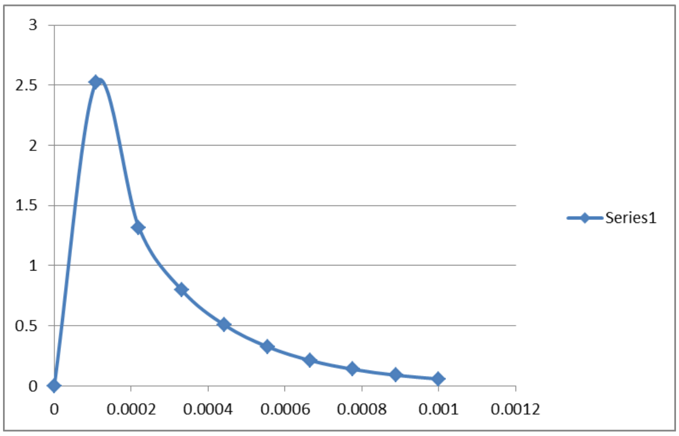

APPENDIX D: Sample calculation using Eurocode-4 formulations

D.1 Design Resistance of CFST-022 column

- Geometrical and material's strength property

Cross Section Dimension: D*T*L (mm)	Concrete strength (f'_c) in (MPa)	Steel Tube yield strength (f_y) in (MPa)
140 * 6.5 * 602	23.8	313.0

$$f'_c = \mathrm{fcm} = 23.8\mathrm{MPa}$$

$$f_{ck} = \mathrm{fcm} - 8 = 15.8\mathrm{MPa}$$

$$\frac{D}{t} = \frac{140}{6.5} = 21.54 \le 90\varepsilon^2 = 90 * \left(\frac{235}{f_y}\right)^{0.5} = 90 * \left(\frac{235}{313}\right)^{0.5} = 77.98 \ldots\ldots \text{Checked for local buckling!}$$

$$A_s = \frac{\pi}{4}(D^2 - (D - 2 * t)^2) = \frac{\pi}{4}(140^2 - (140 - 2 * 6.5)^2) = 2{,}726.117\mathrm{mm}^2$$

$$I_s = \frac{\pi}{64}(D^4 - (D - 2 * t)^4) = \frac{\pi}{64}(140^4 - (140 - 2 * 6.5)^4) = 6{,}087{,}589.699\mathrm{mm}^4$$

$$A_c = \frac{\pi}{4}(D - 2 * t)^2 = \frac{\pi}{4}(140 - 2 * 6.5)^2 = 12{,}667.69\mathrm{mm}^2$$

$$I_c = \frac{\pi}{64}(D - 2 * t)^4 = \frac{\pi}{64}(140 - 2 * 6.5)^4 = 12{,}769{,}820.2\mathrm{mm}^4$$

- Check for local buckling

$$\frac{D}{t} = \frac{140}{6.5} = 21.54 \le 90\varepsilon^2 = 90\left(\frac{235}{313}\right)^{0.5} = 77.984 \ldots\ldots\ldots \mathit{Checked}!$$

- Effective flexural stiffness: $(EI)_{eff}$

$$(EI)_{eff} = E_s I_s + K_e E_{cm} I_c$$

$$\mathrm{Ecm} = 22000 * \left(\frac{\mathrm{fcm}}{10}\right)^{0.3} = 22000 * \left(\frac{23.8}{10}\right)^{0.3} = 28536.18\mathrm{MPa}$$

$$(EI)_{eff} = \left(\frac{200000\mathrm{N}}{\mathrm{mm}^2} * 6087589.699\mathrm{mm}^4\right) + \left(0.6 * \frac{28536.18\mathrm{N}}{\mathrm{mm}^2} * 12769820.2\mathrm{mm}^4\right)$$

$$= 1{,}436{,}159{,}038\mathrm{KNmm}^2$$

Where:-

K_e: Is a correction factor that taken as 0.6

Is: Second moments of area of the structural steel section

Ic: Un-cracked concrete section

- Elastic critical normal force: N_{cr}

$$N_{cr} = \frac{\pi^2 (EI)_{eff}}{L^2} = \frac{\pi^2 * (1{,}436{,}159{,}038KNmm^2)}{(602)^2} = 39111.935KN$$

- Cross-sectional resistance:

$$N_{pl,Rk} = A_s f_y + A_c f_{ck} = 2{,}726.117mm^2 * 313MPa + 12{,}667.69mm^2 * 15.8MPa = 1{,}053.424KN$$

$$\bar{\lambda} = \sqrt{\frac{N_{pl,Rk}}{N_{cr}}} = \sqrt{\frac{1053.424KN}{39111.935KN}} = 0.164$$

For members with zero eccentricity

$$\eta_a = 0.25(3 + 2\bar{\lambda}) = 0.25 * (3 + 2 * 0.164) = 0.832 \leq 1.0 \ldots\ldots \text{checked!}$$

$$\eta_c = 4.9 - 18.5\bar{\lambda} + 17\bar{\lambda}^2 = 4.9 - (18.5 * 0.164) + (17 * 0.164^2) = 2.322 \geq 0 \ldots\ldots \text{checked!}$$

$$f_{cd} = \alpha cc * \frac{f_{ck}}{\gamma c} = 1.0 * \frac{23.8 - 8}{1.5} = 10.53MPa$$

αcc: Coefficient took for long term effects between 0.8 and 1; thus recommended value of 1 were used

A partial safety factor of structural steel γma =1.0 and concrete γc =1.5 used according to EN 1993-1-1, 6.1(1), and EN 1992-1-1, (2.4.2.4) respectively.

$$N_{pl,Rd} = \eta_a A_s f_{yd} + A_c f_{cd}\left(1 + \eta_c \frac{t}{d}\frac{f_y}{f_{ck}}\right)$$

$$N_{pl,Rd} = 0.832 * 2726.117 * \left(\frac{313}{1.0}\right) + 12667.69 * 10.53 * \left(1 + 2.322 * \frac{6.5}{140} * \frac{313}{(23.8 - 8)}\right)$$

$$N_{pl,Rd} = 1128.345KN$$

$$\delta = \frac{A_s * f_{yd}}{N_{pl,Rd}} = \frac{2{,}726.117mm^2 * \left(\frac{313}{1.0}\right) MPa}{1128345N} = 0.756 < 0.9 \ldots\ldots \text{Checked!}$$

D.2 Design Resistance of CFDCST-A1-2 column

- Geometrical and materials' strength property

External Tube				Internal Tube				Column Length
D_{ext} (mm)	t_{ext} (mm)	$f_{y,ext}$ (MPa)	$f'_{c,sw}$ (MPa)	D_{int} (mm)	t_{int} (mm)	$f_{y,int}$ (MPa)	$f'_{c,core}$ (MPa)	L (mm)
426	7.52	302	24.36	219	6.7	316.8	24.36	1300

$$f'_{c,sw} = f'_{c,core} = fcm = 24.36MPa$$

$$f_{ck} = fcm - 8 = 16.36MPa$$

$$\frac{D_{ext}}{t_{ext}} = \frac{426}{7.52} = 56.65 \leq 90\varepsilon^2 = 90 * \left(\frac{235}{f_y}\right)^{0.5} = 90 * \left(\frac{235}{313}\right)^{0.5} = 79.39 \ldots \ldots \text{Checked for local buckling!}$$

$$A_{s,ext} = \frac{\pi}{4}\left(D_{ext}{}^2 - (D_{ext} - 2 * t_{ext})^2\right) = \frac{\pi}{4}(426^2 - (426 - 2 * 7.52)^2) = 9{,}886.497mm^2$$

$$I_{s,ext} = \frac{\pi}{64}\left(D_{ext}{}^4 - (D_{ext} - 2 * t_{ext})^4\right) = \frac{\pi}{64}(426^4 - (426 - 2 * 7.52)^4) = 216{,}492{,}106mm^4$$

$$A_{s,int} = \frac{\pi}{4}\left(D_{int}{}^2 - (D_{int} - 2 * t_{int})^2\right) = \frac{\pi}{4}(219^2 - (219 - 2 * 6.7)^2) = 4{,}468.633mm^2$$

$$I_{s,int} = \frac{\pi}{64}\left(D_{int}{}^4 - (D_{int} - 2 * t_{int})^4\right) = \frac{\pi}{64}(219^4 - (219 - 2 * 6.7)^4) = 25{,}200{,}955mm^4$$

$$A_{c,core} = \frac{\pi}{4}(D_{int} - 2 * t_{int})^2 = \frac{\pi}{4}(219 - 2 * 6.7)^2 = 33{,}199.85mm^2$$

$$I_{c,core} = \frac{\pi}{64}(D_{int} - 2 * t_{int})^4 = \frac{\pi}{64}(219 - 2 * 6.7)^4 = 87{,}712{,}672mm^4$$

$$A_{c,sw} = \frac{\pi}{4}(D_{ext} - 2 * t_{ext})^2 - A_{s,int} - A_{c,core} = \frac{\pi}{4}(426 - 2 * 7.52)^2 - 4{,}468.633mm^2 - 33{,}199.85mm^2 = 94{,}975.94mm^2$$

$$I_{c,sw} = \frac{\pi}{64}(D_{ext} - 2 * t_{ext})^4 - I_{s,int} - I_{c,core} = \frac{\pi}{64}(426 - 2 * 7.52)^4 - 25{,}200{,}955mm^4 - 87{,}712{,}672mm^4 = 1{,}287{,}215{,}562mm^4$$

- Check for local buckling

$$\frac{D}{t} = \frac{426}{7.52} = 56.65 \leq 90\varepsilon^2 = 90\left(\frac{235}{302}\right)^{0.5} = 79.39 \ldots\ldots\ldots. Checked!$$

- Effective flexural stiffness: $(EI)_{eff}$

$$(EI)_{eff} = E_s I_s + K_e E_{cm} I_c$$

$$Ecm_{SW} = Ecm_{core} = 22000 * \left(\frac{fcm}{10}\right)^{0.3} = 22000 * \left(\frac{24.36}{10}\right)^{0.3} = 28735.97MPa$$

$$(EI)_{eff} = \left(\frac{200000N}{mm^2} * 216{,}492{,}106mm^4\right) + \left(\frac{200000N}{mm^2} * 25{,}200{,}955mm^4\right)$$
$$+ \left(0.6 * \frac{28735.97N}{mm^2} * 1{,}287{,}215{,}562mm^4\right) + \left(0.6 * \frac{28735.97N}{mm^2} * 87{,}712{,}672mm^4\right)$$
$$= 72{,}044{,}550{,}286KNmm^2$$

- Elastic critical normal force: N_{cr}

$$N_{cr} = \frac{\pi^2 (EI)_{eff}}{L^2} = \frac{\pi^2 * (72{,}044{,}550{,}286KNmm^2)}{(1300)^2} = 420{,}740.36KN$$

- Cross-sectional resistance:

$$N_{pl,Rk} = A_{s,ext} f_{y,ext} + A_{s,int} f_{y,int} + A_{c,sw} f_{ck,sw} + A_{c,core} f_{ck,core}$$

$$= (9{,}886.49 * 302) + (4{,}468.633 * 316.8) + (94{,}975.94 * 16.36) + (33{,}199.85 * 16.36) = 6{,}498.341KN$$

$$\bar{\lambda} = \sqrt{\frac{N_{pl,Rk}}{N_{cr}}} = \sqrt{\frac{6498.341KN}{420{,}740.36KN}} = 0.1243$$

For members with zero eccentricity

$$\eta_a = 0.25(3 + 2\bar{\lambda}) = 0.25 * (3 + 2 * 0.1243) = 0.81214 \leq 1.0 \ldots\ldots \text{checked!}$$
$$\eta_c = 4.9 - 18.5\bar{\lambda} + 17\bar{\lambda}^2 = 4.9 - (18.5 * 0.1243) + (17 * 0.1243^2) = 2.86342 \geq 0 \ldots\ldots \text{checked!}$$

$$f_{cd,sw} = f_{cd,core} = \alpha cc * \frac{f_{ck}}{\gamma c} = 1.0 * \frac{(24.36 - 8)}{1.5} = 10.91$$

Where:

αcc: Coefficient took for long term effects between 0.8 and 1; the recommended value of 1 was used

A partial safety factor of structural steel γma =1.0 and concrete γc =1.5 used according to EN 1993-1-1, 6.1(1), and EN 1992-1-1, (2.4.2.4) respectively.

$$N_{pl,Rd} = \eta_a A_{s,ext} f_{yd,ext} + A_{s,int} f_{yd,int} + (A_{c,sw} f_{cd,sw} * \left(1 + \eta_c \frac{t_{ext}}{d_{ext}} \frac{f_{y,ext}}{f_{ck,sw}}\right)) + (A_{c,core} f_{cd,core} * \left(1 + \eta_c \frac{t_{ext}}{d_{ext}} \frac{f_{y,ext}}{f_{ck,core}}\right))$$

$$N_{pl,Rd} = 0.81214 * 9{,}886.49 * \left(\frac{302}{1.0}\right) + 4{,}468.633 * \left(\frac{316.8}{1.0}\right) + 94{,}975.94 * 10.91 * \left(1 + 2.86342 * \frac{7.52}{426} * \frac{302}{(24.36 - 8)}\right) + 33{,}199.85 * 10.91 * \left(1 + 2.86342 * \frac{7.52}{426} * \frac{302}{(24.36 - 8)}\right)$$

$$N_{pl,Rd} = 6542.87 KN$$

$$\delta = \frac{A_{s,ext} * f_{yd,ext} + A_{s,int} f_{yd,int}}{N_{pl,Rd}}$$

$$\delta = \frac{9886.49 * \left(\frac{302}{1.0}\right) + 4468.633 * \left(\frac{316.8}{1.0}\right)}{6542868.51} = 0.673 < 0.9 \ldots \ldots \text{Checked!}$$